Efficient Power Allocation Techniques for 5G Cellular Networks

THESIS

Submitted in partial fulfilment
of the requirements for the degree of
DOCTOR OF PHILOSOPHY

by

TRANKATWAR SACHIN RAVIKANT
ID No. 2018PHXF0425H

Under the Supervision of

Dr. Prashant K. Wali

BITS Pilani
Pilani | Dubai | Goa | Hyderabad

BIRLA INSTITUTE OF TECHNOLOGY AND SCIENCE, PILANI
2024

BIRLA INSTITUTE OF TECHNOLOGY AND SCIENCE, PILANI

CERTIFICATE

This is to certify that the thesis entitled, Efficient Power Allocation Techniques for 5G Cellular Networks submitted by Trankatwar Sachin Ravikant ID No. 2018PHXF0425H for award of Ph.D. of the Institute embodies original work done by him under my supervision.

Signature of the Supervisor:

Name: Dr. PRASHANT K. WALI

Designation: Assistant Professor

Date: 28 June 2024

Acknowledgements

To begin, I am extremely grateful to my supervisor, Dr. Prashant K. Wali, for allowing me to pursue and guide me throughout my Ph.D. program. His knowledge and experience have inspired me in my academic research and everyday life. I am very thankful to him for his endless patience, support, kindness, and continuous supervision. He has generously and patiently spent much time discussing research ideas with me. Also, he has consistently pointed out important research queries and has always given me the freedom to explore my interests. Working and learning under his supervision was a great privilege and honor. I am immensely thankful to him.

I would like to thank my doctoral advisory committee members, Prof. Runa Kumari and Dr. Harish V. Dixit, for their technical support in my doctoral study. I am grateful for their valuable time, comments, and suggestions.

I would like to thank the Heads of the Electrical and Electronics Engineering Department, Prof. Subhendu K Sahoo, Prof. Alivelu Manga Parimi (former HoD), and Prof. Sanket Goel (former HoD) for their continuous support and for providing all facilities during my Ph.D. course. I would also like to express gratitude to DRC convener Prof. Radhika Sudha and former DRC conveners Prof. BVVSN Prabhakar Rao, Prof. Prasant Kumar Pattnaik, and Dr. Prashant K. Wali for their help in administrative-related matters.

I would also like to thank the Department of Electrical and Electronics Engineering faculty members for providing me with a conducive environment to learn and grow. I wish to express my thanks to the lab technicians for their discussions and suggestions.

I am also thankful to all my friends in the ADSP Lab for making me part of their daily endeavors. I would like to thank my fellow researchers: Swapna Madam, Sharvani, Priyanka, Anil, Sahith, Nawin, and Jagadheesh. It has been a pleasure working together. I would like to extend my sincere gratitude to my colleague Samit Kumar Ghosh, for assisting me during the initial phase of the research work. I thank my friends Anil Guruvadeyar and Sarath Kumar for helping me economically in various challenging situations.

Finally, I am grateful to my parents, brothers, and family members. Their blessings have helped me in reaching this goal. My heartfelt thanks to my parents-in-law, who have taken care of many of my responsibilities during my doctoral study. I am incredibly thankful to my wife for her patience, prayers, love, and support and for always standing by my side during my research work. It would not have been possible for me to complete my research without the presence of my daughter, Shaarvi.

Abstract

One of the essential areas in the communication field today is wireless communication. Wireless communication aims to provide high-quality, reliable communication for cellular networks. For several decades, wireless cellular technology has advanced from the first generation (1G) to today's fifth generation (5G). Nowadays, wireless communications have evolved into one of the most revolutionary technologies in the industrial, public, and government sectors. Thus, the demand for wireless communication has been increasing continuously. 5G is a wireless technology that has been envisioned to meet these growing demands. Therefore, improving the key requirements is essential to meet the rising demand for 5G wireless networks. The present wireless communication technologies may not be capable of fulfilling these key requirements of 5G wireless networks; therefore, developing advanced technologies is essential. In recent years, several emerging technologies have been developed to improve the essential requirements of 5G networks. Heterogeneous Networks (HetNets) and Non-Orthogonal Multiple Access (NOMA) are among the emerging technologies intended to improve some of the vital requirements of 5G networks.

NOMA technology has been identified as vital in boosting system throughput to meet 5G network demands. To maximize system throughput in a NOMA-based 5G network, the base station (BS) must distribute appropriate transmit power to users. As a result, power allocation (PA) is a crucial challenge for the NOMA-based 5G network's system throughput improvement. User fairness is another equally important parameter that should go hand-in-hand with system throughput for NOMA-based 5G networks. But, to the best of our knowledge, even though there have been works that look at system throughput and user fairness maximization for NOMA-based 5G networks, they looked at these as a single objective optimization problem, where one is the objective and the other is one of the constraints. However, quite often, joint optimization of both system throughput and user fairness is required to make optimal decisions in the face of trade-offs between these equally important but conflicting objectives. In this regard, Chapter 2 formulates a Multi-objective Optimization (MOO) problem to jointly maximize the sum rate and user fairness in a downlink transmission NOMA-based 5G networks through optimal PA under system-imposed constraints. A weighted sum approach is used to turn the MOO into a single-objective optimization problem to make it analytically tractable and provide the desired trade-off between the conflicting objectives. We apply the Lagrange dual decomposition method and the Karush–Kuhn–Tucker (KKT) conditions to achieve the optimal PA. Using optimal PA expressions, we propose an iterative PA algorithm that converges fast enough to be employed in practical NOMA-based 5G networks. We present simulation results to validate our proposed solution. We also compare the proposed system's results with the benchmark methods.

NOMA is based on the concept of multiplexing users at the same time and frequency, which can cause a significant amount of multiple access interference during decoding at each intended receiver. In order to handle this multiple access interference, successive interference cancellation (SIC) is an essential process at the receiver in the NOMA network. To ensure the successful execution of the SIC process, the transmit powers of the users must meet the minimum required gap at the transmitter. However, to the best of our knowledge, to date, no work addresses the joint optimization of sum rate and user fairness while simultaneously considering the minimum power gap constraint. Therefore, in Chapter 3, we formulate and solve a joint sum rate and fairness MOO problem for the downlink NOMA-based 5G network. Along with the usual transmitter power budget and Quality of Service (QoS) constraints, we also consider the user's minimum transmit power gap constraint, which is required for the successful execution of SIC, a constraint ignored at large in the literature. We derive optimal PA coefficients for the proposed method. As part of the validation process, we present simulation results and compare the performance of the proposed system with a system that considers only the sum rate objective.

The use of NOMA in a multicarrier system can further increase the rate of a 5G network. In such a system, the subchannel allocation (SA) and PA are intricately linked and essential for improving system throughput. Chapter 4 work comes up with joint optimization of the SA and PA to maximize the sum rate of the NOMA-based 5G network while sticking to the minimum power gap constraint. Specifically, we formulate an optimization problem to maximize the sum rate by achieving optimal SA and PA while adhering to minimum user rate, minimum power gap, subchannel user rate, and power budget constraints for downlink transmission in multicarrier NOMA networks. To ensure that the proposed method can solve in polynomial time, SA and PA have been obtained in two stages. First, we calculate SA and then PA for each subchannel. In order for our optimization method to work in real-world 5G networks, we propose a fast and low-complexity algorithm. Finally, we present simulation results for the proposed method and compare them with benchmarking schemes. We also compare and examine the performance of the proposed algorithm with existing SA algorithms for our proposed method.

HetNet offers a high data rate, increased capacity, enhanced QoS, reduced latency, and decreased power consumption for 5G networks. Despite the advantages, there are several challenges in HetNets; among them, interference is one of the most significant. Due to densification in a HetNet, interference increases, and consequently, coverage probability decreases for the network. In Chapter 5, we propose an efficient and faster power control algorithm in the downlink to enhance the coverage probability of the K-tier 5G HetNet. We consider the Poisson point process (PPP) to model BS distribution, and Voronoi tessellation provides network coverage areas. We present simulation results to show that the proposed power control algorithm improves

the coverage probability compared to the existing power control algorithm. Furthermore, the proposed power control algorithm's convergence rate is faster than the existing power control algorithm.

Densification in HetNets increases interference while decreasing the rate and outage probability. As a result, NOMA-based HetNets may be employed to minimize cross-tier interference. Thus, it decreases outage probability and increases the system sum rate in order to fulfill 5G network needs. PA is vital for increasing system throughput and reducing outages in NOMA-based HetNets. Hence, Chapter 6 comes up with an optimal PA for downlink transmission NOMA-based HetNets to optimize the system's sum rate and outage probability of the 5G network while adhering to the minimal user rate constraint. We derive a generalized optimal PA coefficient equation for small-cell users of NOMA-based HetNets. Then, utilizing the PA coefficient equation, we present an algorithm to optimize the sum rate and minimize the outage probability. To apply our algorithm in real-world wireless networks, we ensure that our algorithm is both fast and minimal in complexity. Finally, we illustrate simulation results for the proposed method and compare them to OMA systems.

Contents

List of Figures

List of Abbreviations

1G	-	First Generation
2D	-	Two-Dimensional
2G	-	Second Generation
3D	-	Three-Dimensional
3G	-	Third Generation
4G	-	Fourth Generation
5G	-	Fifth Generation
AI	-	Artificial Intelligence
AM	-	Alternating Maximization
AMPS	-	Advanced Mobile Phone System
AR	-	Augmented Reality
AWGN	-	Additive White Gaussian Noise
BS	-	Base Station
CDMA	-	Code Division Multiple Access
CDRT	-	Coordinated Direct and Relay Transmission
CO2	-	Carbon Dioxide
CSI	-	Channel State Information
D2D	-	Device-to-Device
FDMA	-	Frequency Division Multiple Access
GBPS	-	Gigabits Per Second
GSM	-	Global System for Mobile Communications
GPRS	-	General Packet Radio Service
GPS	-	Global Positioning System
HetNet	-	Heterogeneous Network

ICD	-	Intra-Cell Diversity
ICIC	-	Inter-Cell Interference Coordination
ICT	-	Information and Communication Technology
IoT	-	Internet of Things
IGS	-	Improper Gaussian Signaling
IID	-	Independent and Identically Distributed
ITU-R	-	International Telecommunications Union-Radio
ITU	-	International Telecommunication Union
JFI	-	Jain Fairness Index
KBPS	-	Kilobits Per Second
KKT	-	Karush–Kuhn–Tucker
km	-	kilometer
LTE	-	Long-Term Evolution
MBPS	-	Megabits Per Second
MOO	-	Multi-Objective Optimization
MIMO	-	Multiple Input Multiple Output
mmWave	-	millimeter Wave
MHCPP	-	Maern hard-core point process
MISO	-	Multiple Input Single Output
MMS	-	Multimedia Messaging Service
MMSE	-	Minimum Mean Square Error
MRC	-	Maximum Ratio Combining
NOMA	-	Non-Orthogonal Multiple Access
NR	-	New Radio
OFDMA	-	Orthogonal Frequency Division Multiple Access
OMA	-	Orthogonal Multiple Access
PA	-	Power Allocation
PPCP	-	Poisson-Point Cluster Process
PPP	-	Poisson Point Process
QoS	-	Quality of Service
RIS	-	Reconfigurable Intelligent Surface

SA	-	Subchannel Allocation
SIC	-	Successive Interference Cancellation
SINR	-	Signal-to-Interference and Noise Ratio
SIMO	-	Single Input Multiple Output
SIR	-	Signal-to-Interference Ratio
SISO	-	Single Input Single Output
SNR	-	Signal-to-Noise Ratio
TDD	-	Time-Division Duplex
TDMA	-	Time Division Multiple Access
VR	-	Virtual Reality
WCUFSA	-	worst-case user first subcarrier allocation
WCA	-	Worst Case Avoiding
WCF	-	Worst Case First
WSA	-	Worst Subcarrier Avoiding
ZF	-	Zero-Forcing

List of Notations

α	-	Power allocation coefficient.
X	-	Transmitted signal at base station.
S_m	-	Symbol of user m.
P	-	Total transmit power of base station.
α_m	-	Power allocation coefficient of user m.
r_m	-	Received signal at user m.
h_m	-	Complex channel gain from base station to user m.
η_m	-	Complex additive white Gaussian noise.
μ	-	Mean of complex additive white Gaussian noise.
σ^2	-	Variance of complex additive white Gaussian noise.
y_m	-	Received signal at user m after the SIC process.
$SINR_m$	-	Signal-to-interference and Noise Ratio at user m.
R_m	-	Achievable rate for user m.
$\mathbb{R}^2$	-	Spatial distribution in two-dimension.
Φ_i	-	Poisson point process of tier i.
λ_i	-	Density of tier i of Poisson point process.
P_i	-	Transmit power of tier i.
T_i	-	Target SINR of tier i.
x_i	-	Location of a user (which is at the origin) from the base station in the tier i.
P_r	-	Power received by a user.
P_c	-	Coverage probability.
$\mathbb{P}()$	-	Probability that something occurs.
$\bigcup$	-	Union of two or more sets.

M	-	Number of users.
d_i	-	Distance between base station and user i
pl	-	Path loss exponent.
$SINR_m^{imper}$	-	Signal-to-interference and Noise Ratio for imperfect SIC at user m.
ε	-	Residual interference component produced by SIC imperfection.
$U(R_m)$	-	α - fair utility function.
U_{sum}	-	Sum utility.
R_{sum}	-	Sum rate.
l	-	Fairness levels.
P_{BS}	-	Total power budget of base station.
R_{min}	-	Minimum rate requirement for QoS of each user.
ω	-	Weighting coefficient for objective 1.
t_m	-	Assistant variable
$\mathscr{L}$	-	Lagrange function.
χ_m	-	Lagrange multiplier for QoS constraint.
β_m	-	Lagrange multiplier for power budget constraint..
μ_m	-	Lagrange multiplier for assistant variable.
t	-	Iteration index.
$\delta_1, \delta_2,$ and δ_3	-	Step sizes.
$\mathscr{R}$	-	Channel realization.
T^{cv}	-	Total number of iterations for algorithm convergence
JFI	-	Jain fairness index.
Δ_i	-	Determinant of the leading principal sub-matrix of first i rows and i columns of the Hessian matrix.
$\mathbf{A}, \mathbf{C}$	-	Hessian matrix for U_{sum}.
$\mathbf{B}, \mathbf{D}$	-	Hessian matrix for R_{sum}.
z_m	-	Small scale fading parameter.
P_g	-	Minimal power gap between users to execute SIC successfully.
v_m	-	Assistant variable.
ψ_m	-	Lagrange multiplier for SIC constraint.
N	-	Number of subchanels.

T^c	-	Total number of users for multicarrier NOMA network.
M^c	-	maximum number of users per subchannel.
B_N	-	Total bandwidth of network.
B_N^c	-	Bandwidth of subchannel.
$h_{m,n}$	-	Complex channel gain from base station to user m on subchannel n.
$d_{m,n}$	-	Distance between BS and user m on subchannel n.
$z_{m,n}$	-	Complex Gaussian distribution on subchannel n.
X^c	-	Transmitted signal at base station on each subchannel.
P^c	-	Total transmit power per subchannel.
$\alpha_{m,n}$	-	Power allocation coefficient for user m on subchannel n.
$S_{m,n}^c$	-	Symbol of user m on subchannel n.
$\eta_{m,n}$	-	Complex additive white Gaussian noise on subchannel n.
$r_{m,n}$	-	Received signal to the m^{th} user over the n^{th} subchannel.
$y_{m,n}$	-	Received signal for user m over the n^{th} subchannel after the SIC process.
$SINR_{m,n}$	-	Signal-to-interference and noise ratio by user m on subchannel n.
$R_{m,n}$	-	Data rate of user m over subchannel n.
$SINR_{m,n}^{imper}$	-	Signal-to-interference and noise ratio for imperfect SIC by user m on subchannel n.
$\pi_{m,n}$	-	Decoding order of user m on subchannel n.
$\mathbf{S}$	-	Subchannel allocation matrix.
$s_{m,n}$	-	Element of $\mathbf{S}$ matrix for user m and subcarrier n.
α	-	Power allocation matrix.
$\alpha_{m,n}$	-	Element of α matrix for user m and subcarrier n.
ξ	-	Minimum target Signal-to-interference and noise ratio.
$\mathbf{E}, \mathbf{F}$	-	Matrices of the linear simultaneous equation for QoS constraint.
$\mathbf{G}, \mathbf{H}$	-	Matrices of the linear simultaneous equation for SIC constraint.
$\alpha_{m,n}^{'}$	-	PA coefficient of user m on subchannel n for QoS constraint.
$\alpha_{m,n}^{''}$	-	PA coefficient of user m on subchannel n for SIC constraint.
N_1	-	Subchannel 1.
N_2	-	Subchannel 2.
N_3	-	Subchannel 3.

Δ_E	-	Determinant of matrix **E**.
Δ_G	-	Determinant of matrix **G**.
P_i^{sc}	-	Transmit power of BS in a small cell of tier i.
$\text{SINR}(x_i)$	-	SINR of the user connected to BS of location x_i.
κ	-	Tiers indices, Where $\kappa = \{1, 2, ...K\}$.
M^{sc}	-	Number of small cells.
N^{sc}	-	Number of small cell users.
$h_{m,n}^{sc}$	-	Complex Rayleigh fading coefficient from small cell base station m to small cell user n.
$z_{m,n}^{sc}$	-	Rayleigh distribution between small cell base station m to small cell user n.
$g_{m,n}$	-	Complex Rayleigh fading coefficient from macrocell BS to small cell user n in small cell m.
$x_{m,n}$	-	Data intended for n^{th} user in small cell m.
$w_{m,n}$	-	Interference plus noise for n^{th} user in small cell m.
$\alpha_{m,n}^{sc}$	-	Power allocation coefficient from small cell base station m to small cell users n.
$SINR_{m,n}^{sc}$	-	Signal-to-interference and noise ratio of received at the n^{th} small cell user of small cell m.
P^{sc}	-	Transmit power from small base station.
P_k	-	Transmit power from macrocell base station.
B^{sc}	-	Bandwidth of small cell.
$R_{m,n}^{sc}$	-	Data rate of small cell user n in small cell m.
SR^{sc}	-	Sum rate of small cell user n in small cell m.
$R_{m,n}^{sc*}$	-	Target rate of small cell user n of small cell BS m.
ξ_n	-	Target SINR for user n on small cell m.

Chapter 1

Introduction

This chapter provides an overview and the motivation for the research topic. The objectives and summary of the essential contributions of the thesis are expressed. In addition, we provide the structure of the rest of the thesis.

1.1 Overview

Wireless mobile communications have changed tremendously since MacDonald of Bell Telephone Laboratories came up with the idea of cellular communications in 1979 [1]. Wireless communication has become one of the most revolutionary technologies in the industrial, public, and government sectors [2, 3]; thus, it is essential to understand how previous generations developed.

1.1.1 History: From 1G to 5G:

Over the previous four decades, cellular technology has progressed from the first generation (1G), followed by the second generation (2G), third generation (3G), and fourth generation (4G), culminating in today's fifth generation (5G). The 1G mobile communication systems were developed for commercial usage in the 1980s. Advanced mobile phone system (AMPS), the first analog cellular technology, was extensively used in North America [4]. Radiolinja was

the first company in Finland to launch 2G mobile telephony networks in 1991. The global system for mobile communications (GSM) standard was utilized in this network [4]. The key advantage of 2G networks over 1G networks was data services for mobile, initiating with SMS text messaging and advancing to Multimedia Messaging Service (MMS). 2G has a data rate of 14.4 – 64 Kilobits Per Second (KBPS) and a latency of 500 – 1000 milliseconds [5, 6]. The general packet radio service (GPRS) was the first significant step in growing GSM networks toward 3G communication systems. The International Telecommunication Union (ITU) created 3G telecommunication technologies in the early 1980s [7]. In Japan, NTT DoCoMo was the first to commercialize 3G in 2001. Compared to 2G networks, 3G networks provide faster data rates of 2 Megabits Per Second (MBPS), low latency of 200 milliseconds, and more security [5, 6]. 3G provides devices with mobile broadband service of several Mbps. Applications like a Global positioning system (GPS), mobile internet access, mobile TV, video calls, and location-based services were developed employing the bandwidth and location information of 3G devices.

The International Telecommunications Union-Radio (ITU-R) communications sector set the specifications for 4G mobile telecommunication technology standards in March 2008 [8]. Spread spectrum radio technology, which was employed in 3G networks, was phased out in 4G systems. The orthogonal frequency division multiple access (OFDMA) multi-carrier transmission was the fundamental technology in 4G networks. OFDMA has been extensively used to achieve higher data rates in 4G mobile communication systems such as long-term evolution (LTE) and LTE-Advanced [9]. 4G has a latency of 100 milliseconds and a data transmission rate of 200 MBPS - 1 Gigabits Per Second (GBPS) [5, 6]. Following a historical 10-year cycle for every generation, the 5G mobile network is now in the research stage. 5G is expected to be significantly faster than 4G, with peak data speeds of up to 20 GBPS and an average data rate of up to 10 - 100 GBPS [5]. 5G is expected to offer a much lower latency of less than 1 millisecond [6], enabling more instantaneous, real-time access. 5G is expected to be more than just an extension of the existing 4G communication networks. It is expected to support a wide range of scenarios, including smart homes, e-health, industries Internet of Things (IoT), autonomous vehicles, etc. This is due to the exponentially increasing demand for data traffic and the significant impact of future wireless networks on daily human activities. Increased bandwidth, low latency, energy conservation, cost reduction, increased system capacity, and massive device connection are some

of the most significant requirements of 5G [10]. Figure 1.1 shows an evolution of 1G to 5G networks [11].

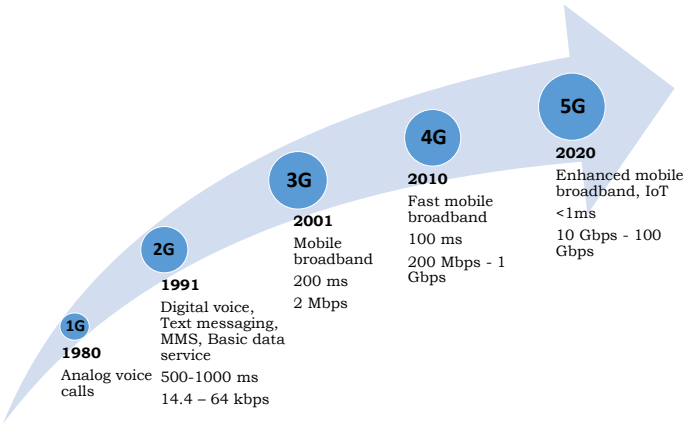

FIGURE 1.1: Evolution of 1G to 5G networks.

1.2 Requirements for 5G:

The fast development of several emergent applications, including artificial intelligence (AI), entertainment and multimedia, augmented reality (AR) and virtual reality (VR), three-dimensional (3D) media, and the IoT, has resulted in a tremendous increase in cellular network traffic. [12]. Global mobile traffic volume was 7.462 exabytes per month in 2010, 60 exabytes per month in 2020, and is expected to reach 600 exabytes per month in 2025 and 5016 exabytes per month in 2030 [13]. This statistic demonstrates the extreme importance of communication system improvement. To meet the ever-increasing demand for 5G networks, it is necessary to improve the key requirements of 5G wireless networks. The key requirements of 5G wireless networks can be summarized as follows:

- **Data Rate:** For more than a century, wireless data traffic has grown at an exponential rate. The race for a faster data rate would continue, necessitating a 10x data rate increase every five years [14]. In the case of 5G, this refers to achieving a peak data rate of at least 1 GBPS when it launched in 2020. Next, it is expected to scale up to 10 GBPS in five years and even 100 GBPS by 2030 [15].

- **Connectivity:** Over the previous few years, millions of sensors have been integrated into homes, cities, industries, and other environments to develop smart life and automated systems. As a result, these services will require a high data throughput as well as reliable connectivity. It is anticipated that the 5G system can support up to one million simultaneous connections per square kilometer (km) [16]. Global mobile traffic volume is predicted to boost 670 times by 2030 compared to 2010 [13]. As compared to 5.32 billion in 2010, the number of mobile subscriptions is anticipated to reach 17.1 billion by 2030 [17].

- **Fairness:** In general, wireless network fairness is achieved by providing adequate Quality of Service (QoS) to all users [18]. Throughout 5G and beyond wireless networks, a large number of devices want an inexpensive QoS at any time, from any location, and regardless of the channel conditions. Thus, it is necessary to take into consideration the issue of fairness for 5G networks.

- **Energy Efficiency:** Due to increased energy consumption and environmental concerns throughout the globe, energy-efficient communications have received a lot of emphasis in academia and industry [19]. By 2020, billions of information and communication technology (ICT) devices have contributed up to 3.5 percent of the world's carbon dioxide (CO2) emissions, and these emissions are expected to be 14 percent by 2040 [20]. In addition, by 2025, it is estimated that the communications sector is expected to account for 20 percent of all global electricity [20]. Furthermore, energy prices are increasing, and worldwide carbon dioxide emissions rise from ICT devices. Thus, the topic of energy-efficient radio management is becoming more engaging.

- **Latency:** Ultra-reliable, low-latency communications have become a critical component of the wireless network. 5G networks are expected to provide low-latency communications by adding features like an end-to-end delay of less than 1 millisecond [15]. According to academic and industry experts, expecting a radio latency value of less than 1 millisecond is one of the significant performance parameters for 5G networks [21].

- **High Coverage:** One of the primary concerns with 5G networks is improving coverage, which affects system performance and end-user experience. Because 5G uses higher frequencies than 4G, it can experience increased attenuation and penetration loss, resulting

in limited coverage. Most of the new 5G spectrum allotments worldwide are time-division duplex (TDD) carriers operating at frequencies of 3.3-3.8 GHz, 28 GHz, or 39 GHz, substantially higher than 4G. This can have an impact on 5G new radio (NR) coverage. [22].

To summarise, Figure 1.2 depicts the key requirements for 5G.

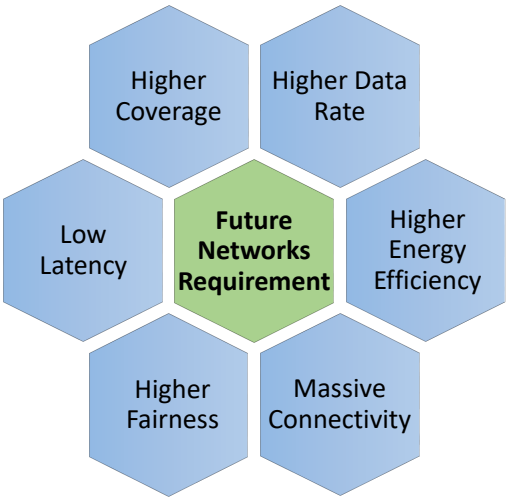

FIGURE 1.2: Key requirements of 5G.

The present wireless communication technologies may not be sufficient to meet the aforementioned critical requirements; therefore, developing of advanced technologies for 5G wireless networks is necessary [23]. Recent years have seen the development of several emerging technologies, including heterogeneous networks (HetNets) [24], millimeter wave (mmWave) [25], non-orthogonal multiple access (NOMA) [26], massive multiple-input multiple-output (MIMO) [27], and device-to-device (D2D) communication [28], among others. This thesis studies NOMA and HetNet, potential multiple access techniques intended to address some of the essential requirements mentioned above the 5G networks [26, 29, 30].

1.3 NOMA

1.3.1 Orthogonal Versus Non-orthogonal Multiple Access Techniques

Multiple access techniques are the key component of the wireless communication system. Multiple access techniques are divided into orthogonal and non-orthogonal categories. In orthogonal multiple access (OMA) techniques, signals transmitted by various users are orthogonal in frequency, time, or code domains to reduce the multiple access interference-effect (see Figure 1.3). Frequency division multiple access (FDMA), time division multiple access (TDMA), code division multiple access (CDMA), and OFDMA are all examples of this principle in use [31]. In contrast to OMA schemes, as shown in Figure 1.3, NOMA works on the principle of users sharing time and frequency resources by separating them into different domains. This separation domain is divided into two regimes: power-based and code-based, resulting in NOMA mechanisms in the power-domain and code-domain, respectively. The focus of this thesis has been on a NOMA scheme operating in the power domain; hereafter, we refer to the power-domain NOMA scheme as NOMA. NOMA serves more than one user at the same time, frequency, and code but at different power levels [32].

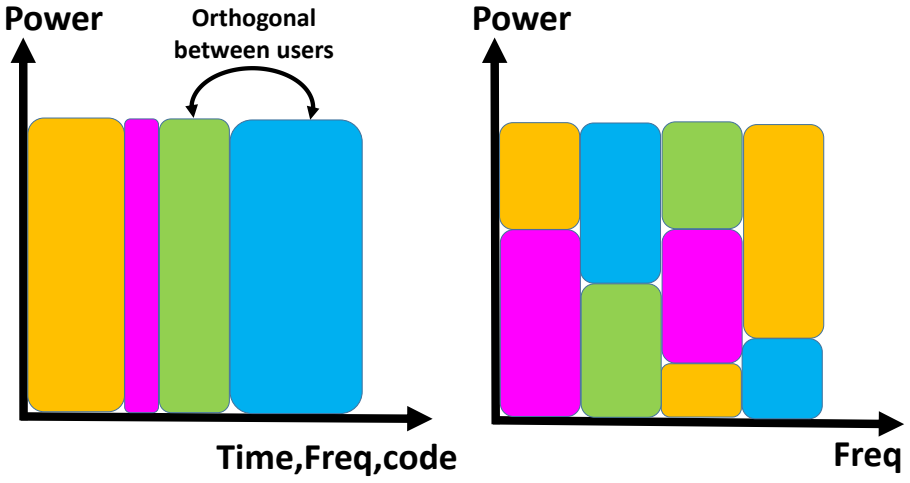

FIGURE 1.3: OMA and NOMA

It may not be possible to meet the above-mentioned key requirements for future communication systems using OFDMA-based OMA alone [33]. All of these requirements are seen as a challenge

in developing new potential communication systems [10]. As a result, NOMA is presented as one of the potential technologies for meeting key requirements of 5G communication systems. NOMA incorporates the concept of superposition coding, which is deployed on the transmitting side, and the principle of successive interference cancellation (SIC), which is implemented on the receiving side [34].

1.3.2 NOMA Fundamentals

NOMA employs two key operations: superposition coding on the transmitter side and SIC on the receiver side.

1.3.2.1 Superposition Coding

The superposition coding for the NOMA network is shown in Figure 1.4. In superposition coding, the modulated signals of several users are superimposed in the power domain. Power domain multiplexing represents the process by which the signals of multiple users are multiplexed via varying power levels depending on the circumstances of their respective channels while maintaining the same time, frequency, and coding resources for all users, as shown in Figure 1.4. Power allocation (PA) coefficient (α) can be used to provide different levels of power to

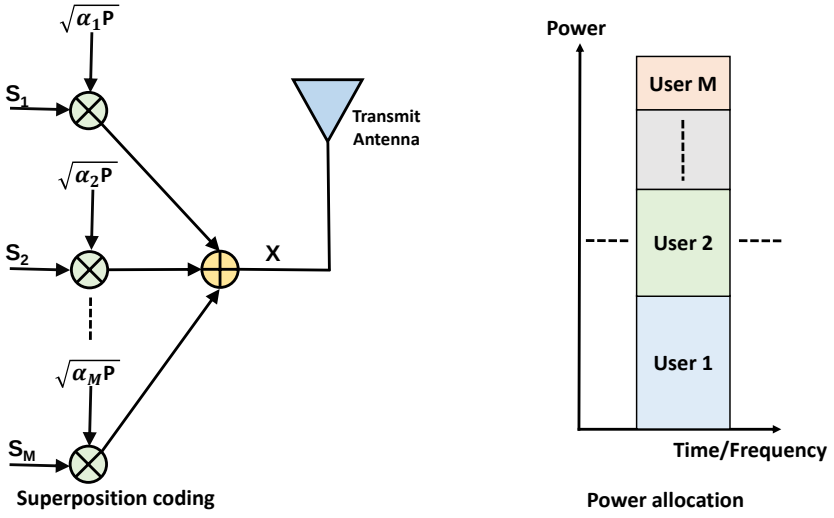

FIGURE 1.4: Superposition coding and power allocation

different users. Thus, in superposition coding, all user signals are multiplied with separate PA

coefficients α, and combined at the base station (BS). As a result, the transmitted signal at BS that uses superposition coding can be expressed as,

$$X = \sum_{m=1}^{M} \sqrt{\alpha_m P}\, S_m, \tag{1.1}$$

where S_m is the symbol of user m, α_m is PA coefficient for user m, and P is total transmit power of BS.

1.3.2.2 Successive Interference Cancellation

The SIC process is performed on the receiver side, as shown in Figure 1.5. In the SIC process,

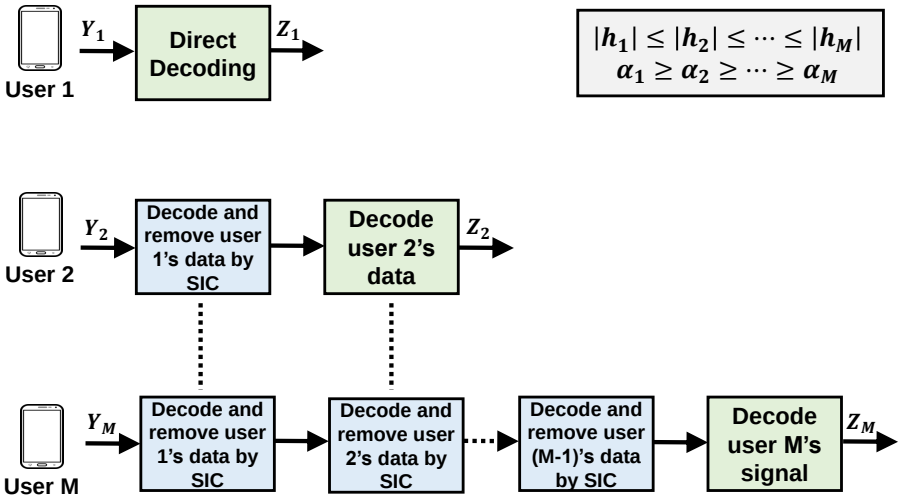

FIGURE 1.5: Successive interference cancellation

data is decoded in the order of diminishing power levels. In each user at the receiver, first, the data corresponding to the user who is provided the highest power in the superposition coding at the BS is decoded directly. Then, the user who is provided the next highest power is decoded by eliminating interference from the preceding decoded user. This process happens till all the user's data is decoded at the receiver [35, 36]. Let the received signal at user m is given by,

$$r_m = h_m X + \eta_m, \tag{1.2}$$

where h_m is the complex channel gain from BS to user m, $\eta_m \sim \mathscr{CN}(\mu, \sigma^2)$ is complex additive white Gaussian noise (AWGN) with zero mean ($\mu = 0$) and variance σ^2 [37, 38]. Without loss

of generality, the channel gains are sorted between the BS and all users in ascending order as $|h_1| \leq |h_2| \leq \cdots \leq |h_M|$. After the SIC process as described above, the decoded signal at the receiver is given by,

$$y_m = h_m \sqrt{\alpha_m P}\, S_m + h_m \sum_{n=m+1}^{M} \sqrt{\alpha_n P}\, S_n + \eta_m, \tag{1.3}$$

1.3.2.3 NOMA in Downlink Transmission

To discuss the downlink transmission of the NOMA network, consider a BS that communicates with M users, as shown in Figure 1.6. We assume a single input and single output (SISO) system

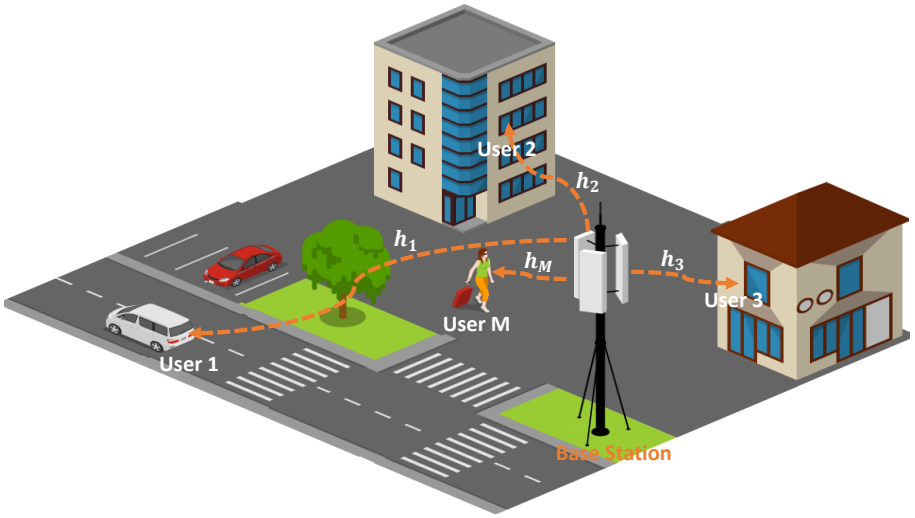

FIGURE 1.6: The downlink transmission of the NOMA network

where the BS uses a single antenna to transmit and the users use a single antenna to receive. Without loss of generality, it is assumed that user 1 is the weakest user in the network and user M is the strongest user. By applying superposition coding at the BS and the SIC process at each user, the signal-to-interference and noise ratio (SINR) as seen by user m can be written as, [36, 37],

$$SINR_m = \frac{\alpha_m P |h_m|^2}{\sum_{n=m+1}^{M} \alpha_n P |h_m|^2 + \sigma^2}, \tag{1.4}$$

Hence, the achievable rate for user m is given by [36, 37],

$$R_m = \log_2(1 + SINR_m) \quad \text{bps/Hz}. \tag{1.5}$$

1.4 Heterogeneous Networks

One of the leading emerging technologies for 5G networks is the deployment of small cells in the cellular network, called a HetNet [39]. In HetNet, low-power small cells (Microcell, Picocell, and Femtocell) are overlaid with a large-power macrocell. The HetNets architecture is anticipated to be crucial to the development of 5G network requirements. Because of network densification, 5G networks will be more diversified and more densely deployed than today's networks. The objective of deploying such small cells is to improve essential features like indoor coverage, user performance at cell-edge, spectrum efficiency using spatial reuse, energy consumption, and capacity. However, due to network densification, intense proliferation, and the same frequency used in all cells, interference in the HetNet can increase [40, 41].

Among each tier of BS, there are differences in the transmit power, target SINR, and BS density in the HetNets [42]. Each cell's transmit power is based on its coverage area. Microcell coverage regions are the greatest, femtocell coverage areas are the smallest, and picocell coverage areas are in the midst [43]. Macro BSs, typically deployed by the operator in a planned layout, provide umbrella coverage. They transmit power typically between 40 W to 100 W. Small cells are deployed on coverage holes or capacity-demanding hotspots, thus following a relatively random placement. Low-power femtocell BS provides a smaller coverage area (less than 100 m), requiring low transmit power (less than 200 mW). Picocell BS provides a 100 m to 200 m coverage area, hence requiring 250 mW to 1 W transmit power [44, 45]. The types of small cells and the design that can support are listed in Table 1.1.

TABLE 1.1: Base station types.

Base station type	**Number of users**	**Coverage (meter)**	**Location**
Femtocell	1 to 30	10 to 100	Indoor
Picocell	30 to 100	100 to 200	Indoor/Outdoor
Microcell	1000 to 2000	100 to 2000	Indoor/Outdoor
Macrocell	$>$ 2000	5000 to 32000	Outdoor

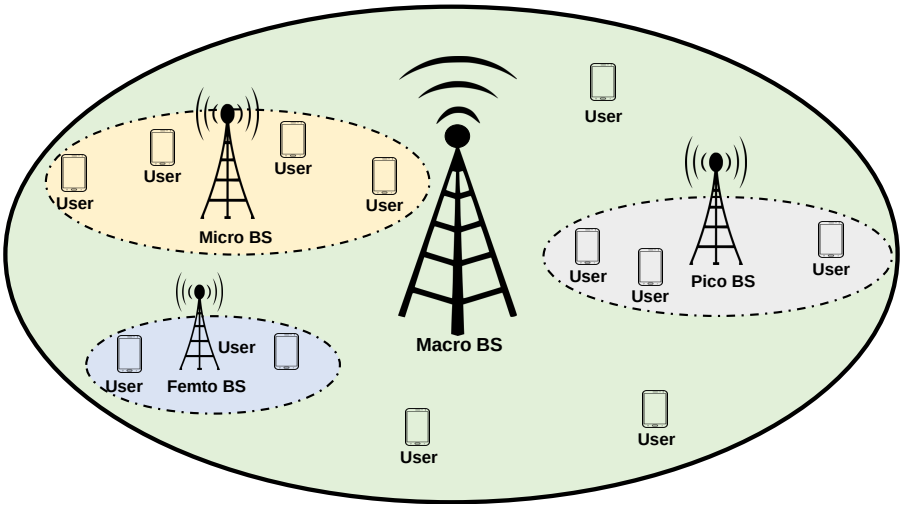

FIGURE 1.7: Representation of 3-tier HetNet, composed of macro, pico, and femto Base Stations.

1.4.1 HetNet in Downlink Transmission

A typical HetNet is shown in Figure 1.7. The Poisson point process (PPP) is used to model BS distribution, and Voronoi tessellation is used to provide network coverage areas for the HetNet. Hence, BSs in the i^{th} tier are spatial distributed in $\mathbb{R}^2$ as a PPP Φ_i of density λ_i, transmit power P_i, and target SINR T_i [42]. Hence, each tier can be distinguished from the others by the tuple $\{P_i, T_i, \lambda_i\}$. Let us place a typical mobile user at the origin. h_i stands for the fading coefficient between the user i and BS. The power received by a user at the origin from the BS at location $x_i \in \Phi_i$ in the i^{th} tier is represented by [42],

$$P_r = P_i h_i \|x_i\|^{-\alpha} \tag{1.6}$$

Where α stands for the path loss exponent. Given that the user is connected to a BS at location x_i, the received SINR can be expressed as [42]:

$$\text{SINR}(x_i) = \frac{P_i h_i \|x_i\|^{-\alpha}}{\sum_{j=1}^{K} \sum_{x \in \Phi_j \setminus x_i} P_j h_j \left\|x_j\right\|^{-\alpha} + \sigma^2} \tag{1.7}$$

Where σ^2 represents the noise power. Now, in a K-tier HetNet, the coverage probability can be modeled as follows [42],

$$P_c(\{P_i\},\{T_i\},\{\lambda_i\}) = \mathbb{P}\left(\bigcup_{i\in\kappa, x_i\in\Phi_i} \text{SINR}(x_i) > T_i\right) \tag{1.8}$$

1.5 Objectives of the Thesis

Wireless communications are now one of the major developments in the industry, public, and government sectors. Hence, the need for wireless communication has increased massively. In order to satisfy the growing need for 5G wireless communication, it is necessary to improve key requirements such as sum rate, fairness, outage probability, and coverage. Among other technologies of 5G, HetNets and NOMA are emerging technologies that enhance the crucial requirements for 5G networks. Hence, this thesis mainly focuses on improving key requirements of HetNets-based and NOMA-based 5G networks. Taking into account the concerns mentioned above, we formulate the following objectives to enhance key requirements of HetNets-based and NOMA-based 5G networks:

1. Joint Sum Rate and User Fairness Maximization for Downlink NOMA Networks.
2. Joint Sum Rate and User Fairness Maximization adhering to the minimum power gap constraint for Downlink NOMA Networks.
3. Sum Rate Maximization for Downlink Multicarrier NOMA Networks.
4. Improve Coverage Probability for Heterogeneous Networks.
5. Improve Sum Rate and Outage Probability for Downlink NOMA Heterogeneous Networks.

1.6 Thesis Outline

The rest of the thesis is organized as follows:

Most NOMA research has focused on single-objective optimization, either of the sum rate or user fairness. However, in many situations, it is essential to consider a multi-objective optimization (MOO) problem to jointly maximize both the sum rate and user fairness to make effective decisions in the face of trade-offs between these two equally important but conflicting objectives. Chapter 2 formulates and investigates the MOO problem in downlink NOMA networks to achieve optimal PA for joint optimization of sum rate and user fairness while maintaining the transmit power budget and QoS constraints.

SIC is an essential constraint in order to prevent co-channel interference at the receiver, which is caused by multiplexing users on the same resource block in NOMA. However, to successfully execute SIC, the NOMA transmitter must maintain a suitable gap between the user's transmit power. Thus, in addition to the user's QoS and transmitter power budget constraints addressed in Chapter 2, we address the minimal transmit power gap constraint in Chapter 3. In this regard, the Chapter 3 research aims to find the optimal PA for downlink NOMA networks in order to maximize the sum rate and user fairness while meeting the minimal transmit power gap, QoS, and transmit power budget constraints.

Multiple access techniques are gaining popularity as the need for high data rates in 5G networks increases. Moreover, multiple access techniques are required to meet the ever-increasing bandwidth requirements. As a result, in addition to PA in the Chapters 2, and 3 optimization problem, we decided to look at the problem of optimal subchannel allocation (SA) in Chapter 4 for NOMA-based 5G network. In Chapter 4, we formulate and investigate the problem of determining optimal SA and PA for maximizing the sum rate while fulfilling the transmit power budget, minimum rate requirement, subchannel user's limit, and minimum power gap constraints in the downlink multicarrier NOMA network. To achieve SA, we investigate the algorithms for SA that are described in papers [46–48] and associate them with our optimization problem.

Current wireless communication technology may not be sufficient to meet the crucial requirements of a 5G network. In recent years, HetNet technology has emerged to fulfill the essential 5G network requirements. Having studied the NOMA technology to improve key parameters of the 5G network in Chapters 2, 3, and 4, in Chapter 5, we investigate improving the coverage probability parameter of the 5G network using HetNet technology. We propose an efficient and faster power control algorithm in the downlink HetNet to enhance the coverage probability.

It is obvious that hybrid systems, particularly those that combine NOMA with other technologies, can further improve system parameters [49]. This motivates us to use NOMA-based HetNets. In Chapters 2, 3, and 4, we investigate improving the performance parameters of the 5G network employing NOMA technology. In Chapter 5, we examine improving the performance parameters for the 5G network using HetNet technology. However, Chapter 6 studies NOMA-based HetNets to improve 5G network performance parameters. Thus, Chapter 6 presents an optimal PA for downlink transmission of NOMA-based HetNets in order to maximize the 5G network's sum rate and outage probability while sticking to the minimal user rate constraint. We derive a generalized equation of the optimal PA for small cell users in NOMA-based HetNets.
Chapter 7 says the conclusions.

Chapter 2

Power Allocation Scheme for Sum Rate and Fairness Trade-off in Downlink NOMA Networks

NOMA is one of the fundamental principles for the 5G wireless network [50]. NOMA is based on the idea that users can share time-frequency resources by splitting them in power-domain and code-domain [51, 52]. This results in power-domain NOMA and code-domain NOMA mechanisms. Our work uses power-domain NOMA. In power-domain NOMA, multiple users are superimposed in the power domain at the transmitter, and at the receiver, users are decoded based on SIC. Hence, the NOMA technique's key idea is that multiple users are served in a single time-frequency block [53]. This is unlike OMA techniques like TDMA and OFDMA that serve a single user in each resource block [53]. Thus, NOMA can achieve a high sum rate (or spectral efficiency) in comparison to OMA techniques, thereby potentially increasing the overall throughput of the system [54, 55]. This has motivated many researchers in the recent past to target the maximization of the sum rate of systems that employ NOMA as a multiple access scheme [36, 51, 56–66]. However, despite an increased throughput, since NOMA is based on the SIC order, the served users might receive unequal achievable rates, which may be troubling in a scenario requiring user fairness [67]. To address this challenge, many authors have considered maximizing the sum rate under user fairness as one of the constraints [68–70], or maximizing the user fairness under the constraint of minimum rate for users and other system imposed

restrictions [71], [72]. Targeting to maximize the sum rate or user fairness as a single objective optimization problem is an important and challenging issue that has been well addressed. Quite often, an optimal PA to jointly maximize both the sum rate and the user fairness is of paramount importance to make efficient decisions in the face of trade-offs between these two equally important but conflicting objectives. Therefore, NOMA needs to be enabled to balance the trade-off between achievable rates and user fairness through optimal PA. However, to the best of our knowledge, such an attempt is missing in the literature. In this regard, this work aims to obtain optimal PA to jointly maximize the sum rate and user fairness under system-imposed constraints. We formulate and solve this as an MOO problem to obtain optimal PA that maximizes the sum rate and user fairness for a NOMA-based system.

The rest of the Chapter is organized as follows. In Section 2.1, we conduct a literature survey of the related works and then motivate and summarize our contributions. We present the system model and problem formulation in Section 2.2. In Section 2.3, we derive the optimal PA solution for the joint sum rate and user fairness optimization problem. Section 2.4 presents simulation results and related discussions for the proposed scheme. Finally, Section 2.5 provides concluding remarks.

2.1 Related Work

In the context of sum rate, the authors in [51] obtain the optimal sum rate of downlink two-user NOMA network for admitting imperfect SIC and minimum QoS requirement constraint. A sub-optimal improper Gaussian signaling circularity coefficient is calculated iteratively to maximize the sum rate. In [56], the authors maximize the sum rate of multiple downlink users for NOMA networks through optimal PA strategy subject to minimum user rate requirements. In [57], the authors investigate optimal PA to maximize the sub-carrier-based NOMA network's sum rate under a minimum rate and a total power constraint. To reduce complexity, two closed-form sub-optimal solutions are also proposed for a two-user situation. Authors in [58] maximize the sum rate using the optimal PA of a MIMO NOMA network with layered transmissions. The authors propose an alternating maximization (AM) algorithm to maximize the sum rate at the BS for known instantaneous channel state information (CSI) and statistical CSI. In [59], the

authors examine the subcarrier and PA for the downlink of a single-cell multicarrier downlink NOMA network. For maximizing the sum rate for the NOMA network, a three-step algorithm named Double Iterative Waterfilling Algorithm is proposed. A secure transmission system for the NOMA network with imperfect CSI for both the eavesdropper's channel and the main channel is studied in paper [60]. An effective algorithm is offered to maximize the reliable secrecy sum rate under transmit power limitations, outage probability, and QoS requirements. The optimization problem of sum rate maximization is formulated for a linearly precoded multiple-input single-output (MISO) downlink transmission NOMA network in manuscript [61]. To solve the optimization problem of sum rate maximization and provide complex precoding vectors, the authors design an iterative algorithm employing the minorization-maximization approach. In [62], the authors study the sum-rate performance of two users and multiple users in the MIMO NOMA network. MIMO-NOMA outperforms MIMO-OMA in both sum and ergodic sum rates in both situations, namely, two users and multiple users. In [36], the proposed MOO methodology efficiently allocates resources in the many-user downlink transmission NOMA network that improves the sum rate while minimizing transmit power subject to the user's QoS requirements, SIC, and transmit power budget. Authors in [63] study the optimization problem to achieve optimal value for both PA and frequency to maximize the sum rate while considering each user's minimum rate requirement constraint in a multiuser NOMA downlink network. The work [64] provides an optimal PA for downlink transmission NOMA-based HetNets to maximize sum rate and outage probability adhering to QoS constraint. The paper [65] looks into PA for maximizing the weighted sum rate in the downlink multiple carriers NOMA systems with imperfect SIC. The paper [66] optimizes subchannel and power to maximize the sum rate while meeting a minimal power gap, minimum user rate, the maximum number of users in a subchannel, and power budget constraints for downlink multicarrier NOMA networks.

Besides the sum rate, user fairness has also gained significant attention in NOMA networks. In this regard, in [67], the maximization of fairness among users with optimal PA is studied by authors for a downlink transmission NOMA network under instantaneous CSI and average CSI knowledge at the transmitter. In [68], authors study optimal PA for energy efficiency maximization and guaranteed user fairness for minimum data rate requirements and maximum transmission power constraints for the MIMO NOMA network. In [72], authors offer a joint NOMA and TDMA scheme in the Industrial Internet of Things, which enables various sensors to

communicate in the same time-frequency resource block by applying the NOMA scheme. Time slot allocation, power control, and user scheduling are simultaneously optimized to maximize the system α - fair utility involving minimum rate constraint and transmit power constraint. In [37], optimization problems are formulated by the authors for the downlink multicarrier NOMA network to optimize fairness and energy efficiency between users concerning the PA and subcarriers. A novel greedy subcarrier assignment method is proposed, which is based on the worst-user first principle. The work in [73] discusses multi-user multi-cluster MIMO systems with downlink NOMA networks. Authors derive closed-form expressions for ergodic rates and outage probability. Multi-user PA coefficients within each sub-group are optimized to maximize fairness for imperfect SIC. The authors introduce an iterative algorithm to present fairness amongst various sub-groups. In the paper [74], the authors investigate the PA and user set selection problem to provide proportional fairness in multi-user downlink NOMA networks. A user-set selection system based on tree searching implements a carefully planned pruning mechanism to eliminate unnecessary user sets in the NOMA network. In [75], the fairness performance is increased for a NOMA-based scheduling scheme for a wireless-powered communication network by irregular user deployment by providing NOMA transmissions for wireless information transfer and wireless energy transfer.

Furthermore, a limited number of works [52, 69–71, 76, 77] address the optimal relationship of user's fairness and sum rate for the NOMA network. The paper [52] gives the joint fairness and sum-rate optimization problem for uplink transmission NOMA network. The authors propose an algorithm for optimal PA, subband assignment, and user grouping for concurrently optimizing fairness and sum rate. The authors present two algorithms; the first algorithm can prevent weak users from starvation and improve fairness, and the second algorithm is applied to obtain PA. The authors in [69] introduce water-filling-based joint PA and a proportional fairness scheduling method to maximize the achievable rate by a quasi-optimal re-partition of the transmission power amongst sub-bands while ensuring a large level of fairness towards resource allocation. The proposed method improves system throughput and user fairness related to either orthogonal signaling or static PA NOMA network. In the paper [70], the average sum rate is maximized considering fading channels, including peak and average power constraints, as well as fairness constraints for a two-user downlink transmission NOMA network. Sum rate maximization is obtained for full and partial CSI, and fairness is taken care of by including a

minimum achievable ergodic rate condition. In the manuscript [71], the optimal PA optimization problem is designed to maximize the instantaneous sum rate with α-fairness for the downlink NOMA network. The user rates are updated based on the instantaneous CSI. The α-fairness is used to measure the qualitative fairness of the instantaneous rate. In the manuscript [76], the author studied proportional fairness scheduling with two users' downlink NOMA networks. The author considered different criteria and achieved optimal PA. The author has shown that the proportional fairness scheduling method maximizes the sum rate and maximizes the least normalized rate which gives proportional fairness and a slight variation of communication rates. The paper [77] addresses work to enable a balanced trade-off between two objectives sum rate and users fairness by employing the MOO problem for designing beamforming in a MISO NOMA system. In this work, a beamforming vector is designed such that the BS can properly allocate the weights of every objective corresponding to the channel conditions and network circumstances. A sequential convex approximations technique is used to determine the weighting coefficients iteratively.

2.1.1 Motivation and Contributions

As stated in [78], the NOMA network's achievable rate is more widespread than that of the OMA network under asymmetric channel conditions. For illustration, in Figure 2(b) in [78], the achievable rate of strong user in NOMA is almost double that of OMA. It is because of superposition coding and SIC used in the NOMA network. In consideration of power-sharing with weak users, the weak user allows a strong user to use the entire bandwidth while allocating a smaller transmission power. As a consequence, a stronger user introduces a small amount of interference to a weaker user. On the other hand, in an OMA network, a significant portion of bandwidth is allocated to a weak user to increase the rate, resulting in a significant reduction in the strong user's achievable rate whose rate is bandwidth restricted. As a result, in a downlink communication network with asymmetric channel conditions between multiple users, NOMA has a more significant opportunity than OMA of improving the trade-off between system sum rate and user fairness [1].

[1]NOMA with appropriate power-sharing and successful SIC achieves a higher rate for the worst user, improving user fairness between near and far users while providing a higher sum rate compared to OMA regardless of channel circumstances.

In some circumstances, multiple objectives of the system need to be optimized simultaneously, which encourages the MOO problem. In particular, many research areas, including engineering, have used MOO to make optimal decisions in the face of trade-offs between two or more objectives that may have a contradiction [79], [80]. Most current NOMA studies focus on a single-objective optimization problem to optimize individual objectives like sum rate, EE, SE, fairness, etc. Therefore, to the best of our knowledge, there is no widely accepted MOO problem for joint configuration of users fairness and sum rate to adequately achieve a trade-off between them with optimal PA under QoS and power budget constraints for the downlink NOMA network, the reason behind this research.

Additionally, the BS should intelligently assess whether it is essential to maximize the sum rate or user's fairness or find a reliable balance between them. Hence, to our understanding, the recent studies [36, 37, 51, 52, 56–76] lack consideration of MOO problems for maximization of sum rate and users fairness in the downlink transmission NOMA networks. Several works [37, 52, 67–76] have studied maximizing sum rate while supporting user fairness for downlink NOMA networks. Despite this, achieving optimal PA for accomplishing a balanced trade-off and concurrently maximizing sum rate and user fairness for maintaining QoS and power budget constraint is missing for downlink NOMA networks. Therefore, we study in-depth interpretation and maximization of sum rate and user fairness for optimal PA in the NOMA downlink network under QoS and power budget limitation. In the paper [77], the authors designed an optimal beamforming vector to maximize the sum rate and user fairness in a MOO problem for the downlink NOMA network. However, the constraints considered in our work are more realistic than the paper [77], which excludes the QoS constraint. Additionally, compared to the paper [77], we also derive a closed-form expression for optimal PA that enables easy and quick changes to the power coefficients as the users channel conditions change. Hence, this Chapter's essential contribution is to get the optimal value of PA for maximization of sum rate and user fairness with QoS condition and power budget restriction in the MOO problem for downlink transmission NOMA network.

The main aspects of the Chapter are summarized as follows:

- We express and study the MOO problem to achieve optimal PA for joint optimization of

sum rate and user fairness in downlink NOMA networks. The objective is to simultaneously enhance the sum rate and user fairness while satisfying the transmit power budget and QoS requirement constraints with optimal PA.

- In our work, we exploit the weighted-sum method where the multi-objectives of maximum sum rate and user fairness can be linearly combined as a single-objective optimization problem by employing a weighting coefficient. Here, the weighting coefficient indicates a trade-off between two objective functions [80], [81].

- The optimization problem of interest is challenging to solve directly due to the complex formulation of a Lagrangian function. We apply a new assistance variable and reformulate the initial problem to a solvable one.

- We use a Lagrange dual decomposition method and Karush–Kuhn–Tucker (KKT) conditions to determine the optimal solution for our MOO problem. Lagrange multipliers can be obtained and updated iteratively by applying the sub-gradient method [82].

- We carry out simulations to validate our analytical expressions and the proposed iterative algorithm. Our results show that the proposed algorithm requires very few iterations for converging to the optimal PA. We also compare the performance of the proposed method with the benchmark methods.

2.2 System Model and Problem Formulation

In this section, we introduce the system model, followed by a discussion of the problem formulation. Let us consider a downlink NOMA-based wireless network, as shown in Figure 2.1, with a BS that communicates with M users. We consider a SISO system in which the BS transmits using a single antenna, and the users receive using a single antenna. Since NOMA uses the power domain for user multiplexing, all users are served at the same time over the same frequency band. Complete knowledge of CSI of all users is assumed at the BS [36]. $\eta_m \sim \mathscr{CN}(\mu, \sigma^2)$ is complex AWGN with zero mean ($\mu = 0$) and variance σ^2. Additionally, we consider channels between BS and all served users to be independently distributed rayleigh fading. The complex channel coefficient between BS and user i is denoted by $h_i \sim \mathscr{CN}(0, d_i^{-pl})$

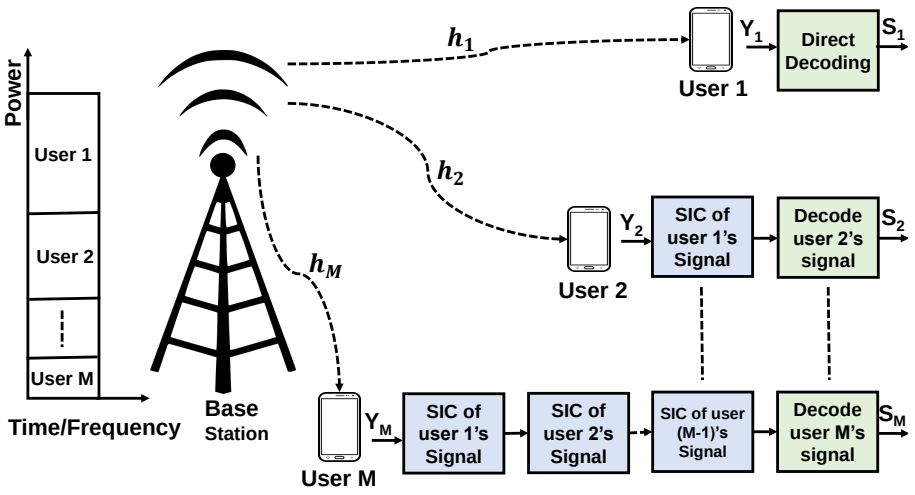

FIGURE 2.1: The system model illustrating the SIC process of downlink transmission NOMA network.

where $i \in (1,2,\cdots,M)$, d_i is the distance between BS and user i, and pl is the path loss exponent [83]. Without loss of generality, we order the channel gains between the BS and all users such that $|h_1| \leq |h_2| \leq \cdots \leq |h_M|$. NOMA performs two fundamental operations, superposition coding, which needs to be done at the transmitter side, and SIC, which is executed at the receiver side. In superposition coding, all user signals are multiplied with separate PA then added together. On the receiver side, SIC is performed where data is decoded in the order of diminishing power levels. First, data corresponding to the user who has been allocated the highest power is decoded directly. Then, the user who has the next highest power is decoded by eliminating interference from the preceding decoded user. This process happens to continue till the intended user's data is decoded. Figure 2.1 depicts the SIC process of downlink transmission of the NOMA network. The BS transmits a multiplexed signal given by,

$$X = \sum_{m=1}^{M} \sqrt{P_m}\, S_m, \tag{2.1}$$

where S_m is the symbol of user m, and P_m is PA for user m. The received signal at user m is given by,

$$r_m = h_m X + \eta_m, \tag{2.2}$$

where h_m is the channel gain from BS to user m, $\eta_m \sim \mathscr{CN}(\mu, \sigma^2)$ is AWGN with zero mean ($\mu = 0$) and variance σ^2. User m performs SIC as described above to obtain the signal y_m given

by,

$$y_m = h_m \sqrt{P_m}\, S_m + h_m \sum_{n=m+1}^{M} \sqrt{P_n}\, S_n + \eta_m, \tag{2.3}$$

The SINR as seen by user m is then given by [36],

$$SINR_m = \frac{P_m |h_m|^2}{\sum_{n=m+1}^{M} P_n |h_m|^2 + \sigma^2}, \tag{2.4}$$

The achievable rate for user m is given by [36],

$$R_m = \log_2(1 + SINR_m) \quad \text{bits/sec/Hz.} \tag{2.5}$$

2.2.1 NOMA Under Imperfect SIC

The NOMA transmitter should ensure a minimal power gap between the user transmit powers for SIC to be successfully executed at the user's end [36]. Each user's SIC is dependent on previous decodings, and errors can propagate and affect the performance of the NOMA network if the minimum power gap is not maintained at the transmitter. Therefore, SIC residual error propagation parameters can be considered in the NOMA systems if the SIC is not executed perfectly. Hence, the SINR for imperfect SIC can be defined as [51, 65, 73, 84],

$$SINR_m^{imper} = \frac{P_m |h_m|^2}{\varepsilon \sum_{n=1}^{m-1} P_n |h_m|^2 + \sum_{n=m+1}^{M} P_n |h_m|^2 + \sigma^2}. \tag{2.6}$$

The factor ε lies between 0, and 1 quantifies the residual interference component produced by this imperfection, where $\varepsilon = 0$ refers to perfect SIC, and $\varepsilon = 1$ refers to entirely imperfect SIC.

We show the achievable rate region for 2 users of a NOMA system as shown in Figure 2.2. The feasible operating region has been obtained for a Signal-to-Noise Ratio (SNR) of 4 for user 1 and SNR of 25 for user 2. As can be seen from Figure 2.2, for different PAs to the two users, different achievable rate combinations can be obtained. For example, point A indicates the case when all the power is allocated to user 1, and point B when all the power is allocated to user 2. Clearly, if the goal is to maximize the sum rate of the system, then we should operate at point B, which corresponds to allocating all the power to user 2. However, this PA results in unfairness to user 1, who is going to get a rate of zero. Also, operating at point A is both unfair to user 2 and

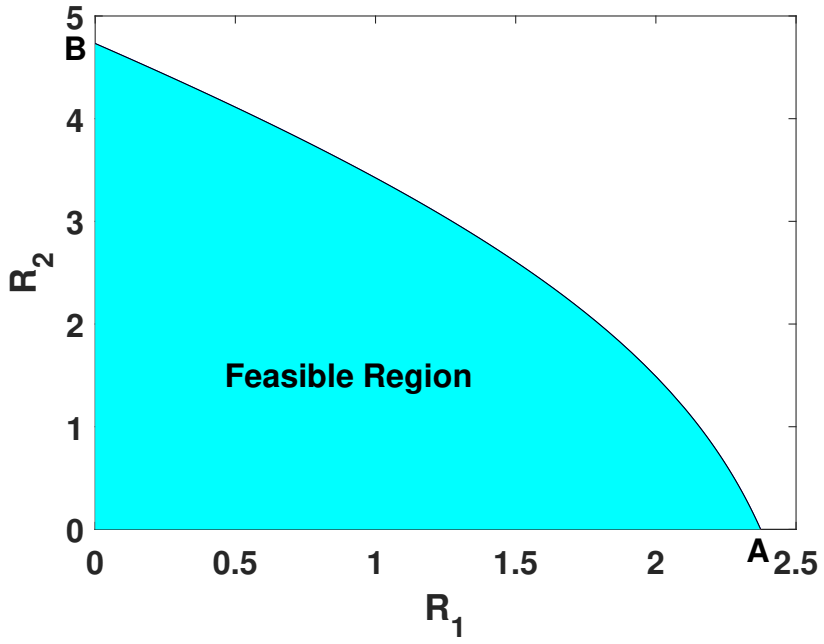

FIGURE 2.2: Capacity Region of a 2-User Downlink NOMA System.

fails to maximize the sum rate as well. Hence, the goal of this Chapter is to find the operating point that jointly maximizes the sum rate and fairness simultaneously. However, to do this, we first need to choose an appropriate measure for user fairness.

Fairness measures are tools to measure fairness levels. They can be classified as quantitative or qualitative. Jain's Index and Entropy measures are quantitative measures, and max-min and proportional fairness are qualitative measures [85]. Jain's index and Entropy measures do not help to identify the unfairly treated individual resources. Jain's index and Entropy measures require complete information of the resource allocation to calculate fairness. max-min fairness can not measure individual fairness and can not measure the level of fairness. However, the α - fair utility function is a generalized form of fairness function. Compared to the fairness mentioned above, α - fairness only uses a single scalar that utilizes different user fairness levels [86]. Hence, in this Chapter, we choose to work with α - fair utility function, which can be expressed as:

$$U(R_m) = \begin{cases} \dfrac{R_m^{1-l}}{1-l}, & l \geq 0,\ l \neq 1, \\ \ln(R_m), & l = 1 \end{cases} \tag{2.7}$$

where l is non-negative and represents different rate fairness levels. In general, an increase in the value of l results in increased fairness among users. For instance, setting $l = 0$ gives

the maximum sum rate, setting $l = 1$ provides proportional fairness, and setting $l \to \infty$ gives max-min fairness [86]. Therefore, in order to achieve the goal of finding the operating point that jointly maximizes the sum rate and user fairness simultaneously using optimal PA for downlink transmission NOMA system, we formulate the following MOO problem:

$$(P1): \max_{P_m} \left(\sum_{m=1}^{M} R_m, \sum_{m=1}^{M} U(R_m) \right), \tag{2.8a}$$

$$\text{s.t.} \sum_{m=1}^{M} P_m \leq P_{BS}, \tag{2.8b}$$

$$R_m \geq R_{min}, \forall m, \tag{2.8c}$$

$$P_m \geq 0, \forall m. \tag{2.8d}$$

where (2.8a) is the vector of objective functions to be jointly maximized. The first function in the vector is the sum rate, and the second function is the sum utility. The constraint in (2.8b) assures BS's combined transmit power to all users is not above the total power budget of BS. The constraint in (2.8c) ensures the minimum rate requirement of each user. The minimum rate requirement constraint is often employed to ensure rate fairness and the QoS of the network. Finally, the constraint in (2.8d) ensures the non-negative transmit power for each user.

2.3 Solution of Multi-objective Optimization Problem

The most extensively used classical methods for solving MOO problems are the weighted sum method and the ε - constraint method [87]. The weighting coefficient is used in the weighted sum method for linearly combining the MOO problem as a single-objective optimization problem. The ε - constraint method optimizes one objective function while constraining the other objective functions to be less than or equal to the specified numerical value [87]. Here, the ε vector must be carefully selected to fall within the particular objective function's minimum and maximum values, which could render this method difficult. In addition, as compared to the ε - constraint approach, the weighted sum approach is easier to implement. Moreover, this weighting coefficient method allows us to have a trade-off between multiple objectives [80], [81]. This is also in line with our motivation to achieve optimal PA for accomplishing a balanced trade-off and concurrently maximizing sum rate and user fairness for maintaining QoS and power budget constraints.

Therefore, we use the weighted sum method in our Chapter to solve the optimization problem $(P1)$. Hence, the MOO problem $(P1)$ is converted to a single objective optimization problem as:

$$\begin{aligned}(P2): \max_{P_m} \ & \omega \sum_{m=1}^{M} R_m + (1-\omega) \sum_{m=1}^{M} U(R_m), \\ & \text{s.t. } (2.8b),\ (2.8c),\ (2.8d).\end{aligned} \tag{2.9}$$

Where ω is the weighting coefficient for objective 1 and $(1-\omega)$ is the weighting coefficient for objective 2, such that $0 \leq \omega \leq 1$ [88]. Higher values of ω favor maximizing the system sum rate, whereas lower values of ω favor user fairness. Therefore, for a given l, the trade-off between sum rate and fairness can be achieved by adjusting ω. Note that $(P2)$ in its current form is tough to solve using the Lagrange dual decomposition method and KKT conditions since the fairness objective function is dependent on the achievable rates, which have a non-linear form. Thus, the optimization problem $(P1)$ is first formulated and then converted to a convex optimization problem, for which the solution obtained is always the optimal one [82]. In order to overcome this non-linear problem, we judiciously identify that we can reduce the difficulty in solving this problem if we define a new assistant variable t_m for user m, and rewrite $(P2)$ as [89]:

$$(P3): \max_{P_m} \ \omega \sum_{m=1}^{M} R_m + (1-\omega) \sum_{m=1}^{M} U(t_m), \tag{2.10a}$$

$$\text{s.t. } (2.8b),\ (2.8c),\ (2.8d),$$

$$t_m \leq R_m, \forall m. \tag{2.10b}$$

Observe that when the weighted objective function in $(P3)$ is maximized, $U(\cdot)$ is an increasing function, and t_m must be equal to R_m [89]. Hence, $(P2)$ and $(P3)$ would, therefore, have the same solution. Therefore, we can solve $(P3)$ instead of $(P2)$. This motivates us to now apply the Lagrange dual decomposition method [82] to $(P3)$. Doing so gives the following Lagrangian function:

$$\begin{aligned}\mathscr{L}(P_m, \chi_m, \beta_m, \mu_m) = & \omega \sum_{m=1}^{M} R_m + (1-\omega) \sum_{m=1}^{M} U(t_m) + \sum_{m=1}^{M} \chi_m (R_m - R_{min}) + \beta_m (P_{BS} - \sum_{m=1}^{M} P_m) \\ & + \sum_{m=1}^{M} \mu_m (R_m - t_m),\end{aligned} \tag{2.11}$$

Solving the above Lagrangian function consists of two sub-problems. The first one is the Application layer optimization problem with variable t, and the second one is the Physical layer optimization problem with variable P. Hence, the Application layer optimization problem can be written as follows:

$$h_1 = \max_{t} g_1(t_m), \tag{2.12}$$

where,

$$g_1(t_m) = (1-\omega)\sum_{m=1}^{M} U(t_m) - \sum_{m=1}^{M} \mu_m t_m. \tag{2.13}$$

and the physical layer optimization problem can be written as:

$$h_2 = \max_{P_m} g_2(P_m), \tag{2.14}$$

where,

$$g_2(P_m) = \omega \sum_{m=1}^{M} R_m + \sum_{m=1}^{M} \chi_m(R_m - R_{min}) + \beta_m(P_{BS} - \sum_{m=1}^{M} P_m) + \sum_{m=1}^{M} \mu_m R_m. \tag{2.15}$$

The α-fair utility function in Eqn. (2.7) consists of two cases: $l = 1$ and $l \geq 0$. Therefore, we will discuss the optimal solution of $g_1(t_m)$ of Eqn. (2.12) separately for $l = 1$ and $l \geq 0$ as follows:

Case I ($l = 1$): In this case, the second term $\sum_{m=1}^{M} \mu_m t_m$ in (2.13) is a linear function of t_m, and $U(t_m) = \ln(t_m)$ is a strictly concave function of t_m. Hence, $g_1(t_m)$ is a concave function of t_m. Therefore, by applying the KKT conditions [82], the closed-form expression for t_m in Case I can be obtained by taking the first partial derivative of $g_1(t_m)$ *w.r.t* t_m and equating to zero. Hence,

$$\frac{\partial g_1(t_m)}{\partial t_m} = \frac{(1-\omega)}{t_m} - \mu_m = 0 \implies t_m^* = \frac{(1-\omega)}{\mu_m}. \tag{2.16}$$

Case II ($l \geq 0$): As shown in Appendix A, $g_1(t_m)$ is concave function of t_m. Therefore, by applying the KKT conditions, the closed-form expression for t_m in Case II can be obtained, as shown in Appendix C. Hence,

$$t_m^* = \sqrt[l]{\frac{(1-\omega)}{\mu_m}}. \tag{2.17}$$

To obtain optimal PA ${P_m}^*$, we first show that $g_2(P_m)$ is a concave function of P_m (refer Appendix B). Therefore, the closed-form expression for P_m^* can be derived using the KKT conditions (refer

to Appendix D for the derivation) as shown in the given Eqn. (2.18) with $[P]^+ = \max(0, P)$ and ϕ_m as shown in Eqn. (2.19).

$$P_m^* = \left[\frac{(\omega + \chi_m + \mu_m)\,|h_m|^2 - \phi_m \left(\sum_{n=m+1}^{M} P_n\,|h_m|^2 + \sigma^2 \right)}{\phi_m\,|h_m|^2} \right]^+, \tag{2.18}$$

$$\phi_m = \beta_m\, log(2) + \sum_{i=1}^{m-1} \frac{(\omega + \chi_i + \mu_i)\,(P_i{}^2(|h_i|^2)^2)}{\left(\sum_{j=i}^{M} P_j\,|h_i|^2 + \sigma^2 \right) \left(\sum_{k=i+1}^{M} P_k\,|h_i|^2 + \sigma^2 \right)}. \tag{2.19}$$

Now, the Lagrange multipliers can be obtained and updated in an iterative manner using a sub-gradient method [82]:

$$\chi_m(t+1) = [\chi_m(t) + \delta_1(t)(R_{min} - R_m)]^+, \forall m, \tag{2.20}$$

$$\beta_m(t+1) = \left[\beta_m(t) + \delta_2(t) \left(\sum_{m=1}^{M} P_m - P_{BS} \right) \right]^+, \tag{2.21}$$

$$\mu_m(t+1) = [\mu_m(t) + \delta_3(t)(t_m - R_m)]^+. \tag{2.22}$$

where $\delta_1, \delta_2,$ and δ_3 are step sizes for Eqn. (2.20), Eqn. (2.21), and Eqn. (2.22) respectively and t is the iteration index. There are various sorts of step size rules used in the subgradient method. We choose step size according to a diminishing step size rule explained in [90]. Using the expressions that we have derived, we now propose an iterative algorithm 1 to obtain the optimum PA (P_m^*) for the sum rate and user fairness maximization for downlink communication NOMA system.

Now we analyze the time complexity of our proposed algorithm 1. The convergence rate and the number of arithmetic operations decide the algorithm's time complexity. Since algorithm 1 has M users, updating the sum rate and fairness at line 3 in algorithm 1 requires M worst-case computation time. We can see that the Eqn. (2.19) for ϕ_i contains the product of two summations. The first summation sums up most of the M terms, while the second summation adds the max of $(M-1)$ terms. Consequently, the amount of time it takes to compute ϕ_i at line 7 algorithm 1 in the worst-case scenario is $M(M-1)$ for M users. Following that, updating P_i in Eqn. (2.18) depends on ϕ_i. Note that, inside the inner loop, P_i takes more computing time than an assistant variable, P_i, Lagrange multipliers, sum rates, and fairness. Thus, it is important to observe that P_i at line 8 algorithm 1 takes the greatest computation time inside the loops. As a result, the

Algorithm 1 Iterative Optimal Power Allocation Algorithm

1: Requires: σ^2, P_{BS}, R_{min}, M, pl, l, t, ω, and $\mathscr{R}$,
2: Requires: h, P, χ, β, and μ for all users.
3: Evaluate initial rates and user fairness for M users;
4: **for** until sum rate/User fairness start repeating **do**
5: **for** $m = 1$ to M **do**
6: $t = t + 1$;
7: Update $\phi_m(t)$ using Eqn. (2.19);
8: Update $P_m(t)$ using Eqn. (2.18);
9: Update $t_m(t)$ using Eqn. (2.16) if $l = 1$ else Updates $t_m(t)$ using (2.17) if $l \geq 0$;
10: Update $\chi_m(t)$, $\beta_m(t)$, and $\mu_m(t)$ using Eqn. (2.20), Eqn. (2.21), and Eqn. (2.22) respectively;
11: Update rates and user fairness for M users;
12: **end for**
13: **end for**

worst-case calculation time of P_i in line 8 for each iteration of the inner loop is $M^2(M-1)$. Since the inner loop (lines 5 to 12) repeats M times, the worst-case complexity of the inner loop is $M^3(M-1)$. Assume the total number of iterations for algorithm 1 convergence is T^{cv}. Therefore, the outer loop repeats T^{cv} times. As a result, the overall worst-case time complexity for the outer loop is $M^3(M-1)\,T^{cv}$ for M users. P_i in line 8 has a higher worst-case computation time than in line 3. As a result, our proposed algorithm's worst-case run time complexity for M users is $\mathscr{O}(M^4\,T^{cv})$. Note that the number of users that are multiplexed per subband is usually limited to 2-3 in most of the literature for downlink PA in NOMA-based systems in order to limit the SIC complexity. Hence, M can be safely assumed to be less than or equal to 3 users making the proposed algorithm practically feasible for a technology like 5G [91], [92].

2.3.1 Effect on the Proposed Method in the Absence of Minimum Rate Requirement Constraint.

In Sections 2.2 and 2.3, we discussed the sum rate and fairness maximization with the constraints given for M users downlink transmission NOMA network in our optimization problem $(P1)$. Here, we drop the minimum rate requirement constraint in the optimization problem $(P1)$ to obtain the optimal PA for the sum rate and fairness maximization. Therefore, the optimization

problem $(P4)$ can be written as:

$$(P4): \max_{P_m} \left(\sum_{m=1}^{M} R_m, \sum_{m=1}^{M} U(R_m) \right), \tag{2.23a}$$

$$\text{s.t.} \sum_{m=1}^{M} P_m \leq P_{BS}, \tag{2.23b}$$

$$P_m \geq 0, \forall m. \tag{2.23c}$$

We use the same steps and method discussed in the Section 2.3 to obtain the optimization problem $(P4)$ solution. However, all the steps and explanations involved are overlooked due to the similarity and simplicity.

2.3.2 Single-objective Optimization Scheme.

We introduce a single-objective optimization problem by removing the user fairness objective from the optimization problem $(P1)$ in order to reduce computational complexity. Hence, the optimization problem $(P5)$ may be expressed as:

$$(P5): \max_{P_m} \sum_{m=1}^{M} R_m, \tag{2.24a}$$

$$\text{s.t.} \sum_{m=1}^{M} P_m \leq P_{BS}, \tag{2.24b}$$

$$R_m \geq R_{min}, \forall m, \tag{2.24c}$$

$$P_m \geq 0, \forall m. \tag{2.24d}$$

To solve the optimization problem $(P5)$, we follow the same steps and methodology as in section 2.3. However, all of the steps and explanations involved are ignored due to their similarity and simplicity.

2.3.3 Discussion on Fairness

The α-fair utility function measures the fairness of a single user. However, if we wish to measure fairness across all network users, JFI is a widely used quantitative measure of fairness. Thus, we

can use JFI in simulation to determine system fairness. We consider JFI in terms of achievable rates defined as [71, 72, 93–96]:

$$JFI = \frac{\left(\sum_{i=1}^{M} R_i\right)^2}{M\sum_{i=1}^{M} R_i^2} \tag{2.25}$$

This definition in Eqn. (2.25) demonstrates that JFI accepts continuous values in the range $[1/M; 1]$. $JFI = 1$ refers to the fairest rate allocation, in which all users receive the same rate allocations. On the other hand, $JFI = 1/M$ denotes the least fair rate allocation, in which all rate allocations are given to a single user.

2.4 Simulation Results

This section discusses the simulation results of our proposed MOO problem. Also, we compare the simulation results of the proposed method $(P1)$ with the optimization methods $(P4)$, $(P5)$, and paper [56]. We use MATLAB to perform simulations. In the simulation, the performance parameters for all users are obtained over 10^5 channel gain realizations of Rayleigh fading, and then we take the average of these performance parameters. Unless otherwise stated, the values of the simulation parameters used to generate the plots are mentioned in Table 2.1. These parameter

System Parameter	**Values**
Channel realization $(\mathscr{R})$	10^5
Number of users (M)	3 and 4
Total power budget of BS (P_{BS})	10 Watt
Variance of AWGN noise (σ^2)	1
The minimum required rate for QoS (R_{min})	1 Bits/Sec/Hz
Weighting coefficient (ω)	0.5
Fairness level (l)	0.5

TABLE 2.1: The simulation values for various parameters

values have been taken from the paper [36]. Table 2.2 presents the initial and converged system parameter values for the proposed MOO method in the three-users and four-users downlink NOMA networks. In our simulations, we randomly initialize the PA as $P_1 = P_2 = P_3 = 5W$ for three users case and $P_1 = P_2 = P_3 = P_4 = 5W$ for four users case, regardless of our MOO problem's objectives and constraints. There is no specific reason for choosing $5W$ power values for three and four user cases, respectively. However, it is important to note that these random

System parameter	Initial value		Converged value	
	3 Users	4 Users	3 Users	4 Users
P_1	5	5	5.903	7.440
P_2	5	5	1.545	1.786
P_3	5	5	0.332	0.426
P_4	–	5	–	0.163
Total Power from BS	15	20	7.779	9.815
R_1	0.5154	0.3679	1.5386	1.5207
R_2	0.9469	0.5591	1.7663	1.4430
R_3	5.4288	0.9656	1.9793	1.1096
R_4	–	5.6594	–	1.4390
SR	6.8911	7.5520	5.2842	5.5123
JFI	0.5167	0.4268	0.9897	0.9870

TABLE 2.2: Initial and converged system parameter values for downlink NOMA networks

initializations of the PA must converge to optimal PA values in order to jointly maximize sum rate and user fairness while satisfying the (2.8b), (2.8c), and (2.8d) constraints of the optimization problem $(P1)$. The random initialization of PA results in an initial total transmit power of 15 W for three users, violating the power budget constraint as shown in Table 2.2. However, our algorithm ensures convergence of optimal PA $P_1 = 5.903W, P_2 = 1.545W$, and $P_3 = 0.332W$ for three users and $P_1 = 7.440W, P_2 = 1.786W, P_3 = 0.426W$, and $P_4 = 0.163W$ for four users, as specified in Table 2.2. These results in a total transmit power of $7.779W$ for three and $9.815W$ for four user cases, satisfying the power budget constraint (2.8b). From Table 2.2, we can also see that the convergence achievable rates in the three users and the four users cases are very close, highlighting the effectiveness of our proposed algorithm with respect to user fairness while also maximizing the sum rate.

Each user's transmit power is shown graphically in Figure 2.3 and Figure 2.4 to demonstrate how they change with each iteration of an algorithm 1 of our method for three users and four users instances. The iteration index is shown on the horizontal axis, and the vertical axis indicates the parameter of interest. Figure 2.3 shows that the transmit power of user 1 starts at $5W$ and finally converges to $5.903W$ as the number of iterations reaches 8. We can make similar observations for user 2 and user 3 from Figure 2.3. Hence, the optimal transmit power of user 1, user 2, and user 3 is $5.903W$, $1.545W$, and $0.332W$, respectively, making the total transmit power equal to $7.779W$, which is less than the power budget constraint of $P_{BS} = 10W$. Figure 2.4 shows

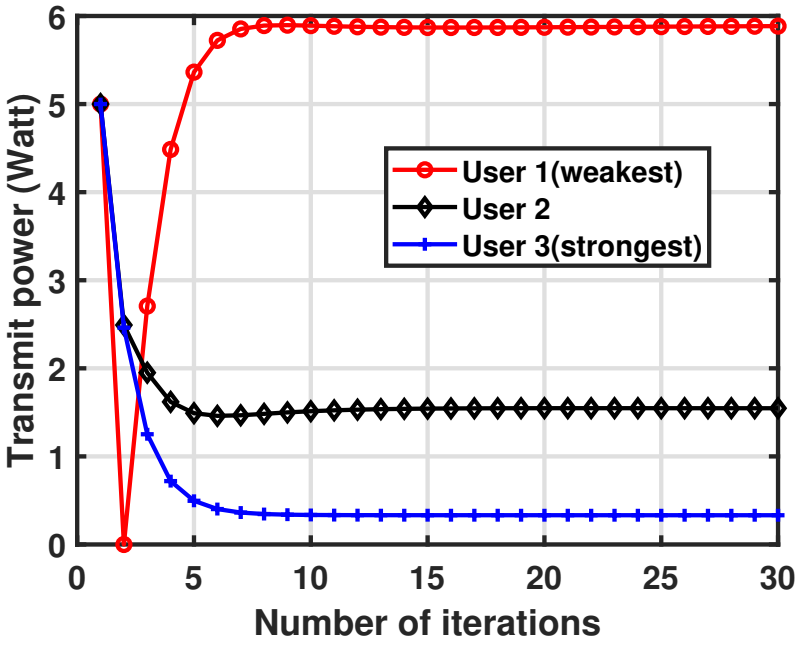

FIGURE 2.3: Transmit power versus the number of iterations for the proposed method for three users downlink communication NOMA network.

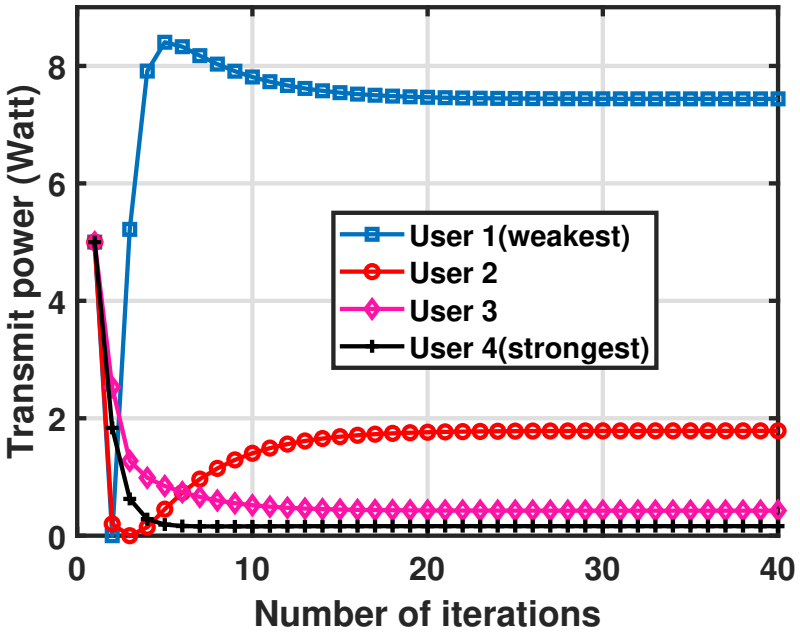

FIGURE 2.4: Transmit power versus the number of iterations of an algorithm for the proposed method for four users downlink communication NOMA network.

transmit power versus the number of iterations for four users with a similar conclusion. Observe

that the user with the worst channel conditions receives the largest transmit power, while the user with the best channel conditions receives the least transmit power.

Similarly, we can observe the convergence of rates to optimal values of each user in Figure 2.5, Figure 2.6, and Figure 2.7 for the three-user proposed method, four-user proposed method, and $(P4)$ method with three-user, respectively, as initially noted in Table 2.2. In addition,

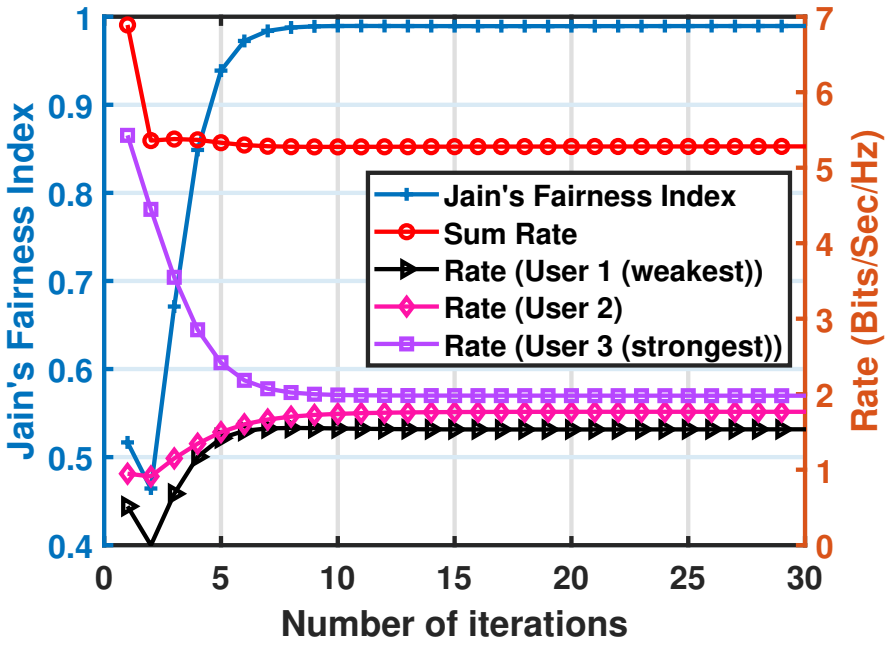

FIGURE 2.5: Sum rate, Jain's fairness index, and individual rates against the number of iterations for the proposed method for three users downlink communication NOMA network.

the sum rate and JFI of the proposed and (P4) methods are shown in Figures 2.5, 2.6, and 2.7. Note that in the three-user and four-user scenarios of $(P1)$, the optimal rates for all users are greater than or equal to R_{min} = 1 Bits/Sec/Hz. It must be anticipated from constraint (2.8c) in the MOO problem $(P1)$. On the other hand, the $(P4)$ optimization method overlooked the minimum rate constraint (2.8c) from the optimization problem(P1). As a result, user rates in the $(P4)$ method may take any value, and we can see that the user 3 rate ($R_3 = 0.8662$ Bits/Sec/Hz) is lower than the R_{min}. Figures 2.5, 2.6, and 2.7 show the relationship between individual rates and user fairness versus iteration numbers of an algorithm 1. These figures depict how the JFI evolves in terms of rate allocation at each iteration for the proposed methodology and $(P4)$ optimization method. In the case of three users, the JFI is equal to 0.5167 for initial randomly

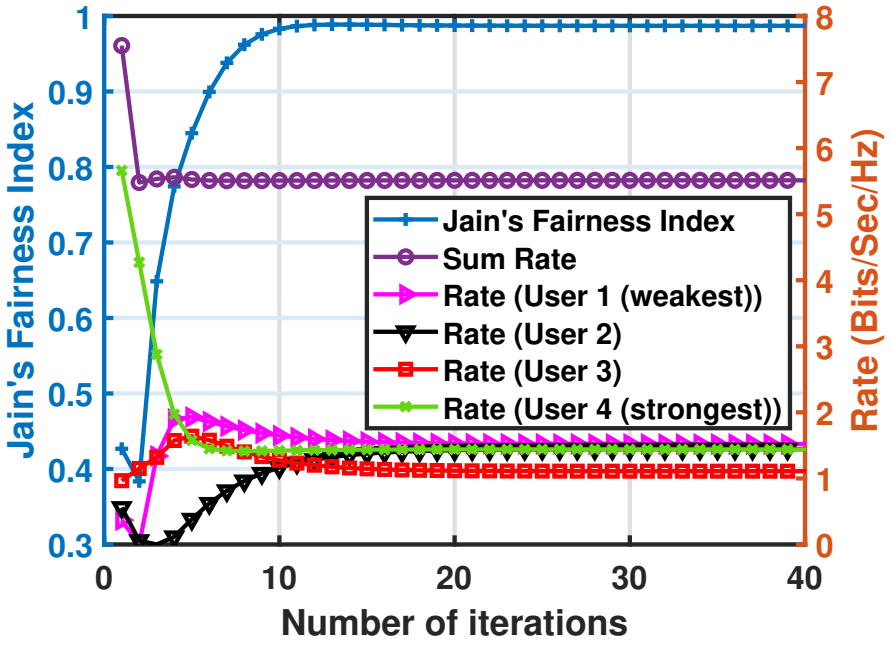

FIGURE 2.6: Sum rate, Jain's fairness index, and individual rates against the number of iterations for the proposed method for four users downlink communication NOMA network.

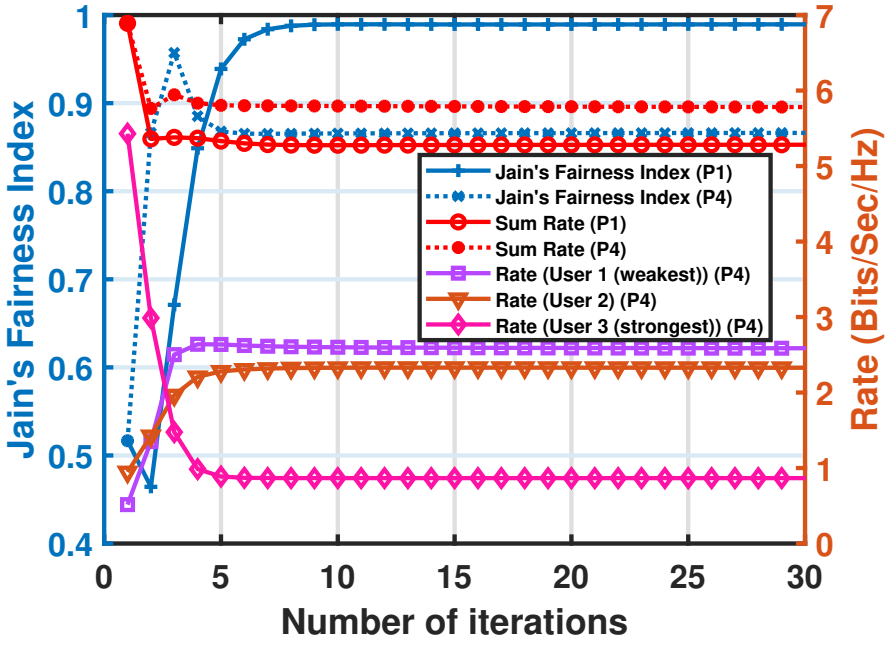

FIGURE 2.7: Sum rate, Jain's fairness index, and individual rates against the number of iterations for the $(P4)$ problem for three users downlink communication NOMA network.

chosen user rates and converges to 0.9897 when the number of iterations approaches 8. Figure 2.6 shows a similar observation for the four-users case; JFI is 0.4268 for the initial value and then concentrates on 0.9870. This clearly demonstrates that our proposed MOO algorithm maximizes user fairness objective. On the other hand, the primary JFI is 0.5167 in the $(P4)$ scheme, and then the algorithm 1 converges the JFI to 0.8664, as shown in Figure 2.7. The $(P4)$ optimization scheme's sum rate (at $\omega = 0.5$) is higher than the proposed method $(P1)$ due to fewer constraints of the $(P4)$ optimization method than the proposed method. However, the JFI of the $(P4)$ optimization scheme is lower than that of the proposed method $(P1)$ because the $(P4)$ method does not account for a minimum rate constraint (2.8c), resulting in more unfair rate allocations than the proposed method $(P1)$. It is observed that after initially assigned random PA, the proposed algorithm requires only 8 iterations to converge, demonstrating that it has a fast convergence rate and effectiveness to be deployed in practical NOMA networks.

Figure 2.8 depicts the sum rate and JFI concerning the number of iterations of an algorithm 1 for the three users for the problem $(P1)$ with $\omega = 0.5$, problem $(P1)$ with $\omega = 1$, problem (P5), and the single-objective scheme in [56]. It is worth noting that the objectives and constraints of

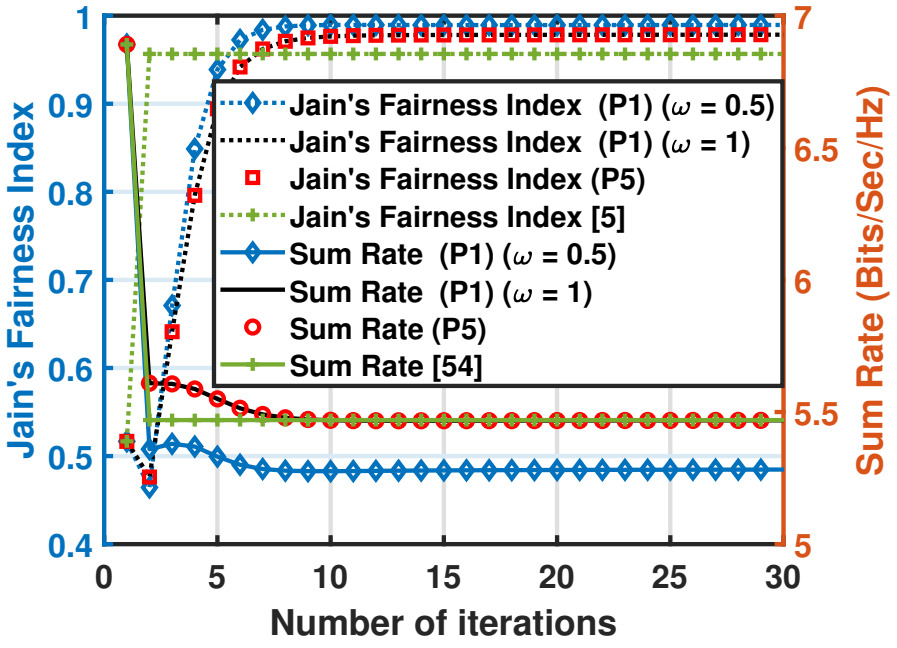

FIGURE 2.8: Sum rate and Jain's fairness index concerning the number of iterations for the three users for the proposed problem $(P1)$ with $\omega = 0.5$, proposed problem $(P1)$ with $\omega = 1$, single objective scheme $(P5)$, and the single-objective problem of [54].

the single-objective optimization problem $(P5)$ and the single-objective optimization problem of [56] are the same. Also, when $\omega = 1$, problem $(P1)$ is the same as problems $(P5)$ and [56]. As a result, the optimal sum rate for $(P1)$ with $\omega = 1$, $(P5)$, and [56] problems must be the same, as illustrated in Figure 2.8. The JFI of the $(P5)$ problem is greater than the JFI of the [56] optimization problem. The problem $(P5)$ has a full weight $(\omega = 1)$ towards the sum rate objective but no weight towards user fairness. Whereas, in the proposed method $(P1)$ with $\omega = 0.5$, it gives equal weight to the sum rate and fairness objectives. Consequently, the sum rate of the problem $(P1)$ with $\omega = 0.5$ must be less than the problem $(P1)$ with $\omega = 1$, $(P5)$ and [56], but the JFI of problem $(P1)$ (with $\omega = 0.5$) greater than problem $(P1)$ with with $\omega = 1$, $(P5)$, and [56], as depicted in Figure 2.8.

In Figure 2.10, we plot the sum rate and user's fairness as a function of the number of iterations of an algorithm 1 for different residual component (ε) in a 3 users case (using the imperfect SINR Eqn. 2.6). As can be seen from the figures, when ε increases, residual interference increases

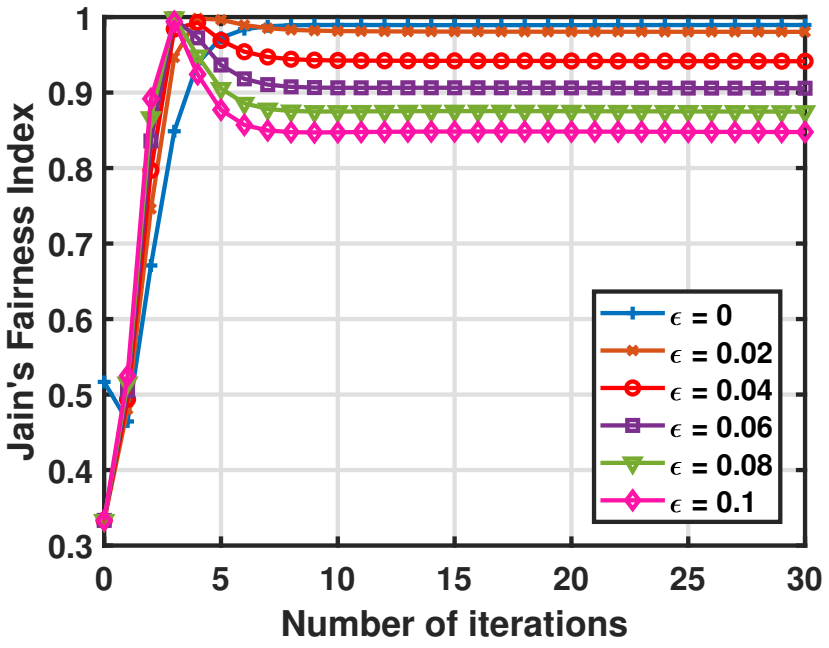

FIGURE 2.9: Jain's fairness index vs. the number of iterations for different residual components in the downlink NOMA network with three users.

for all users (except the weakest user) in the NOMA network, and thus, the sum rate and user's fairness for the proposed method decreases. The SIC operation in the NOMA network directly

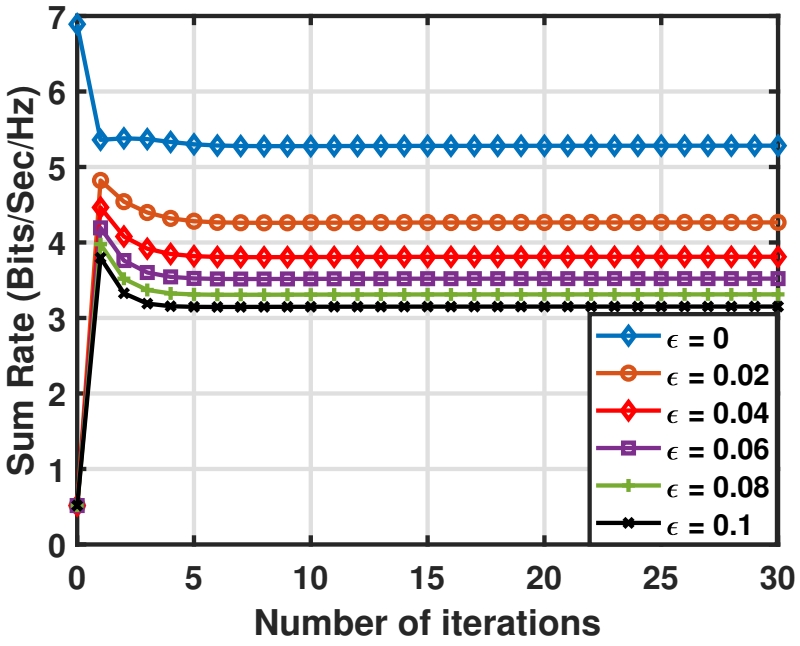

FIGURE 2.10: Sum rate vs. the number of iterations for different residual components in the downlink NOMA network with three users.

decodes the weakest user (user 1). In this way, the weakest user is spared from the effects of imperfect SIC. For the proposed ($P1$) method, with a 10% increase in residual interference, the sum rate drops by 40.35% while JFI drops by 14.42%. Figure 2.11 illustrates the user's fairness as converging with the number of iterations of algorithm 1 for different fairness levels (l) for three users downlink NOMA network. As per the α - fair utility function (Eqn. 2.7), fairness among users increases when the fairness level increases. Therefore, we can observe in Figure 2.11 that as l increases, the proposed method fairness increases. However, it is worth noting that for large l from 5 to 50, JFI rises by a small amount from 0.9905 to 0.9907. As a result, using a large value of l to maximize the overall rate is fruitless.

Figure 2.12 shows the sum rate and user fairness versus the number of iterations of algorithm 1 for two strong and one weak user in a three-user downlink NOMA network. Without loss of generality, we assume user 1 is the weakest, and users 2 and 3 are the strong compared to user 1 in the three-user case. We fix the channel coefficients using the relationship $h_2 \approx h_3$ and $h_2 = Xh_1$, where X is a uniformly distributed random number between 10 and 15. This ensures that h_2 and h_3 are greater than h_1 by a factor of at least 10 all the time. In this case, the JFI converges to 0.7378, and the sum rate converges to 5.7820. Due to the significant difference in

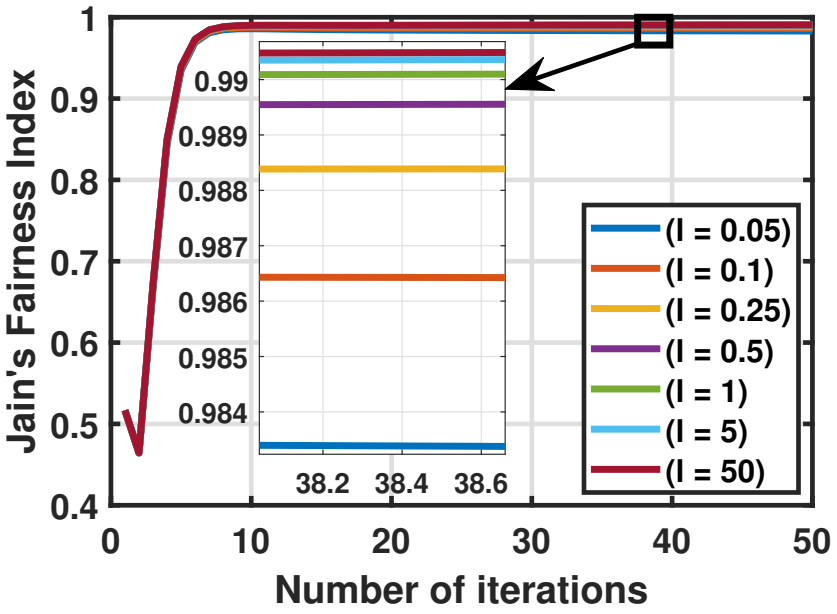

FIGURE 2.11: Jain's fairness index vs. the number of iterations for different fairness levels in the downlink NOMA network with three users.

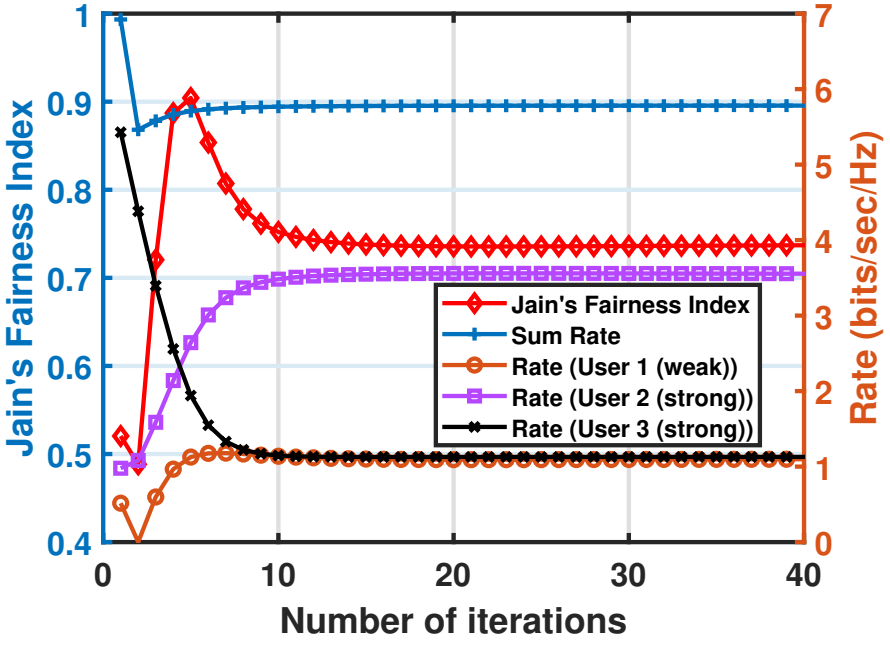

FIGURE 2.12: Sum rate and Jain's fairness index vs. the number of iterations for two strong and one weak user in the downlink NOMA network with three users.

channel conditions between strong and weak users, users get lower JFI in this two strong and one weak case compared to the $|h_1| \leq |h_2| \leq |h_3|$ case (discussed in Figure 2.5).

Figure 2.13 illustrates the achievable sum rate and JFI as a function of the weighting coefficient (ω) using the proposed PA algorithm. The horizontal axis indicates ω, the left side of the y-axis

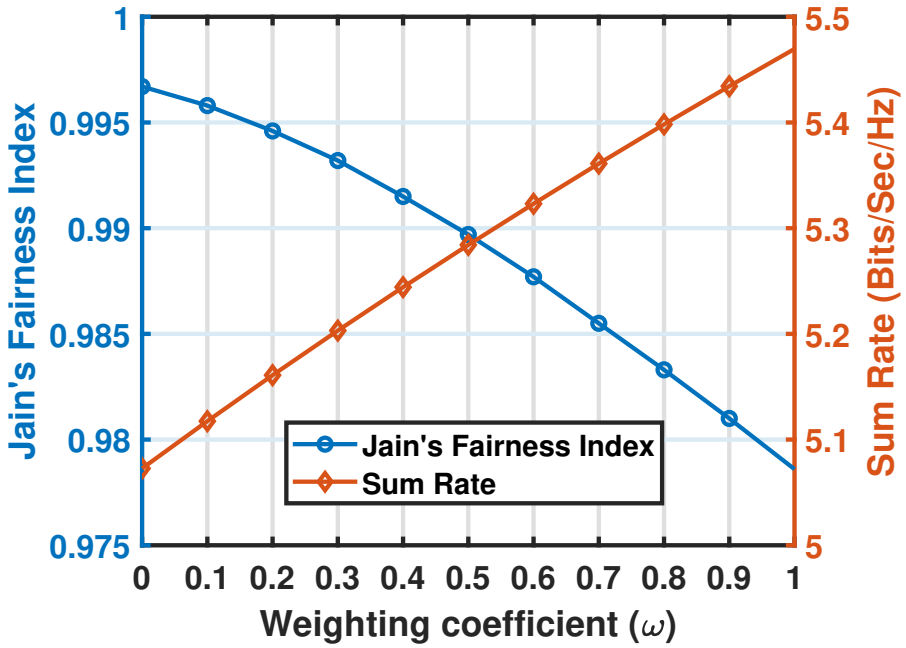

FIGURE 2.13: Sum rate and Jain's fairness index against weighting coefficient in the downlink NOMA network with three users.

shows the sum rate and the right side of the y-axis indicates JFI. In Figure 2.13, as expected and as shown by our PA algorithm, the maximum sum rate is achieved at $w = 1$ at the cost of the lowest fairness, whereas maximum fairness is achieved at $w = 0$ at the cost of the lowest sum rate. However, the results obtained using our algorithm in Figure 2.13 also show that a desired trade-off between the sum rate and fairness is possible with an appropriate choice of ω. As seen from the figure, our algorithm shows the sum rate increases monotonically, and the fairness decreases monotonically as we increase ω. Hence, it is possible to choose optimal point ω^* where both the sum rate and the fairness are jointly maximized. As illustrated in Figure 2.13, selecting $w = 0.51$ resulted in a good trade-off between these performance parameters.

2.4.1 Comparison with OMA

In Figure 2.14, we compare our proposed NOMA network's sum rate and user fairness with that of a conventional OMA network for different total transmit power of BS. Figure 2.14 shows that

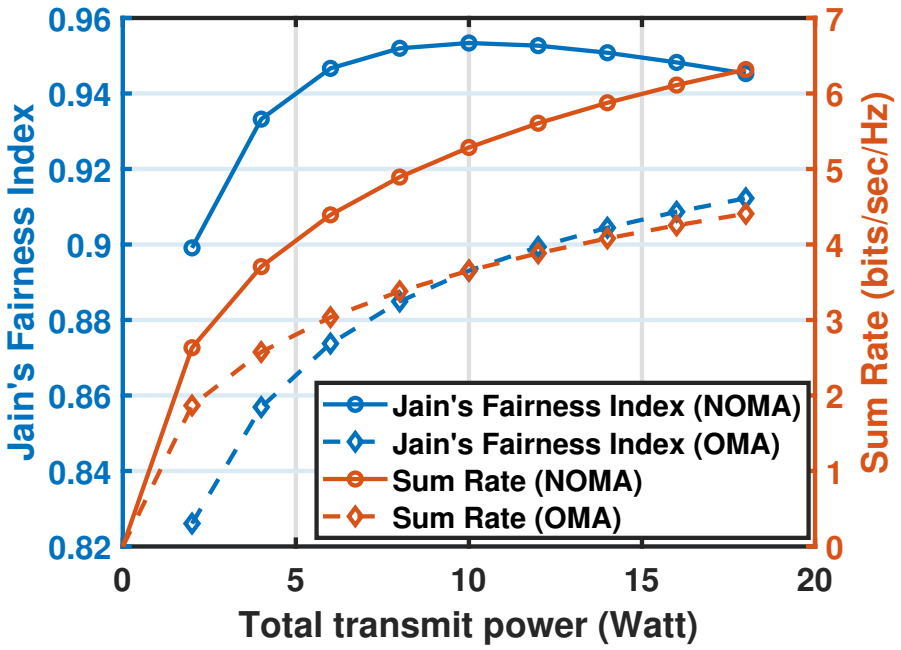

FIGURE 2.14: Sum rate and Jain's fairness index vs. total transmit power from BS in downlink NOMA and OMA networks with three users.

the sum rate for OMA and NOMA networks gradually increases with the total transmit power. JFI for OMA increases with the increase in total transmit power; however, JFI for NOMA first increases and then decreases to a further rise in total transmit power. Additionally, the NOMA sum rate and fairness are always higher than the OMA sum rate and fairness. This is because each user in OMA must share bandwidth with all other users compared to NOMA, in which each user uses the entire bandwidth but is separated from other users in the power domain. Moreover, for Figure 2.14, as the transmit power increases, the separation between sum rates of NOMA and OMA increases. This happened because PA is linked to the SIC process. When the BS's transmit power is low, the user with the small PA is greatly affected by noise, resulting in a sum rate degradation of NOMA compared to the OMA. This is indeed what we see in Figure 2.14 for low transmit power. However, if the transmit power is sufficiently high, the receiver can detect the signal more accurately, and SIC can be carried out more efficiently, resulting in a significant rate increase. As a result, we can see a more increase in the NOMA sum rate than the OMA sum rate at higher transmit power, as shown in Figure 2.14.

2.5 Summary

This Chapter presented a MOO scheme to investigate the trade-off between sum rate and user fairness for downlink transmission NOMA networks. The work investigated a novel approach and demonstrated that the proposed technique works well for the NOMA network. First, we formulated an original MOO problem for maximization of sum rate and user fairness with transmit power and QoS requirement constraints while optimizing PA. Using the weighted sum method, we transformed a MOO problem into a single-objective optimization problem. We applied the Lagrange dual decomposition method and KKT conditions to solve the optimization problem. Finally, simulation results show that the maximization of sum rate and user fairness for downlink NOMA networks.

In the future, we aim to investigate the performance of our proposed method for the study of downlink NOMA networks in the presence of an imperfect SIC constraint. Furthermore, the performance of our proposed method for downlink transmission in NOMA-based heterogeneous networks is one that we would like to study further.

NOMA is based on the concept of multiplexing users at the same time and frequency, which might result in a substantial amount of multiple access interference during decoding at each intended receiver. Hence, SIC is a crucial process employed at the receiver of a NOMA network to mitigate this interference caused by multiple access. However, to ensure the successful execution of the SIC process, each user's transmit power must meet the minimum required gap, which is defined as the minimum transmit power gap constraint. We address the minimum transmit power gap constraint in Chapter 3, in addition to the user's QoS and transmitter power budget constraints investigated in Chapter 2. In this context, the study presented in Chapter 3 aims to determine the optimal PA for downlink NOMA networks to optimize the sum rate and user fairness while meeting the minimum transmit power gap, QoS, and power budget constraints.

Chapter 3

Power Allocation for Joint Sum Rate and Fairness Optimization in Downlink NOMA Networks

Future broadband wireless networks need to be capable of meeting the enormous demand for high-speed data transmission. NOMA has been recognized as one of the important enabling elements to satisfy such a demand. [38, 65, 70]. The fundamental idea of NOMA is that several users are served in a single time-frequency block, in contrast to the OMA method, which serves a single user in each resource block [35, 38, 51, 52, 67]. As a result, NOMA is found to give a higher data rate and spectrum efficiency than OMA [52, 65, 77, 97]. Therefore, in recent years, many researchers in academia and industry have been inspired to further investigate ways to maximize the sum rate of the NOMA networks.

Despite the importance of the sum rate, user fairness is an equally important factor in NOMA networks [67, 77]. When there is a possibility that users with poor gains may be unable to access the channel, we can take advantage of fairness at the cost of reduced throughput [76, 77]. In addition, as NOMA aims to serve multiple users through non-orthogonal resource allocation, it is desirable to realize a trade-off between sum rate and user fairness [67, 71]. Designing such a trade-off between the sum rate and fairness in a NOMA network is highly dependent on distributing the total transmit power among users at the BS NOMA transmitter [52, 67, 70, 71, 76, 98]. However,

the distribution of the total transmit power should be done in a way that in addition to the network and user constraints, NOMA technology's constraint should also be satisfied.

To this end, in addition to the users' QoS and transmitter power budget constraints, we should also consider the co-channel interference between NOMA multiplexed users at the receiver. Since NOMA multiplexes users on the same resource block, it results in co-channel interference between the multiplexed users [37]. Hence, SIC may help decrease interference at the receivers [35, 36, 65, 98]. However, for the SIC to be appropriately executed at the user's end, the NOMA transmitter should ensure a sufficient gap between the user transmit powers [35, 36, 98]. In this respect, this research aims to find the optimal PA coefficients among multiplexed users for downlink NOMA networks to jointly optimize the sum rate and user fairness while satisfying users' QoS, transmit power budget, and users' minimum transmit power gap constraints.

The rest of the Chapter is organized as follows. Section 3.1 discusses the related literature, motivation, and summary of our contributions. Section 3.2 presents the downlink NOMA system model and the MOO problem formulation. Section 3.3 derives the optimal PA coefficients and provides an iterative algorithm for the solution of the MOO problem. The proposed MOO problem's simulation results and related discussions are presented in Section 3.4. Finally, the Chapter is concluded in Section 3.5.

3.1 Related Work

We begin with sum rate maximization articles, particularly those that deal with the SIC constraint in addition to other constraints. To maintain consistency in the discussion in this CHapter, if the SIC process at the receiver is imperfect, then interference from multiplexed co-users with lower channel coefficients is not completely eliminated when decoding a user's signal. Henceforth, imperfect SIC in this Chapter means there are some residues of user interference even after successive interference cancellation. The optimal PA for maximizing the weighted sum rate in a downlink multi-carrier NOMA network with imperfect SIC in addition to power budget and power order constraints are investigated in the manuscript [65].To optimize the sum rate for downlink NOMA networks, the study [38] proposed an optimal PA scheme that considers the imperfect SIC, the power budget, and the minimum rate constraints. The study [35] optimizes

user clustering and PA for downlink and uplink NOMA networks to maximize the sum rate. This study includes a sufficient gap between users transmitting power constraint in addition to power budget, QoS, one user can be allocated to at most one cluster while at least two users are grouped into one cluster, and total frequency resource constraints. The authors of [51] maximize the sum rate of a two-user downlink NOMA network while considering the imperfect SIC along with QoS constraints. The sum rate is maximized by calculating the optimal improper Gaussian signaling (IGS) circularity coefficient. The study [97] comes with an optimization problem that solves the precoding matrix and PA to optimize system throughput by employing imperfect SIC for downlink MIMO NOMA with power budget and minimum rate requirement for weak user constraints. The research [36] proposes a MOO problem for optimally allocating power in a downlink transmission NOMA network in order to maximize the sum rate while minimizing transmit power under the constraint of the minimum power gap among users, along with QoS and power budget constraints. The research [99] explores the performance of a NOMA-based satellite-terrestrial system in terms of outage performance, ergodic sum rate, and system throughput in the presence of imperfect SIC and CSI while satisfying the QoS requirement.

We now examine sum rate studies that ensure a desired fairness level without addressing the SIC constraint while considering other constraints. In [70], the authors optimize the PA to maximize the average sum rate for two-user downlink transmission with delay-tolerant transmission over fading channels, incorporating peak and average power and minimum individual rate constraints. Sum rate maximization is achieved for both complete and partial CSI, and fairness is ensured by including a minimum achievable ergodic rate requirement. In article [67], a downlink transmission NOMA network studies the maximization of fairness in terms of rate under full CSI and outage probability under average CSI with optimal PA. The research [52] employs zero-forcing (ZF) and minimum mean square error (MMSE), and the paper [100] employs maximum ratio combining (MRC) and MIMO SIC receiver algorithms to solve the joint fairness and sum rate optimization problem for uplink transmission NOMA networks. The authors in [52, 100] offers a method for concurrently improving fairness and sum rate through optimal PA, subband assignment, and user grouping. [52, 100] constrained power budget, number of users per subband, and number of subbands per user.The author investigated proportional fairness scheduling in a two-user downlink NOMA network in the research [76]. The author demonstrated that the proportional fairness scheduling approach optimizes both the sum rate and

the least normalized rate with optimal PA, resulting in proportional fairness and a slight variation in transmission rates. The optimal PA optimization problem in the paper [71] is intended to optimize the instantaneous sum rate with α - fairness for the downlink NOMA network under the power budget constraint. The user rates are updated based on the instantaneous CSI. The work [37] formulates an optimization problem for a downlink multicarrier NOMA network to optimize fairness and EE amongst users in terms of PA and subcarriers. The optimization problem has QoS requirements, the transmission power of the BS, the power budget for each subchannel, and the user limit on the subcarrier constraints. First, the worst-case user first subcarrier allocation (WCUFSA) algorithm is presented to allocate subcarriers. Then, optimal PA is achieved to improve the energy efficiency further and guarantee maximum fairness for NOMA users. The authors offer a water-filling-based joint PA and a proportional fairness scheduling approach in [69] to optimize the achievable rate by a quasi-optimal repartition of transmission power among subbands while assuring a high resource allocation fairness. The paper [72] proposed a joint NOMA and TDMA scheme in the Industrial IoT, which allows several sensors to communicate in the same time-frequency resource block using the NOMA method. Time slot allocation, power control, and user scheduling are optimized simultaneously to maximize the system α - fair utility with minimum rate, available transmission time allocated to all sensors, and transmit power constraints.

Some researchers have studied the sum rate that ensures user fairness while considering the SIC constraint in addition to other constraints. The research [77] addresses a MOO problem to jointly optimize sum rate and fairness for designing optimal beamforming in a MISO NOMA network by incorporating SIC power order in addition to the total transmit power constraints. The objective of the study [98] is to maximize the fairness in the data rates of different users while optimizing PA in a NOMA network by taking the minimum gap among users' powers as well as QoS, power budget constraints into consideration. The article [68] investigates the optimal PA for maximizing energy efficiency for MIMO NOMA networks with SIC power order as well as weak user QoS requirements, user fairness, and maximum transmission power constraints.

3.1.1 Motivation and Contributions

The majority of research on NOMA till now has been on single-objective optimization, either of the sum rate or fairness. However, in many situations, multiple system objectives need be optimized simultaneously. Quite often, it is essential to employ MOO to jointly optimize both sum rate and user fairness with respect to PA in order to make effective decisions in the face of trade-offs between these two equally important but conflicting objectives. Also, since NOMA is based on the idea of multiplexing users at the same time and frequency, it can cause a significant amount of multiple access interference during the decoding process at each intended receiver. In order to handle this multiple access interference, SIC is an important process at the receivers in a NOMA network. But, to make the SIC process successful, the transmit power of all the users must satisfy the minimum required gap. However, to the best of our knowledge, there has been no work till now that addresses the joint optimization of sum rate and users fairness while also considering the minimum power gap constraint. Even though [77] jointly maximizes the sum rate and user fairness, it does so with respect to the beamforming vector and not users' power allocation and without considering the power gap constraint. Only a few works [35, 36, 98] guarantee a minimal gap between users' transmission powers, but these papers do not address the MOO problem for joint sum rate and fairness maximization. Hence, to the best of our knowledge, a work that considers the joint optimization of sum rate and users fairness under the transmit power budget, users QoS, and minimum gap between users transmit power constraints is missing in the literature. In order to fill this important gap in the literature, we investigate the MOO problem for joint maximization of sum rate and user fairness through optimal PA while adhering to a sufficient power gap constraint between the users' transmit powers in addition to the transmit power budget and users's QoS constraints. In this regard, the main contributions of the Chapter are summarized as follows:

- We formulate and study the MOO problem to achieve optimal PA in downlink NOMA networks. The MOO problem jointly optimizes the sum rate and user fairness while meeting the minimum transmit power gap between users, power budget, and QoS requirements through optimal PA.

- We run Monte Carlo simulations to verify our analytical expressions and the proposed iterative algorithm. Our simulations show that the proposed algorithm requires only a few iterations to converge to the optimal PA coefficients.

- We show through our derived analytical expressions and simulations the trade-off between the sum rate and user fairness as the weighting coefficient that indicates the amount of importance given to each objective is varied. This also helps us to compare the proposed method's performance with a single objective benchmark scheme that considers only the sum rate objective in a network.

- Using our investigations, we also show that as the minimum power gap increases, except for the weakest user, other users restrictions increase with their power. Thus, the sum rate performance degrades with the increase in the minimum power gap. Hence, we conclude that there is an optimal power gap that needs to be chosen for the best performance of the network.

While our investigation of the MOO problem provides a lot of insights into how we can bring a meaningful trade-off between sum rate and user fairness under the said constraints, it has to be noted that the formulated problem poses sufficient challenges to solve because of the complicated nature of objective functions and the additional power gap constraint that is included in our work. In order to circumvent the challenges, as will be seen in the subsequent sections, we judiciously include a new assistance variable to convert the original problem into a solvable problem. Further, we adopt the weighted-sum method, which allows the MOO problem of maximizing sum rate and user fairness to be linearly combined into a single-objective optimization problem [77,80,81] using a weighting coefficient that enables a desired trade-off between these conflicting objectives. Following that, we derive the optimal solution to our MOO problem using a Lagrange dual decomposition method and KKT conditions. Hence, overall, considering the importance of the problem that is formulated, the challenges that such a problem formulation poses to get solved and the numerous insights that our investigation provides, this work can be considered important for the literature.

3.2 System Model and Problem Formulation

This section discusses the downlink NOMA network system model and formulation of the MOO problem for joint sum rate and user fairness maximization using optimal PA. Consider a downlink NOMA-based wireless network with a BS that communicates with M users, as shown in Figure 3.1. We assume a SISO system where the BS uses a single antenna to transmit, and

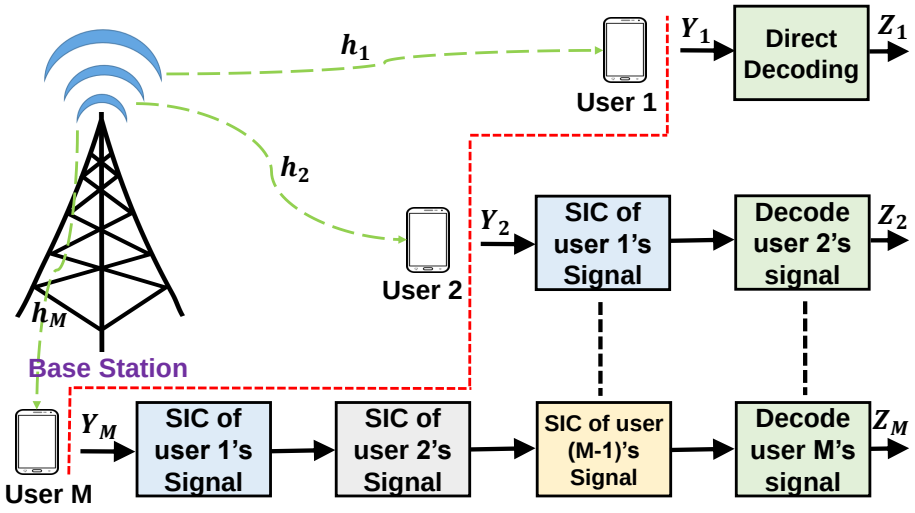

FIGURE 3.1: The system model illustrating the SIC process of downlink transmission NOMA network.

the users use a single antenna to receive. NOMA is based on the idea that users can share time-frequency resources by splitting them into power-domain and code-domain [51, 52]. This results in power-domain NOMA and code-domain NOMA mechanisms. We utilize power-domain NOMA user multiplexing, which enables us to serve all users at the same time across the same frequency band [37, 38, 67, 68, 71]. NOMA employs superposition coding at the transmitter, and at the receiver, it uses SIC decoding [35, 67, 71]. In superposition coding, all user signals are multiplied with separate PA coefficients and then combined at the BS. As a result, the transmitted signal at BS that uses superposition coding can be expressed as Eqn. (1.1). The received signal at user m is given by Eqn. (1.2). We assume the channels between the BS and all served users to have rayleigh fading with independent distribution [67, 77], represented by $h_m = z_m d_m^{-pl}$ and z_m is the small scale fading parameter that follows a complex Gaussian distribution i.e., $z_m \sim \mathscr{CN}(0,1)$ whre $m \in (1,2,\cdots,M)$, d_m is the distance between BS and user m, and pl is the path loss exponent [37, 71]. Without loss of generality, we sorted the channel gains between

the BS and all users in ascending order as $|h_1| \leq |h_2| \leq \cdots \leq |h_M|$. Further, we assume that the CSI is perfectly known at the BS [36, 37]. The SIC process for the downlink transmission of the NOMA network is illustrated in Figure 3.1. After the SIC process as described above, we can obtain the signal y_m at user m given by Eqn. (1.3). The SINR as seen by user m can be written as Eqn. (1.4). Hence, the achievable rate for user m is given by Eqn. (1.5).

Fairness measurements are tools for determining the amount of fairness. The fairness measurements can be characterized as quantitative or qualitative based on their quantitative ability. Quantitative measurements include JFI and Entropy, while qualitative measures include max-min and proportional fairness [85, 86]. JFI and Entropy measures do not help identify resources that have been treated unfairly. Additionally, JFI and Entropy measures need complete information on resource allocation to obtain fairness [86]. In max-min fairness measures, maximizes the user service by providing the lowest service to the maximum allocated resource. It may result in network inefficiency. max-min fairness does not measure individual fairness and the amount of fairness [86]. On the other hand, an α - fair utility function is a generalized form of the fairness function. Compared to the fairness mentioned above, an α - fair utility function measures individual fairness and does not require complete information. An α - fair utility function uses a single scalar to represent various levels of user fairness [71, 86]. As a result, in this study, we prefer to use the α - fair utility function, which may be represented as [71, 77, 86],

$$U(R_m) = \begin{cases} \dfrac{R_m^{1-l}}{1-l}, & l \geq 0,\ l \neq 1, \\ \ln(R_m), & l = 1. \end{cases} \tag{3.1}$$

Where l represents different fairness levels of achievable rate R_m. We incorporate the constraint of minimum power gap for successful SIC into our optimization problem, which can be represented as follows [35, 36, 98],

$$\alpha_m P|h_{m+1}|^2 - \sum_{i=m+1}^{M} \alpha_i P|h_{m+1}|^2 \geq P_g, \text{for } m = 1, 2, \cdots, M-1. \tag{3.2}$$

where P_g is the minimal power gap between users to implement the SIC procedure successfully. From Eqn. (3.2), primary decoded users must be given more power than later decoded users to ensure successful SIC in NOMA networks. Furthermore, there should be a reasonable difference in transmission power between users.

Next, we frame the MOO problem to determine the operating point that simultaneously optimizes the sum rate and user fairness using optimal PA for downlink NOMA networks. This MOO problem can be written as $(P1)$,

$$(P1): \max_{\alpha_m} \left(\sum_{m=1}^{M} R_m, \sum_{m=1}^{M} U(R_m) \right), \tag{3.3a}$$

$$\text{s.t. } \alpha_m P|h_{m+1}|^2 - \sum_{i=m+1}^{M} \alpha_i P|h_{m+1}|^2 \geq P_g,$$

$$\text{for } m = 1, 2, \cdots, M-1. \tag{3.3b}$$

$$R_m \geq R_{min}, \forall m, \tag{3.3c}$$

$$\sum_{m=1}^{M} \alpha_m P \leq P_{BS}, \tag{3.3d}$$

$$\alpha_m \geq 0, \forall m. \tag{3.3e}$$

Where Eqn. (3.3a) denotes objective functions to be maximized simultaneously. The first function is the sum rate, and the second function is the sum utility. The constraint in Eqn. (3.3b) ensures minimum power gap for successful SIC process in NOMA. In the context of QoS, the constraint in Eqn. (3.3c) implies the requirement that the data rate of each user must not fall below the minimum user data rate R_{min}. The constraint in Eqn. (3.3d) ensures that the network's overall transmit power does not exceed BS's total power budget P_{BS}. Finally, the constraint in Eqn. (3.3e) assures that each user has a non-negative transmit power.

3.3 Solution of Multi-objective Optimization Problem

This section will provide the optimal solution for an M users downlink NOMA network in terms of both sum rate and user fairness maximization. Later in this section, we also discuss benchmark schemes. The weighted sum and ε-constraint methods are the two most often adopted classical methods for solving MOO problems [87]. In the weighted sum method, a weighting coefficient linearly combines the MOO problem into a single-objective optimization problem. The ε-constraint method optimizes one objective function while constraining the others to be less than or equal to a defined numerical value [87]. The ε vector in the ε-constraint method must be carefully chosen to fall within the minimum and maximum values of the objective

function, which might make this approach challenging. However, the weighted sum method is more straightforward to implement than the ε-constraint method. Furthermore, we may make a trade-off between multiple objectives using the weighting coefficient method. This is also consistent with our aim of reaching optimal PA to achieve a balanced trade-off while simultaneously optimizing the sum rate and user fairness. Thus, we use the weighted sum method to solve the MOO problem $(P1)$. This results in a MOO problem $(P1)$ being converted into a single objective optimization problem, which is as follows [77, 80, 81],

$$(P2): \max_{\alpha_m} \omega \sum_{m=1}^{M} R_m + (1-\omega) \sum_{m=1}^{M} U(R_m),$$
$$\text{s.t. } (3.3b),\ (3.3c),\ (3.3d),\ (3.3e).$$

where ω is a weighting coefficient, such as $0 \leq \omega \leq 1$. The ω shows a tradeoff between two objectives, i.e., higher ω values support maximizing the sum rate, while lower ω values favor maximizing user fairness. Note that the fairness objective function is neither convex nor concave with regard to α. Hence, the optimization problem $(P1)$ becomes non-convex. Therefore, the solution for $(P1)$ may not be global. We recognize that the fairness objective function can be converted to a concave function by creating a new assistant variable v_m for the user m [89], and then $(P2)$ is written as,

$$(P3): \max_{\alpha_m} \omega \sum_{m=1}^{M} R_m + (1-\omega) \sum_{m=1}^{M} U(v_m),$$
$$\text{s.t. } (3.3b),\ (3.3c),\ (3.3d),\ (3.3e).$$
$$v_m \leq R_m, \forall m. \tag{3.4a}$$

As stated in [89], when the weighted objective function in $(P3)$ is to be maximized, $U(\cdot)$ must be an increasing function, and v_m must be equal to R_m. Then, $(P2)$ and $(P3)$ would have the same solution. As a result, instead of $(P2)$, we can solve $(P3)$. We may now use the Lagrange dual decomposition method to solve the optimization problem $(P3)$ [36, 70, 82]. As a result, the

following Lagrangian function is obtained as,

$$\mathscr{L}(\alpha_m,\psi_m,\chi_m,\beta_m,\mu_m)=\omega\sum_{m=1}^{M}R_m+(1-\omega)\sum_{m=1}^{M}U(v_m)+\sum_{m=1}^{M}\chi_m(R_m-R_{min})+$$
$$\sum_{m=1}^{M-1}\psi_m\left(\alpha_m P|h_{m+1}|^2-\sum_{i=m+1}^{M}\alpha_i P|h_{m+1}|^2-P_g\right)+\beta_m(P_{BS}-\sum_{m=1}^{M}\alpha_m P)+\sum_{m=1}^{M}\mu_m(R_m-v_m), \tag{3.5}$$

There are two sub-problems in solving the above Lagrangian function. The first is a problem of application layer optimization with variable v, and the second is a problem of physical layer optimization with variable α. Hence, the problem of application layer optimization may be expressed as,

$$T_1=\max_{t}\ g_3(v_m), \tag{3.6}$$

where,

$$g_3(v_m)=(1-\omega)\sum_{m=1}^{M}U(v_m)-\sum_{m=1}^{M}\mu_m v_m. \tag{3.7}$$

and the physical layer optimization problem can be written as:

$$T_2=\max_{\alpha_m}\ g_4(\alpha_m), \tag{3.8}$$

where,

$$g_4(\alpha_m)=\omega\sum_{m=1}^{M}R_m+\sum_{m=1}^{M}\chi_m(R_m-R_{min})+\beta_m(P_{BS}-\sum_{m=1}^{M}\alpha_m P)+$$
$$\sum_{m=1}^{M-1}\psi_m\left(\alpha_m P|h_{m+1}|^2-\sum_{i=m+1}^{M}\alpha_i P|h_{m+1}|^2-P_g\right)+\sum_{m=1}^{M}\mu_m R_m \tag{3.9}$$

In Eqn. (3.1), the α-fair utility function has two cases: $l=1$ and $l\geq 0$. As a result, for $l=1$ and $l\geq 0$, we can study the optimal solution of T_1 of Eqn. (3.6) independently as follows.

Case I ($l=1$): In this case, $U(v_m)=\ln(v_m)$ is a strictly concave function of v_m. Therefore, the first term $(1-\omega)\sum_{m=1}^{M}U(v_m)$ is a strictly concave function of v_m. The second term $\sum_{m=1}^{M}\mu_m v_m$ in (3.7) is a linear function of v_m. Hence, $g_3(v_m)$ is a concave function of v_m. Thus, by using the KKT conditions [82], one may derive the closed-form formula for v_m in case I by obtaining the first partial derivative of $g_3(v_m)$ with respect to v_m and equating to zero. Hence,

$$\frac{\partial g_3(v_m)}{\partial v_m}=\frac{\omega}{v_m}-\mu_m=0\implies v_m^*=\frac{\omega}{\mu_m}. \tag{3.10}$$

Case II ($l \geq 0$): $g_3(v_m)$ is a concave function of v_m, as demonstrated in Appendix E. As a result, the closed-form formula for v_m in case II can be computed by applying the KKT conditions, as shown in Appendix G. Therefore, we get v_m^* as,

$$v_m^* = \sqrt[l]{\frac{(1-\omega)}{\mu_m}}. \tag{3.11}$$

To derive optimal PA coefficients α_m^*, we first demonstrate in Appendix F that $g_4(\alpha_m)$ is a concave function of α_m. As a result, as seen in Appendix H, the closed-form expression for α_m^* can be determined using the KKT conditions as stated in Eqn. (3.12) with $[\alpha]^+ = \max(0,\alpha)$ and $\mathscr{T}_m$ as given in Eqn. (3.13).

$$\alpha_m^* = \left[\frac{(\omega+\chi_m+\mu_m)P|h_m|^2 - \mathscr{T}_m\left(\sum_{n=m+1}^{M}\alpha_n P|h_m|^2+\sigma^2\right)}{\mathscr{T}_m P|h_m|^2}\right]^+, \tag{3.12}$$

$$\begin{aligned}\mathscr{T}_m &= \beta_m P - \psi_m P|h_{m+1}|^2 + \\ &\sum_{i=1}^{m-1}\left(\psi_i P|h_{i+1}|^2 + \left(\frac{(\omega+\chi_i+\mu_i)P|h_i|^2}{\sum_{j=i+1}^{M}\alpha_j P|h_i|^2+\sigma^2} - \frac{(\omega+\chi_i+\mu_i)P|h_i|^2}{\sum_{j=i}^{M}\alpha_j P|h_i|^2+\sigma^2}\right)\right)\end{aligned} \tag{3.13}$$

Now, using a sub-gradient method, the Lagrange multipliers can be calculated and updated iteratively, as described below [82],

$$\psi_m(t+1) = \left[\psi_m(t) + \delta_1(t)\left(P_g - \alpha_m P|h_{m+1}|^2 + \sum_{i=m+1}^{M}\alpha_i P|h_{m+1}|^2\right)\right]^+, \quad \text{for } m = 1,2,\cdots,M-1, \tag{3.14}$$

$$\chi_m(t+1) = [\chi_m(t) + \delta_2(t)(R_{min} - R_m)]^+, \forall m, \tag{3.15}$$

$$\beta_m(t+1) = \left[\beta_m(t) + \delta_3(t)\left(\sum_{m=1}^{M}\alpha_m P - P_{BS}\right)\right]^+, \tag{3.16}$$

$$\mu_m(t+1) = [\mu_m(t) + \delta_4(t)(v_m - R_m)]^+. \tag{3.17}$$

where δ denotes the step size, and t represents the iteration index. The subgradient method uses a variety of different step size rules. We pick the step size in accordance with the rule of diminishing step sizes described in [90]. Once the equations are derived, we can present an

iterative algorithm 2 for obtaining the optimal PA coefficients for the MOO problem $(P1)$ of jointly maximizing the sum rate and user fairness.

Algorithm 2 Iterative Optimal Power Allocation Algorithm

1: Requires: P, σ^2, P_{BS}, R_{min}, M, P_g, pl, l, t, ω, and $\mathscr{R}$;
2: Requires: h, α, ψ, χ, β, μ, and δ for all users;
3: Calculate initial rates and user fairness for M users;
4: **for** until sum rate/user fairness repeats **do**
5: **for** $m = 1$ to M **do**
6: $t = t + 1$;
7: Update $\mathscr{T}_m(t)$ using Eqn. (3.13);
8: Update $\alpha_m(t)$ using Eqn. (3.12);
9: Update $v_m(t)$ using Eqn. (3.10) if $l = 1$ else update $v_m(t)$ using Eqn. (3.11) if $l \geq 0$;
10: Update $\psi_m(t)$ using Eqn. (3.14);
11: Update $\chi_m(t)$ using Eqn. (3.15);
12: Update $\beta_m(t)$ using Eqn. (3.16);
13: Update $\mu_m(t)$ using Eqn. (3.17);
14: Update rates and user fairness for M users;
15: **end for**
16: **end for**

Now we study the time complexity of our proposed algorithm. Since algorithm 2 has M users, it takes M worst-case computation time to update the sum rate and fairness at line 3. It is important to note that line 8 takes the most computing time inside the loop. The worst-case time computation of $\mathscr{T}_m$ in Eqn. (3.13) is M^2. Line 8 updates α_m using Eqn. (3.12), which depends on $\mathscr{T}_m$. Thus, the worst-case time computation of α_m is M^3. Since the inner loop (line 5 to line 15) repeats M times, the inner loop's worst-case complexity is M^4. Assume that the total number of iterations required for algorithm convergence is T^{cv}. As a result, our proposed method's worst-case run time complexity for M users is $\mathscr{O}(M^4\, T^{cv})$.

3.3.1 Benchmark: Single-objective Optimization

It is worth noting that our proposed MOO problem $(P1)$ jointly optimizes the sum rate and user fairness. In certain circumstances, it may be necessary to optimize only the sum rate of a NOMA network in order to decrease computing complexity. Consequently, subsection 3.3.1 provides the single-objective optimization problem $(P4)$ by omitting the user fairness objective of the MOO problem $(P1)$. As a result, section III-B of work [36] provides a benchmark for the MOO

problem $(P1)$. In $(P4)$, we find the optimal PA for maximizing the sum rate while keeping the minimum transmit power gap between users, QoS, and power budget constraints in mind. As a result, the optimization problem $(P4)$ may be stated as follows:

$$(P4): \max_{\alpha_m} \sum_{m=1}^{M} R_m,$$
$$\text{s.t. } (3.3b),\ (3.3c),\ (3.3d),\ (3.3e).$$

We solve the optimization problem $(P4)$ using the same steps and method as in Section 3.3 due to the similarities in solving the optimization problem. As a result, all steps and explanations are ignored.

3.4 Simulation Results

This section discusses the simulation results for our proposed MOO problem. Additionally, we compare the simulation results to the benchmark method. The performance parameters for all users are obtained in the simulation across 10^5 channel gain realizations of Rayleigh fading, and then we take the average of these performance parameters. Table 3.1 lists the values of the simulation parameters used to generate the plots unless otherwise stated. We have set the

TABLE 3.1: The simulation values for various parameters

System Parameter	**Values**
Channel realization $(\mathscr{R})$	10^5
Number of users (M)	3
Total transmit power from BS (P)	10 W
Total power budget of BS (P_{BS})	10 W
Variance of AWGN noise (σ^2)	1
The minimum required rate for QoS (R_{min})	1 bps/Hz
Minimum power gap among different users (P_g)	1.5
Weighting coefficient (ω)	0.5
Fairness level (l)	0.75

user's minimum power gap to 1.5 $(P_g = 1.5)$. The proposed solution ensures power gaps of constraint (3.3b) for the given user's channel conditions. Table 3.2 shows the proposed MOO problem's initial and converged system parameter values. In our simulations, we randomly

TABLE 3.2: Initial and converged system parameter values for downlink NOMA networks

System Parameter	**Initial value**	**Converged value**
α_1	0.1	0.6501
α_2	0.1	0.1066
α_3	0.1	0.0222
Transmit power from BS to user 1	1 W	6.50 W
Transmit power from BS to user 2	1 W	1.07 W
Transmit power from BS to user 3	1 W	0.22 W
Total transmit power from BS	3 W	7.792 W
R_1	0.35 bps/Hz	1.68 bps/Hz
R_2	0.75 bps/Hz	1.38 bps/Hz
R_3	4.23 bps/Hz	2.34 bps/Hz
SR	5.33 bps/Hz	5.40 bps/Hz
JFI	0.51	0.95

initialize the PA coefficients as $\alpha_1 = \alpha_2 = \alpha_3 = 0.1$, as shown in Table 3.2, regardless of our MOO problem's objectives and constraints. On the other hand, our method guarantees that the optimal PA coefficients converge to $\alpha_1 = 0.6501, \alpha_2 = 0.1066, \alpha_3 = 0.0222$, resulting in a total transmit power of 7.79 W that meets all constraints of $(P1)$ while also concurrently optimizing sum rate and fairness. Table 3.2 shows that, as expected by NOMA principles, the user with the worst channel conditions receives the most transmit power. In contrast, the user with the best channel conditions receives the least transmit power. Additionally, we can observe in Table 3.2 that randomly initialized PA coefficients provide rates that are not ensuring the QoS constraint. On the other side, once the algorithm converges, all user rates satisfy the QoS constraint. Those rates converge very near to one another, demonstrating the effectiveness of our proposed method in terms of user fairness while simultaneously maximizing the sum rate.

Figures 3.2 and 3.3 show graphically how each user's transmit power and rate change with each iteration of our algorithm 2. The iteration index is shown on the horizontal axis, while the parameter of interest is displayed on the vertical axis. Figure 3.2 shows that user 1's transmit power begins at 1 W and eventually converges to 6.50 W as the number of iterations approaches 35. We may draw similar conclusions from Figure 3.2 for users 2 and 3. As a result, the optimal transmit power of users 1, 2, and 3 is 6.50 W, 1.07 W, and 0.22 W, respectively, resulting in a

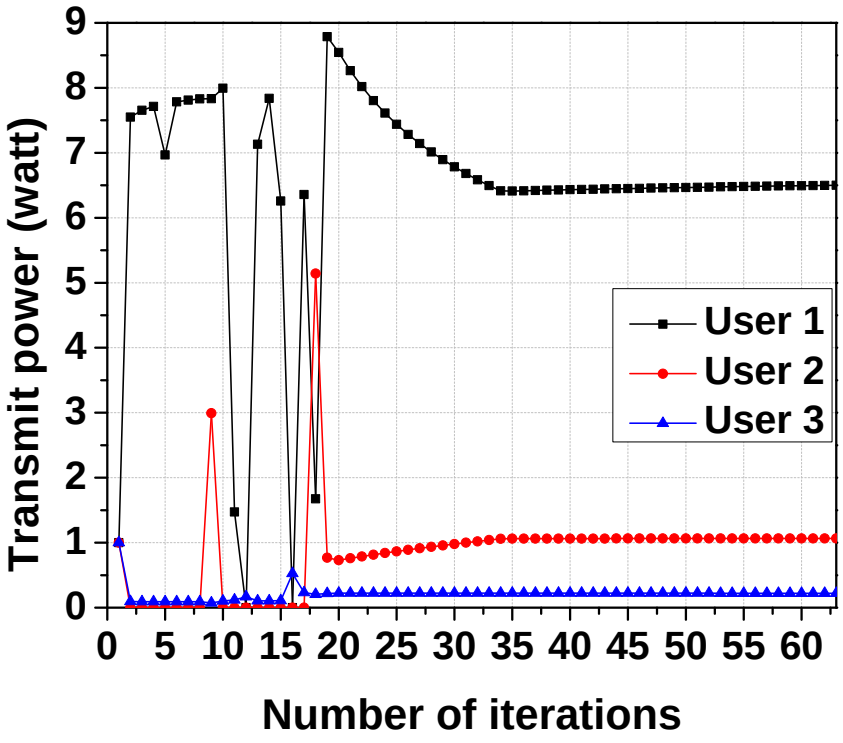

FIGURE 3.2: Transmit power vs. the number of iterations for downlink NOMA network.

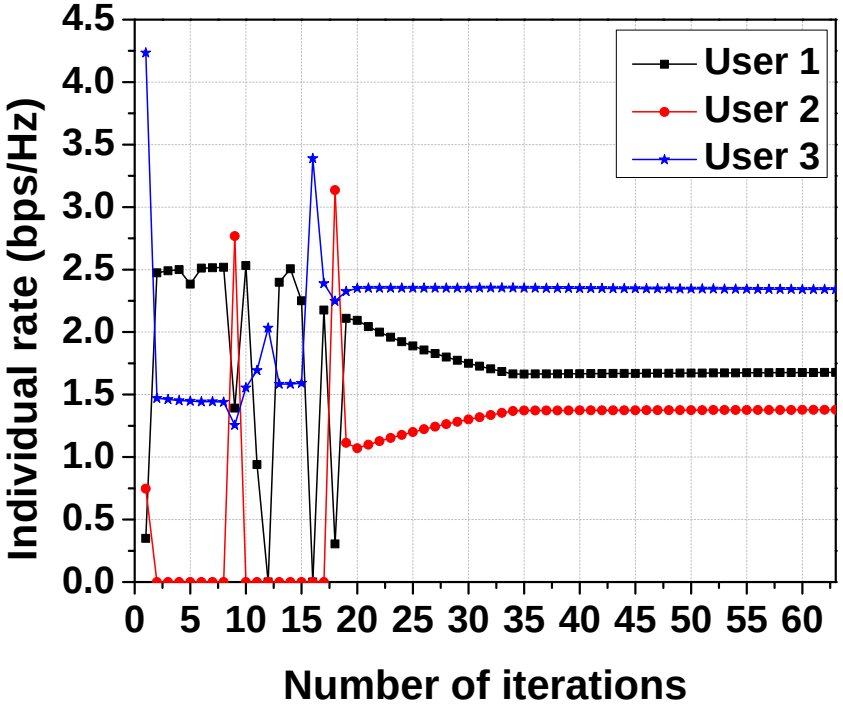

FIGURE 3.3: Individual rates vs. the number of iterations for downlink NOMA network.

total transmit power of 7.79 W, which is less than the power budget constraint (P_{BS} = 10 W). Thus it ensures power budget constraint. In Figure 3.3, individual rates converge to optimal values of 1.68 bps/Hz, 1.38 bps/Hz, and 2.34 bps/Hz for users 1, 2, and 3. Note that all user's optimal rates are higher than R_{min} = 1 bps/Hz, which is expected given constraint (3.3c) in the MOO problem ($P1$). The proposed method only needs about 35 iterations to converge once the first random PA coefficients are given, proving that it has a fast convergence rate and is effective enough to be implemented in practical networks like 5G networks.

Figure 3.4 illustrates the sum rate versus the number of iterations for various weighting coefficients (ω) in the proposed and benchmark methods. The ω allows for a choice between the

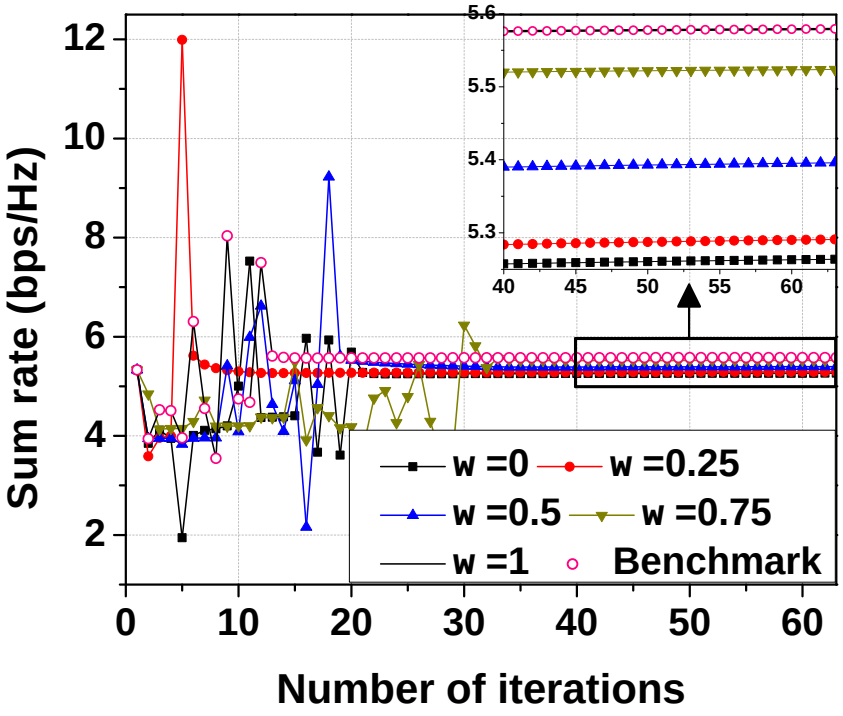

FIGURE 3.4: Sum rate vs. the number of iterations for various weighting coefficients in downlink NOMA network.

sum rate and fairness. Higher ω values support increasing the sum rate, while lower ω values support increasing user fairness. Thus, when seen in Figure 3.4, as ω grows, so does the sum rate. When ω = 1, the sum rate is entirely favored, and fairness is completely ignored. Hence, the benchmark and the ω = 1 case are the same. As a result, the ω = 1 and benchmark plots intersect, as illustrated in Figure 3.4.

Figure 3.5 depicts JFI versus iteration count for various weighting coefficients (ω) in the proposed and benchmark methods. The JFI for $\omega = 0.5$ is equal to 0.51 for initially randomly

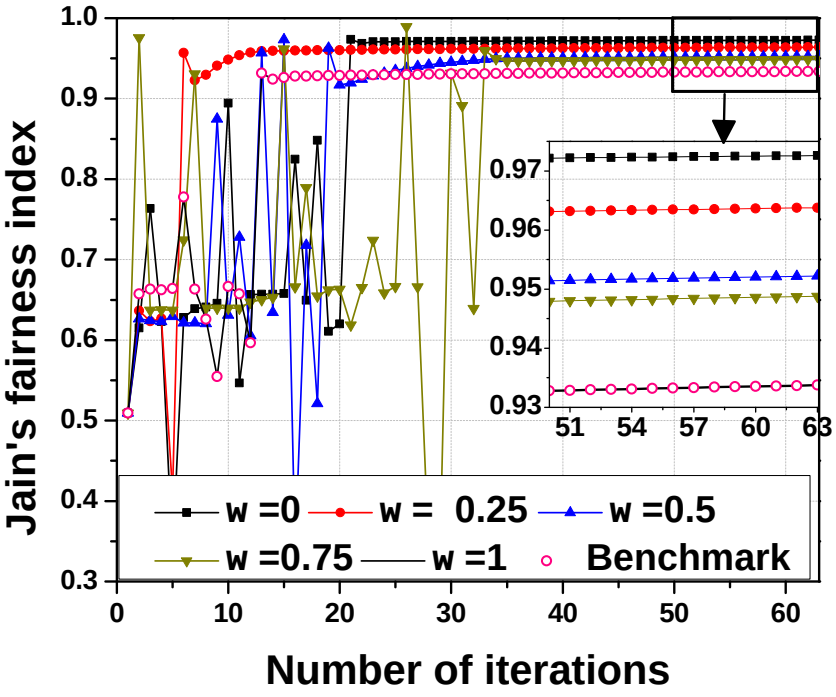

FIGURE 3.5: JFI vs. the number of iterations for different weighting coefficients in downlink NOMA network.

chosen PA coefficients and grows to 0.95 when iterations exceed 35. This indicates clearly that our proposed MOO method maximizes user fairness. In Figure 3.5, when ω increases, the fairness decreases. Figure 3.5 shows that plots overlap for $\omega = 1$ and the benchmark method, which is expected. Figure 3.6 depicts the achieved sum rate and JFI over the weighting coefficient. ω is indicated on the horizontal axis, the sum rate is shown on the left side of the y-axis, and JFI is indicated on the right side of the y-axis. For problem $(P1)$, as anticipated, at $\omega = 0$, the maximum sum rate is achieved at the cost of the lowest fairness. Furthermore, when $\omega = 1$, maximum fairness is achieved at the cost of the lowest sum rate. However, the BS can choose an appropriate value for the weighting coefficient ω in order to achieve a good balance between the sum rate and fairness. As shown in Figure 3.6, choosing $\omega = 0.52$ results in a good trade-off between these performance parameters. Figure 3.7 depicts the proposed method's sum rate versus iteration count for different power gaps (P_g). When P_g increases, the sum rate decreases for the proposed method. This is because when P_g increases, the PA coefficients decrease (except for the PA of the weakest user). The reason for the decrease in PAs is that users,

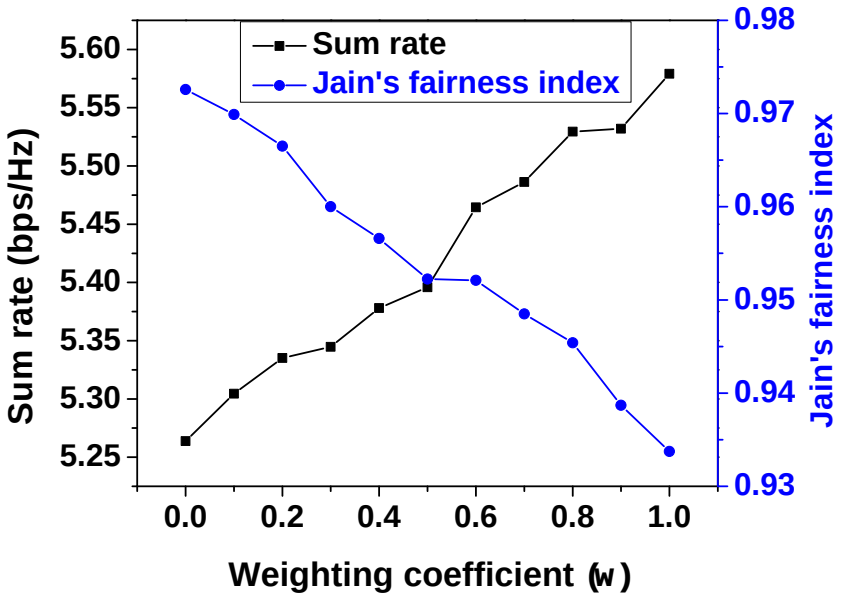

FIGURE 3.6: Sum rate and JFI against weighting coefficient in downlink NOMA network.

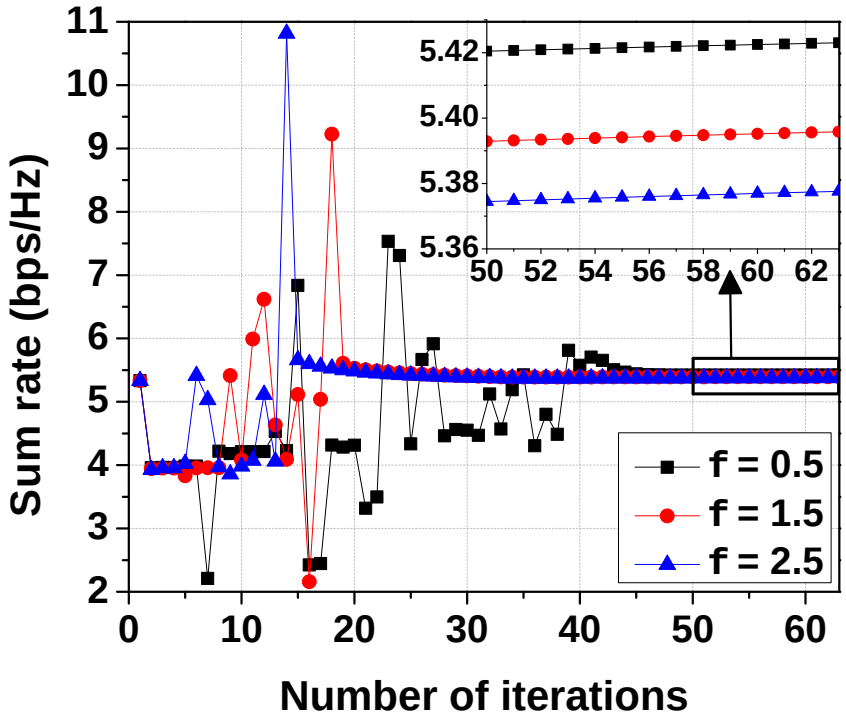

FIGURE 3.7: Sum rate vs. the number of iterations for various power gaps in the downlink NOMA network.

excluding the weakest, must meet the SIC process's power gap criterion (3.3b). The weakest user is provided the most power. Hence, this user directly decoded in the NOMA network's SIC procedure. Therefore, the weakest user is exempt from meeting the power gap condition

between decoded and non-decoded users. As a result, P_g does not affect the PA coefficient of the weakest user. Figure 3.8 illustrates the proposed method's transmit power versus total power budget (P_{BS}) for various weighting coefficients (ω). According to constraint (3.3d), when P_{BS}

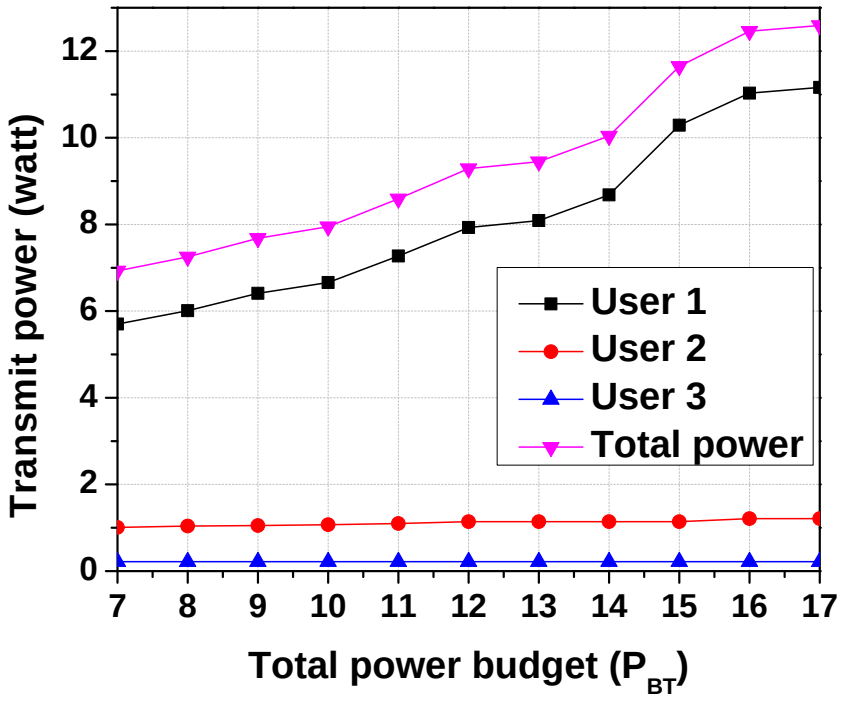

FIGURE 3.8: Transmit power vs. total power budget for downlink NOMA network.

increases, transmit power for all users should increase. However, because of the minimum power gap constraint (3.3b), all users except the weakest have limitations when it comes to increasing transmit power. As a result, we can see in Figure 3.8 that the transmit power for the weakest user grows rapidly while the transmit power for other users increases gradually. Figure 3.9 shows the sum rate against the total power budget for different weighting coefficients in the proposed method. According to the discussion mentioned above, when P_{BS} increases, so does the transmit power for all users. As a result, the network's overall rate increases.

3.5 Summary

This research presented a MOO method for investigating the trade-off between sum rate and user fairness in downlink communication NOMA networks incorporating the minimum power

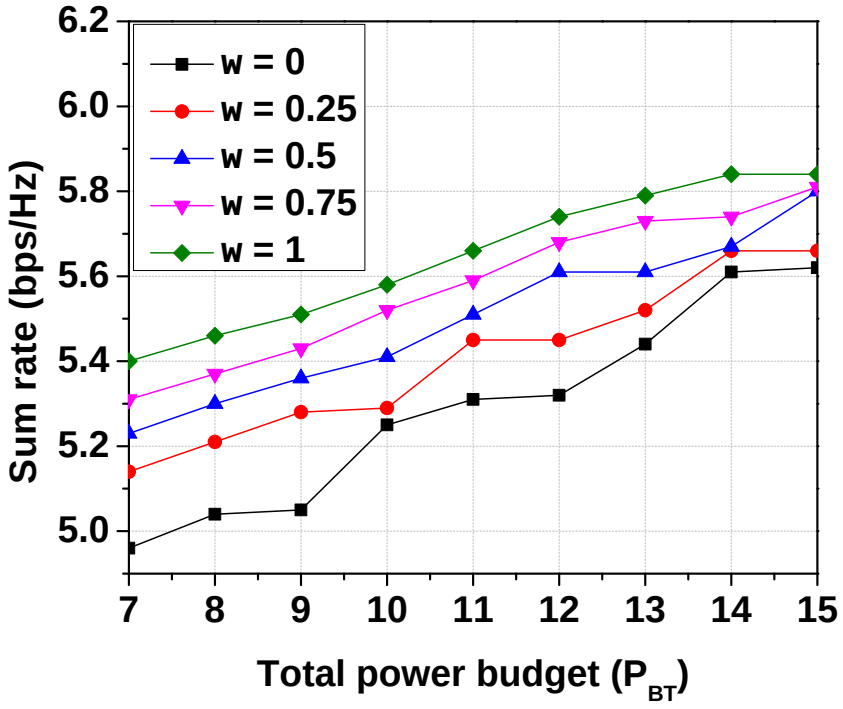

FIGURE 3.9: Sum rate vs. total power budget for various weighting coefficients in downlink NOMA network.

gap for successful SIC constraint. The study looks at a novel approach and demonstrates that the proposed method performs well in downlink NOMA networks. First, we formulated the MOO problem for jointly maximizing sum rate and user fairness while optimizing PA under a minimum power gap among users, transmit power, and QoS requirement constraints. Then, we converted a MOO problem to a single-objective optimization problem using the weighted sum method. In order to solve the optimization problem, we used the Lagrange dual decomposition method and the KKT conditions. Finally, simulation results show how downlink NOMA networks can maximize the sum rate and be fair to all users while maintaining a quick convergence rate for the proposed method. We also compared our method's performance to that of benchmark methods.

As 5G networks require more data rates, multiple access techniques are becoming more popular. Additionally, multiple access technique is needed to meet the rising bandwidth requirements. Hence, in addition to the PA optimization problems in Chapters 2 and 3, we will next move on to study the optimal SA problem in Chapter 4. In Chapter 4, we formulate and study the problem of determining optimal SA and PA for maximizing the sum rate.

Chapter 4

Joint Subchannel and Power Optimization for Sum Rate Maximization in Downlink Multicarrier NOMA Networks

For more than a century, wireless data traffic has grown at an exponential rate. The race for a faster data rate would continue, necessitating a 10x data rate increase every five years [14]. In the case of 5G, this refers to achieving a peak data rate of at least 1 GBPS when it launched in 2020. Next, it is expected to scale up to 10 GBPS in five years, and even 100 GBPS by 2030 [15]. Thus, the data rate of wireless networks must be increased in order to keep up with the rising demand for data rate in wireless networks. OFDMA has been widely investigated and implemented in 4G mobile communication networks for sum rate maximization [101], [102]. However, in OFDMA, orthogonal channel access can restrict spectral efficiency since one user per time slot can only access each subchannel. To enhance spectrum efficiency, NOMA enables several users to be multiplexed on the same subchannel. As a result, the NOMA network can achieve a higher sum rate, potentially improving the system's overall throughput compared to the OMA network [54]. Therefore, in recent times, many researchers have been motivated to maximize the sum rate of the NOMA system. The maximization of the sum rate in the NOMA network massively depends on sharing appropriate transmit power from the BS to all the users. NOMA operates on the principle of sharing time-frequency resources among users by separating them into other domains [103]. The separation domain is split into power-based and code-based, resulting in

power-domain NOMA and code-domain NOMA mechanisms, respectively. In power-domain NOMA, different powers are given to the different users based on the channel conditions [104]. PA coefficients can be used to provide different power to different users. Therefore, PA is an essential tool for the sum rate maximization in the NOMA network.

In order to enhance spectrum efficiency, NOMA multiplexes users on the same subchannel; unfortunately, this leads to co-channel interference amongst the multiplexed users [105]. However, for the successful execution of SIC, a minimum power gap needs to be maintained among users [36, 98, 106, 107], which is included in our work. The world's future wireless network demand is expected to increase massive data traffic for networks. NOMA has recently received a lot of attention as a potential contender for future wireless networks. Therefore, multiple carrier techniques have become increasingly popular due to the increasing demand for high data rates in NOMA networks. Multiple access techniques are necessary to meet the rapidly growing bandwidth requirement. Further, expecting all users to share the same amount of bandwidth may be impractical in terms of complexity. In certain cases, the problem of using the whole available bandwidth by all users may become prohibitive [37]. Consequently, NOMA can leverage multicarrier systems to create practical wireless communication networks. Multicarrier NOMA enables a limited number of users to use a subset of subcarriers at the same time. In such a scenario, it is clear that SA and PA are inextricably linked, with both having an influence on the overall system rate. Also, to prevent the imminent spectrum crisis caused by limited bandwidth and a growing number of users, an efficient method for adaptive bandwidth and PA is needed [37]. In this regard, this chapter seeks to determine SA and PA for the NOMA downlink network to maximize the sum rate while maintaining the total power budget, quality of service minimum power gap for SIC, subchannel user limit, and QoS constraints.

4.1 Related Work

We begin by discussing papers on the PA for sum rate maximization under SIC constraint. Authors in [106] analyze the power budget, QoS, and minimum power gap constraints in order to optimize the sum rate for both downlink and uplink NOMA networks. The optimal PA, resource blocks, and user groups are found in the cluster. A MOO problem is formulated in

paper [36] to maximize rate and minimize transmission power for a downlink NOMA network with constraints on minimum rate requirement, power budget, and minimum power gap. The objective of the paper [98] is to improve the fairness of data rates across users while optimizing PA in a NOMA system while taking into account QoS, power budget, and minimum power gap constraints. Paper [107] formulated and solved the PA technique for improving the spectral efficiency of NOMA-enabled IoT devices under the transmit power, QoS, and minimum power gap constraints. The work in [65] formulates and studies the optimization problem of PA and user scheduling to maximize the weighted sum rate. A downlink multi-carrier NOMA network's power budget and SIC error constraints are included.

SA and PA are interconnected factors contributing to high system performance in multicarrier NOMA systems. Thus, we next discuss SA and PA optimization works in the NOMA network for sum rate maximization. The authors of the study [37] maximize energy efficiency and user fairness by optimizing SA and PA and providing power budget and QoS constraints. The optimization problem is split into two stages, SA and PA, to reduce computational complexity. In paper [108], the authors maximized sum rate, energy efficiency, and maximin fairness in downlink NOMA network with joint optimization of PA and SA under QoS and power order constraints. The work [109] proposed a joint SA and PA optimization problem to maximize weighted sum rate utility in a downlink NOMA network with a total power budget, individual power restriction for each user, and the maximum number of multiplexed users on each subchannel. The manuscript [110] investigates SA and PA to balance the sum rate improvement and the power consumption in downlink NOMA networks. The Lyapunov optimization method solves this problem with minimal user QoS and maximum transmit power constraints. The problem of SA and PA to maximize sum rate in NOMA heterogeneous small cell networks is investigated in [111], taking into account energy harvesting and cross-tier interference. The objective of the paper [112] is to optimize the sum rate of the NOMA heterogeneous network, including macro and small cells, by assigning subchannels and power following total power, QoS, and cross-tier interference requirements. The manuscript [113] studied the PA and SA optimization problem to maximize the sum rate utility for downlink NOMA networks, considering individual and overall power budgets and the maximum number of users multiplexed on each subcarrier. The work [114] examined the SA and PA method for the sum rate of cognitive NOMA systems that takes channel uncertainty and user's QoS, interference temperature, and

transmission power constraints. NOMA-based IoT has been presented in an article [115] as an optimization problem of achievable rate for optimizing user clustering, PA, and bandwidth allocation to minimize the number of channels while meeting the QoS requirements. The authors of the research [116] formulated the problem of maximizing overall system capacity and spectral efficiency by optimizing the SA and PA in the downlink NOMA system. The paper [117] aims to maximize the weighted total sum rate in a downlink NOMA system by optimizing the SA and PA while considering user fairness. The optimal joint PA and SA approach for multicarrier NOMA systems under power constraint and maximum users on each subchannel constraint is studied in the paper [118]. The paper [119] investigates the PA and SA schemes for maximizing total system capacity and user fairness in multicarrier NOMA systems with energy harvesting. An efficient user scheduling and PA problem for sum rate maximization is investigated in [120] for multi-mell, multicarrier NOMA networks. The problem is separated into two subproblems. The user scheduling for fixed power is the first problem, and PA is the second problem. Work [121] addresses the optimization problem of user association, transmit PA, sub-channel assignment, and multiple access technique selections for hybrid OMA-NOMA Wireless Networks to optimize the sum rate under a minimum rate requirement and power constraints.

There have been some recent works for sum rate maximization. The maximum sum rate is obtained in the manuscript [122] by optimizing the phase matrix of the reconfigurable intelligent surface (RIS) subject to maximum power constraints of the RIS-aided uplink NOMA network with direct links. Due to the non-convexity of the problem, two methods have been proposed. Paper [123] studies the throughput and outage probability of coordinated direct and relay transmission (CDRT) based downlink NOMA with direct links to the near user and the far user. The author shows the importance of choosing the PA coefficient and target symbol rates to boost the near user throughput while ensuring the desired far user throughput. The work [124] studies the outage probability and ergodic sum rate of the NOMA-based overlay cognitive radio network for Industry 5.0 using Nakagami-m channels. The performance of an adaptive multi-user underlay NOMA network with multiple near-users and far-users is investigated in the paper [84]. The authors employ an intelligent user selection and switching between cooperative NOMA, non-cooperative NOMA, and OMA to ensure high throughput at the selected far user while ensuring the desired performance at the selected near user. The authors also show that careful

consideration of target rates and the PA coefficient is essential. A Joint Maximum-Likelihood detector guarantees reliable multi-user detection in the uplink IoT Single Input Multiple Output (SIMO)-NOMA system in work [125]. The authors proposed a scheme showing effectiveness in removing the error floor.

4.1.1 Motivation and Contributions

The papers [37, 108–121] maximize the sum rate by optimizing both SA and PA; however, the SIC constraint is ignored. Some articles investigated the SIC constraint but failed to consider SA and PA together to maximize the sum rate. In particular, articles [36, 65, 98, 106, 107] investigated maximizing sum rate while dealing with the SIC constraint and other constraints such as power budget, QoS, and minimum rate requirement constraints. However, these NOMA studies have not addressed the SA problem. In summary, to the best of our knowledge, existing works in the literature have ignored the optimization of SA and PA together, along with the SIC constraint for the sum rate maximization. Therefore, we are motivated to maximize the sum rate by optimizing SA and PA while adhering to the minimum power gap for SIC, QoS, power budget, and subchannel user limit constraints for the downlink multicarrier NOMA network.

The salient aspects of the Chapter are summarized as follows:

- We formulate and analyze the SA and PA optimization problem to maximize the sum rate while satisfying the power budget, QoS, subchannel user limit, and minimum power gap constraints in the downlink multicarrier NOMA network.
- We study the SA algorithms from articles [46–48] and associate them with our optimization problem $(P1)$ to obtain SA. We compare and examine the performance of each algorithm for our proposed method.
- Then, the PA solution is obtained using a linear optimization problem and concavity of the sum rate. In addition, we conclude that our solution is unique to the proposed method.
- We perform simulations as part of the validation process for our proposed optimization problem. Additionally, we compare the proposed method's performance to the benchmark method. We compare greedy [46], worst subcarrier avoiding (WSA) [47], worst case

avoiding (WCA), and worst case first (WCF) [48] algorithms performance to problem $(P1)$. We conclude that the WCF algorithm provides a higher sum rate of the NOMA network than greedy, WSA, and WCA algorithms for the proposed problem.

The rest of the Chapter is organized as follows. We present the system model and problem formulation in Section 4.2. In Section 4.3, we derive the SA and PA solution for the proposed optimization problem. Section 4.4 presents simulation results and relevant discussions for the proposed scheme. Finally, Section 4.5 provides concluding remarks.

4.2 Problem Statement

This section introduces the downlink NOMA network system model and formulates the optimization problem for maximizing the sum rate with SA and PA.

4.2.1 System Model

We consider a downlink multicarrier NOMA-based wireless network with N subcarriers and the total number of T^c users. Figure 4.1 illustrates SA for our downlink multicarrier NOMA network. In Figure 4.1, M^c represents the maximum number of users per subchannel and N

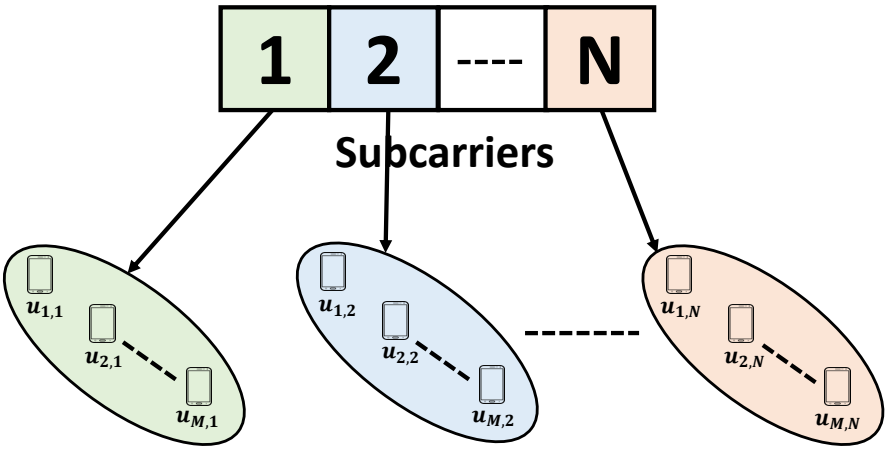

FIGURE 4.1: Subcarrier assignment for downlink multicarrier NOMA network.

stands for the number of subchannels, where $m \in (1,2,\cdots,M^c)$ and $n \in (1,2,\cdots,N)$. After assigning all users to subchannels, we employ the NOMA technique in each subchannel. We employ power-domain NOMA user multiplexing, with all users serviced simultaneously over the same frequency range [54]. The power-domain NOMA mechanism uses superposition coding at the transmitter and SIC at the receiver. Figure 4.2 depicts the SIC process in each subcarrier for our downlink NOMA network. The words subchannel and subcarrier are used interchangeably

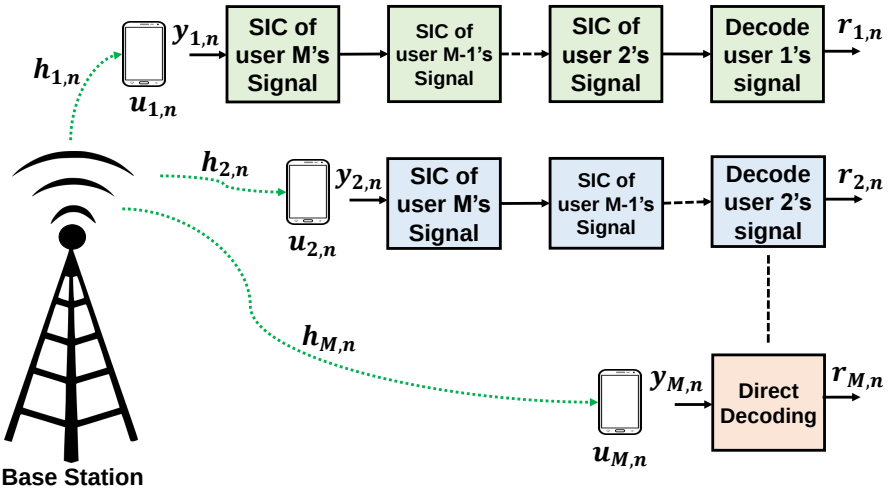

FIGURE 4.2: SIC process in each subcarrier for multicarrier downlink NOMA network.

in this Thesis. The network's total bandwidth is B_N Hz is split into N subchannels of subchannel bandwidth B_N^c, for each $n \in N$, such that $\sum_{n\in N} B_n^c = B_N$. We consider Rayleigh fading channel with channel coefficient between BS and user m on subchannel n is denoted by $h_{m,n} = z_{m,n} d_{m,n}^{-pl}$, where $d_{m,n}$ is the distance between BS and user m, and pl is the path loss exponent, and $z_{m,n}$ is a complex Gaussian distribution, $z_{m,n} \sim \mathscr{CN}(0,\,1)$ [37, 108]. We consider channels between BS and all users are independently distributed.

Without losing generality, we arrange channel coefficients between BS and all users on n^{th} subchannel in a descending order as $|h_{1,n}| \geq |h_{2,n}| \geq \cdots \geq |h_{M^c,n}|$. According to this order on each subchannel, at the NOMA network's transmitter side, each user's PA coefficient is first multiplied by the total transmit power, and then these signals are added together. The BS transmits a multiplexed signal on each subchannel n is given by,

$$X^c = \sum_{m=1}^{M^c} \sqrt{\alpha_{m,n} P^c}\, S_{m,n}^c, \tag{4.1}$$

where P^c denotes the total transmit power per subchannel. $\alpha_{m,n}$ is PA coefficient for user m on subchannel n, and $S^c_{m,n}$ is the symbol of user m on subchannel n. The SIC process is carried out on each subchannel on the receiver side of the NOMA network. In the SIC process, the data of the higher power user, i.e. user M, is first decoded directly, then the data of the next highest power user (user M^c-1) is decoded by canceling the interference generated from the previously decoded user (user M^c). This process continues until we have decoded all the user's data. The SIC method is illustrated in Figure 4.2. We can present the received signal to the m^{th} user over the n^{th} subchannel as given below,

$$r_{m,n} = h_{m,n} X^c_n + \eta_{m,n}, \tag{4.2}$$

where $\eta_{m,n} \sim \mathscr{CN}(0, \sigma^2)$. Thus, using the SIC working discussed above, the received signal $r_{m,n}$ for user m is represented by,

$$y_{m,n} = \left(\sqrt{\alpha_{m,n} P^c}\, S^c_{m,n} + \sum_{i=m+1}^{M^c} \sqrt{\alpha_{i,n} P^c}\, S^c_{i,n} \right) h_{m,n} + \eta_{m,n}, \tag{4.3}$$

The signal-to-interference and noise ratio (SINR) as seen by user m on subchannel n is then written as [108],

$$SINR_{m,n} = \frac{\alpha_{m,n} P^c \cdot |h_{m,n}|^2}{|h_{m,n}|^2 \cdot \sum_{i=1}^{m-1} \alpha_{i,n} P^c + \sigma^2}, \tag{4.4}$$

According to Shannon's capacity formula, the data rate of user m over subchannel n is written as [108],

$$R_{m,n} = B^c_N \log_2(1 + SINR_{m,n}) \quad \text{bps}. \tag{4.5}$$

4.2.1.1 Imperfect SIC

For SIC to be successfully executed at the user's end, the NOMA transmitter should ensure a minimal power gap between the user transmit powers [36]. If the minimal power gap is not maintained at the transmitter, errors may propagate and degrade the performance of the NOMA network (since each user's SIC depends on previous decodings). As a result, SIC residual error propagation can be considered in NOMA systems if the SIC is not executed perfectly. Therefore,

the SINR for imperfect SIC can be represented as [51, 65, 84],

$$SINR_m^{imper} = \frac{\alpha_{m,n} P^c |h_{m,n}|^2}{\sum_{i=1}^{m-1} \alpha_{i,n} P^c |h_{m,n}|^2 + \varepsilon \sum_{j=m+1}^{M^c} \alpha_{j,n} P^c |h_{m,n}|^2 + \sigma^2} \tag{4.6}$$

The residual interference component produced by this imperfection is quantified by the factor ε, which ranges from 0 to 1. Perfect SIC has an $\varepsilon = 0$, whereas fully imperfect SIC has an $\varepsilon = 1$.

4.2.2 Problem Formulation

In NOMA, signals for all users are superimposed at the transmitter and decoded at each user executing the SIC process. The SIC process decodes and subtracts the signals in sequence until it gets its desired signal. However, the decoding order for each user must match the user index in the cancellation sequence. In the case of a mismatch, users will not receive their signals. As a result, the SIC decoding order is a critical issue in SIC process execution, which we are addressing in this work. Let $\pi_{m,n} \in \{0,1\}$ represent the decoding order of user m on subchannel n. Based on this order, we can implement the SIC process. For user m, users $m+1$ to user M^c are removed with the SIC process, and then user m decodes its own signal. In this case, to guarantee that the SIC can be performed successfully, decoding order $\pi_{i,n}$, for $i = 1$ to $m-1$ must be assigned to 1, and $\pi_{i,n}$, for $i = m+1$ to M^c must be assigned to 0 for $|h_{m,n}|^2 \geq |h_{m+1,n}|^2, \forall m$. Otherwise, $\pi_{i,n}$, for $i = 1$ to $m-1$ must be assigned to 0, and $\pi_{i,n}$, for $i = m+1$ to M^c must be assigned to 1. Hence, SINR for user m on subchannel n can be written as,

$$SINR_{m,n} = \frac{\alpha_{m,n} P^c |h_{m,n}|^2}{\pi_{m,n} |h_{m,n}|^2 \sum_{i=1}^{m-1} \alpha_{i,n} P^c + \pi_{m,n} |h_{m,n}|^2 \sum_{i=m+1}^{M^c} \alpha_{i,n} P^c + \sigma^2}, \tag{4.7}$$

We can now formulate an optimization problem $(P1)$ for obtaining SA and PA in the downlink NOMA network, taking into account practical considerations such as subchannel users limit, QoS, power budget, and minimum power gap constraints, as follows:

$$(\text{P1}) : \max_{\mathbf{S},\alpha} \sum_{n=1}^{N} \sum_{m=1}^{M^c} s_{m,n} R_{m,n}, \tag{4.8a}$$

$$\textbf{s.t. } \text{C}_1 : R_{m,n} \geq R_{min}, \ \forall m, n, \tag{4.8b}$$

$$\mathrm{C}_2 : s_{m,n}\alpha_{m,n}P^c \left|h_{m-1,n}\right|^2 - \sum_{i=1}^{m-1} s_{i,n}\alpha_{i,n}P^c \left|h_{m-1,n}\right|^2$$

$$\geq P_g, \text{for } m = 2,3,\cdots,M^c, \forall n, \tag{4.8c}$$

$$\mathrm{C}_3 : \sum_{m=1}^{M^c} s_{m,n}\alpha_{m,n}P^c \leq 1, \forall n, \tag{4.8d}$$

$$\mathrm{C}_4 : \sum_{m=1}^{T} s_{m,n} \leq M^c, \forall n, \tag{4.8e}$$

$$\mathrm{C}_5 : s_{m,n} \in \{0,1\}, \forall m,n. \tag{4.8f}$$

where $\mathbf{S} = [s_{m,n}]_{T\times N}$ stands for SA matrix and $s_{m,n}$ is an element of $\mathbf{S}$ that becomes one if user m is multiplexed on subcarrier n and zero otherwise, $\alpha = [\alpha_{m,n}]_{M\times N}$ denotes the PA matrix and $\alpha_{m,n}$ is an element of α. In the context of QoS, constraint Eqn. (4.8b) implies the requirement that the data rate of each user must not fall below the minimum user data rate R_{min}. The constraint in Eqn. (4.8c) ensures the minimum power gap required for the successful execution of the SIC process in NOMA for each subchannel n. P_g is the minimum required power gap. According to Eqn. (4.8d), the total power of all users on a subchannel is less than or equal to P. Eqn. (4.8e) guarantees that a single subcarrier can support up to M^c users. Finally, Eqn. (4.8f) employs a subcarrier assignment variable.

4.3 Solution of Optimization Problem

The global optimal solution to an optimization problem $(P1)$ is difficult to find in polynomial time, so we no longer insist on having an efficient method to determine the global optimal solution in polynomial time. Instead, we should strive for approximation or locally optimal solutions in polynomial time, which is more feasible in practice [126]. According to [47,48,127], it is possible to achieve PA and SA of the optimization problem $(P1)$ by using separate power and subcarrier allocation without sacrificing much performance but significantly reducing implementation complexity. As a result, this Chapter implies that power and subcarrier distribution takes place in two stages. After SA, PA is done based on the channels of the subcarriers that have been assigned to various users.

4.3.1 Subchannel Assignment Scheme

This subsection presents a low-complexity SA algorithm based on the assumption of equal power across subchannels. The SA algorithm goal is to maximize the sum rate by efficiently allocating users to the subchannels. To do so, we studied the SA algorithms from [46–48] and associated them with our problem (P1). The greedy method is presented in paper [46], the WSA algorithm is proposed in the article [47], and WCA and WCF algorithms are presented in the article [48]. To demonstrate the functioning of each algorithm, we use a general channel quality matrix $\mathbf{H_{NT^c}}$ with a total of N subchannels to accommodate a total of T^c users in the network and a maximum of M^c users per subchannel. To begin, let us look at the greedy algorithm.

4.3.1.1 Greedy Algorithm

In the greedy method, a subcarrier is always assigned to M^c users who have the best channel characteristics among the remaining users who still need subcarriers. SA is performed sequentially from the first to the final subchannel. The first subchannel is assigned to M^c users who have the best channel quality for this subchannel. The next subchannel is then assigned to M^c users who have the best channel qualities among the remaining users. This process is repeated until the final subchannel is reached. In summary, the greedy algorithm is presented in the following algorithm 3. The reduced complexity of the greedy algorithm is a clear benefit. However, the

Algorithm 3 Greedy Algorithm

Initialize: $M^c, \mathscr{M} = \emptyset, \mathscr{N} = \{1,2,\cdots,N\}, \mathscr{T} = \{1,2,\cdots,T^c\}, \tilde{\mathscr{T}} = \mathscr{T}$
Repeat:
1) For each subchannel n_i, assign user t^* with best channel quality:
$t^* = \underset{t\in\tilde{\mathscr{T}}}{\operatorname{argmax}} \{h_{t,n_i}\}, n_i \in \mathscr{N}, \forall t.$
2) Remove user t^* from $\tilde{\mathscr{T}}$: $\tilde{\mathscr{T}} \leftarrow \tilde{\mathscr{T}} - \{t^*\}$.
3) Add user t^* to $\mathscr{M}$: $\mathscr{M} \leftarrow \mathscr{M} \cup \{t^*\}$.
Stop if $|\mathscr{M}| = M^c$.

algorithm may be forced to allocate users subchannels with extremely low channel quality later in the allocation process because of a lack of alternative possibilities.

4.3.1.2 Worst Subchannel Avoiding Algorithm

The WSA algorithm [47] ensures that users do not get subchannels with the worst channel quality. First, the channel with the worst quality is determined for each of the subchannels. Next, the subchannels are ordered ascendingly by their poorest channel qualities. As a final step, users are assigned subchannels from the first row to the last row, following the greedy algorithm's rules outlined in Section 4.3.1.1. In summary, the WSA algorithm can be described as shown in algorithm 4.

Algorithm 4 WSA Algorithm

Initialize: $M^c, \mathscr{N} = \{1,2,\cdots,N\}, \mathscr{T} = \{1,2,\cdots,T^c\}$
1) Find each subchannel's worst channel quality:
$h_{n_i}^{min} = \underset{t\in\mathscr{T}}{\text{argmin}}\{h_{t,n_i}\}, n_i \in \mathscr{N}$.
2) Arrange subchannels in ascending order according to the worst channel qualities as, $\{n_1, n_2, \cdots, n_N\}$, if $h_{n_1}^{min} \leq h_{n_2}^{min} \leq \cdots h_{n_N}^{min}$.
3) Based on the above order, apply the greedy algorithm to assign users to each subchannel.

4.3.1.3 Worst Case Avoiding Algorithm

We can classify the WSA algorithm as a subcarrier-oriented WSA algorithm because it can avoid assigning the $(N-1)$ worst channels when there are total N subchannels [47]. When the WCA algorithm is in use, it always tries to stay away from the worst subchannels as much as it can. The WCA algorithm avoids more bad subchannels than the subcarrier-oriented WSA algorithm. When the WCA algorithm is used, it first places the users in ascending order based on their subcarrier's poorest channel quality. Then, the greedy algorithm is used to assign subcarriers to users one at a time, from the first to the last column. The WCA algorithm is provided, as shown in algorithm 5.

4.3.1.4 Worst Case First Algorithm

In the WCF algorithm, users are reordered based on the channel quality of available subcarriers. Specifically, at each step, the algorithm determines the unassigned user's worst channel quality using just the available subcarriers, rather than the worst channel quality using all available

Algorithm 5 WCA Algorithm

Initialize: $M^c, \mathscr{N} = \{1,2,\cdots,N\}, \mathscr{T} = \{1,2,\cdots,T\}, \tilde{\mathscr{N}} = \mathscr{N}$

1) Find each user's worst channel quality:
$h_{ti}^{min} = \underset{n\in\mathscr{N}}{\text{argmin}}\{h_{ti,n}\}, ti \in \mathscr{T}$.

2) Arrange users in ascending order according to the worst channel qualities as,
$\{t_1,t_2,\cdots,t_T\}$, if $h_{t_1}^{min} \leq h_{t_2}^{min} \leq \cdots h_{t_{T^c}}^{min}$.

3) Based on the above order, assign subchannels one at a time from the first user to the last user.
For t_i user, subchannel n^* is assigned as,
$n^* = \underset{n\in\tilde{\mathscr{N}}}{\text{argmax}}\{h_{t_i,n}\}, ti \in \mathscr{T}$.

4) Remove subchannel n^* from $\tilde{\mathscr{N}} : \tilde{\mathscr{N}} \leftarrow \tilde{\mathscr{N}} - \{n^*\}$, if subchannel n^* has been assigned to M users.

subcarriers, as the WCA algorithm does. In summary, the WCF algorithm can be stated as follows in algorithm 6.

Algorithm 6 WCF Algorithm

Initialize: $M^c, \mathscr{N} = \{1,2,\cdots,N\}, \mathscr{T} = \{1,2,\cdots,T\}, \tilde{\mathscr{N}} = \mathscr{N}, \tilde{\mathscr{T}} = \mathscr{T}, \mathscr{M}_n = \emptyset$

Repeat:

1) Find each user's worst channel quality:
$h_{ti}^{min} = \underset{n\in\tilde{\mathscr{N}}}{\text{argmin}}\{h_{ti,n}\}, ti \in \tilde{\mathscr{T}}$.

2) Find the user with a minimum of the worst channel quality:
$t^* = \underset{t\in\tilde{\mathscr{T}}}{\text{argmin}}\{h_t^{min}\}$.

3) Assign user t^* to the subchannel n^* with the best channel quality:
$n^* = \underset{n\in\tilde{\mathscr{N}}}{\text{argmax}}\{h_{t^*,n}\}, t^* \in \mathscr{T}$.

4) $\mathscr{M}_n \leftarrow \mathscr{M}_n \cup \{n^*\}$.

5) Remove user t^* from $\tilde{\mathscr{T}} : \tilde{\mathscr{T}} \leftarrow \tilde{\mathscr{T}} - \{t^*\}$.

6) Remove subchannel n^* from $\tilde{\mathscr{N}} : \tilde{\mathscr{N}} \leftarrow \tilde{\mathscr{N}} - \{n^*\}$, if subchannel n^* has been assigned to M users.

Stop if $\tilde{\mathscr{T}} = \emptyset$.

We can apply and evaluate the performance of each discussed algorithm for our problem. All of the algorithms presented so far provide an **S** matrix. Next, we can then proceed with acquiring the PA of users in each subchannel.

4.3.2 Power Allocation Method

Since the SA algorithms discussed in the previous Section 4.3.1 assigned all users to different subchannels, we can utilize this section to solve the PA of the optimization problem $(P1)$. As a consequence, using obtained $\mathbf{S}$ matrix, the PA optimization problem $(P2)$ can be expressed as follows,

$$\text{(P2)}: \max_{\alpha} \sum_{m=1}^{M^c} \sum_{n=1}^{N} s_{m,n} R_{m,n}, \tag{4.9a}$$

$$\textbf{s.t.}\ (4.8b), (4.8c), \text{and}\ (4.8d).$$

Our first step is to determine the solution of the PA coefficients for constraint (4.8b) and constraint (4.8c) on each subchannel. Next, we can evaluate the proposed method's PA coefficients for this common region on each subchannel. To get the solution of PA coefficients on constraint (4.8b) in the problem $(P2)$, we simplified constraint (4.8b) as shown below,

$$\frac{\alpha^{'}_{m,n} P^c \cdot |h_{m,n}|^2}{|h_{m,n}|^2 \cdot \sum_{i=1}^{m-1} \alpha^{'}_{i,n} P^c + \sigma^2} \geq \xi, \forall m$$

Here, $\alpha^{'}_{m,n}$ is the PA coefficient of user m on subchannel n for constraint (4.8b) in the problem $(P2)$, and ξ is the minimum target SINR, which is $\xi = 2^{R_{min}} - 1$. By substituting $\alpha_{m,n} = 1 - \sum_{\substack{i=1, \\ i \neq m}}^{M^c} \alpha_{i,n}$ into the above equation and solving, we get,

$$\xi \sum_{i=1}^{m-1} \alpha^{'}_{i,n} + \sum_{\substack{i=1, \\ i \neq m}}^{M^c} \alpha^{'}_{i,n} \leq (1 - \xi u_m), \forall m \tag{4.10}$$

Here, $u_m = \frac{\sigma^2}{P^c \cdot |h_{m,n}|^2}$. We have M^c equations with M^c unknown to M^c users on subchannel n for Eqn. (4.10). As a result, we may employ linear simultaneous equations to get the solution in all user's α. A matrix equation of linear simultaneous equations of the form $\mathbf{E} \cdot \alpha^{'}_{m,n} = \mathbf{F}$ can represent Eqn. (4.10). Where matrix $\mathbf{E}$ of size $M^c \times M^c$ is represented by Eqn. (4.11) and matrix

$\mathbf{F}$ of dimension $M^c \times 1$ is represented by Eqn. (4.12).

$$\mathbf{E} = \begin{bmatrix} 0 & 1 & 1 & \cdots & 1 \\ (1+\xi) & 0 & 1 & \cdots & 1 \\ (1+\xi) & (1+\xi) & 0 & \ddots & 1 \\ \vdots & \ddots & \ddots & \ddots & \vdots \\ (1+\xi) & (1+\xi) & (1+\xi) & \cdots & 0 \end{bmatrix} \tag{4.11}$$

$$\mathbf{F} = \begin{bmatrix} 1-\xi u_1 & 1-\xi u_2 & 1-\xi u_3 & \cdots & 1-\xi u_{M^c} \end{bmatrix}^T \tag{4.12}$$

Where T is the matrix's transpose. Now, solving the above linear simultaneous equations gives us the solution to the PA coefficients $\alpha'_{m,n}$. Matrix $\mathbf{E}$ is a non-singular matrix, as shown in Appendix I. As a result, the unknown matrix $\alpha'_{m,n}$ in the given system of linear simultaneous equations has a unique solution. The next step is to solve constraint (4.8c) in $(P2)$ to get the solution of constraint (4.8c) on the PA coefficients across subchannel n; the explanation is shown below.

$$\alpha''_{m,n} P^c \left|h_{m-1,n}\right|^2 - \sum_{i=1}^{m-1} \alpha''_{i,n} P^c \left|h_{m-1,n}\right|^2 \geq P_g, \text{for } m = 2,3,\cdots,M^c. \tag{4.13}$$

Here, $\alpha''_{m,n}$ is the PA coefficient of user m on subchannel n for constraint (4.8c) in $(P2)$. For user m on subchannel n, put, $\alpha_{m,n} = 1 - \sum_{\substack{i=1, \\ i\neq m}}^{M^c} \alpha_{i,n}$, solving, we get,

$$\left(2\sum_{i=1}^{m-1} \alpha''_{i,n} + \sum_{i=m+1}^{M^c} \alpha''_{i,n}\right) P^c \left|h_{m-1,n}\right|^2 \leq P^c \left|h_{m-1,n}\right|^2 - P_g, \text{for } m = 2,3,\cdots,M^c. \tag{4.14}$$

From Eqn. (4.14), we have $(M^c - 1)$ equations with $(M^c - 1)$ unknown to M^c users on subchannel n; and from constraint (4.8d) in the problem $(P2)$, we receive one more equation. Eqn. (4.14) may be written as a matrix equation with linear simultaneous equations of the form $\mathbf{G} \cdot \alpha''_{m,n} = \mathbf{H}$. Matrix $\mathbf{G}$ has a dimension $M^c \times M^c$ as shown in Eqn. (4.15), and matrix $\mathbf{H}$ has a dimension

$M^c \times 1$ indicated in Eqn. (4.16).

$$\mathbf{G} = \begin{bmatrix} 1 & 1 & 1 & \cdots & 1 \\ 2P^c\left|h_{1,n}\right|^2 & 0 & P^c\left|h_{1,n}\right|^2 & \cdots & P^c\left|h_{1,n}\right|^2 \\ 2P^c\left|h_{2,n}\right|^2 & 2P^c\left|h_{2,n}\right|^2 & 0 & \ddots & P^c\left|h_{2,n}\right|^2 \\ \vdots & \ddots & \ddots & \ddots & \vdots \\ 2P^c\left|h_{M^c-1,n}\right|^2 & 2P^c\left|h_{M^c-1,n}\right|^2 & 2P^c\left|h_{M^c-1,n}\right|^2 & \cdots & 0 \end{bmatrix} \tag{4.15}$$

$$\mathbf{H} = \begin{bmatrix} 1 & P^c\left|h_{1,n}\right|^2 - P_g & P^c\left|h_{2,n}\right|^2 - P_g & \cdots & P^c\left|h_{M-1,n}\right|^2 - P_g \end{bmatrix}^T \tag{4.16}$$

Now, solving the above linear simultaneous equations provides the solution to the PA coefficients $\alpha''_{m,n}$. Matrix $\mathbf{G}$ is a non-singular matrix, as demonstrated in Appendix J. As a result, the above system of linear simultaneous equations has a unique solution of unknown matrix $\alpha''_{m,n}$. The solution for each user of Eqn. (4.10) is less than or equal to the corresponding element of the $\alpha'_{m,n}$ matrix since we obtained the solution by choosing equal to rather than less than or equal to in Eqn. (4.10). Similarly, the solution for each user of (4.14) is less than or equal to the corresponding element of the $\alpha''_{m,n}$ matrix. The sum rate function is a concave-down and strictly increasing function for $\alpha_{m,n}$ (the proof is given in Appendix K). Consequently, the smaller between the corresponding element of α' and α'' is the PA coefficient for each user for maximizing the sum rate. Hence, we obtained the PA coefficient matrix α^* for maximizing the sum rate. In the context of the preceding description, we present algorithm 7 for determining the α^* over each subchannel to maximize the sum rate in a NOMA downlink communication system. In the algorithm 7, we first determine the SIC decoding order of the NOMA, followed by the SA and PA. We obtain decoding order $\pi_{m,n}$ from lines 4 to 8 in algorithm 7. The $\mathbf{S}$ matrix can be calculated using one of the greedy, WSA, WCA, or WCF methods in algorithm 7, line 9. In line 11 of algorithm 7, we calculated the upper limits α' and α'' for the constraints of $(P2)$. We can obtain α^* from lines 13 to 19 of algorithm 7. Thus, we achieve the maximum sum rate on the subchannel for α^* in the downlink NOMA network while adhering to power budget, QoS, and minimum power gap constraints.

Algorithm 7 Power allocation for each subchannel.

Requires: $\mathscr{R}$, P^c, M^c, N, R_{min}, P_g, σ^2, η, **E**, **F**, **G**, and **H**.
for $n = 1$ to $\mathscr{R}$ **do**
    Generate channel quality matrix;
    if $|h_{m,n}|^2 \geq |h_{m+1,n}|^2, \forall m$ **then**
        $\pi_{i,n} = 1$, for $i = 1$ to $m-1$, and $\pi_{i,n} = 0$, for $i = m+1$ to M^c;
    else
        $\pi_{i,n} = 0$, for $i = 1$ to $m-1$, and $\pi_{i,n} = 1$, for $i = m+1$ to M^c;
    end if
    Calculate **S** matrix using Greedy/WSA/WCA/WCF algorithm;
    Given $\mathbf{E} \cdot \alpha^{'} = \mathbf{F}$ and $\mathbf{G} \cdot \alpha^{''} = \mathbf{H}$;
    Compute matrix $\alpha^{'}$ and $\alpha^{''}$;
    for $n = 1$ to N **do**
        for $m = 1$ to M^c **do**
            if $\alpha^{'}_{m,n} \leq \alpha^{''}_{m,n}$ **then**
                $\alpha^{*}_{m,n} = \alpha^{'}_{m,n}$;
            else
                $\alpha^{*}_{m,n} = \alpha^{''}_{m,n}$;
            end if
        end for
        Find sum rate over n subchannel;
    end for
    Compute network's sum rate;
end for
Find mean of $\alpha^{*}_{m,n}$ and sum rate;

4.3.3 Complexity Analysis

This section analyzes the complexity of SA algorithms and the proposed algorithm. Our analysis assumes that $M^c \geq N$. The greedy algorithm finds M^c number of users for each subcarrier. The number of required operations for all M^c users allocation is $\frac{M^c(M^c-1)}{2}$. As a result, the greedy algorithm has a time complexity of $\mathscr{O}(M^{c2})$. The total number of operations for the WSA algorithm is about $N(M^c-1) + 2N\ln(N) + \frac{M^c(M^c-1)}{2}$, yielding a time complexity of $\mathscr{O}(M^{c2})$. The WCA algorithm orders the M users from worst to best channel qualities. This process requires $M^c(N-1) + 2M^c\ln(M^c)$ calculations. Then, $(M^c-N)(N-1) + \frac{N(N-1)}{2}$ operations are required for the SA. Hence, the number of operations required by the WCA algorithm can be expressed as $M^c(N-1) + 2M^c\ln(M^c) + (M^c-N)(N-1) + \frac{N(N-1)}{2}$. Hence, the WCA algorithm has $\mathscr{O}(M^cN)$ time complexity. The SA process of the WCF algorithm is the same as the WCA algorithm, except for the user order. The WCF algorithm requires

$M^c(N-1)+\frac{M^c(M^c-1)}{2}+\frac{(N-1)(N-2)}{2}+\frac{N(N-1)}{2}+(M^c-N)(N-1)$ number of operations. After solving, the time complexity of the WCF algorithm can be obtained as $\mathcal{O}(M^{c2})$. Table 4.1 summarises the time complexity of the above-discussed SA algorithms.

TABLE 4.1: Time complexity of various SA algorithms

Algorithm	Time complexity
Greedy	$\mathcal{O}(M^{c2})$
WSA	$\mathcal{O}(M^{c2})$
WCA	$\mathcal{O}(M^cN)$
WCF	$\mathcal{O}(M^{c2})$

We can now study algorithm 7's time complexity. The algorithm's time complexity is defined as the number of iterations and arithmetic operations performed. We have a maximum of M^c users in each subchannel of our NOMA network, which means that solving a system of linear simultaneous equations has a time complexity of at most M^{c3} on each subchannel. The overall time complexity of linear simultaneous equations is $M^{c3}N$ if N subchannels are in the system. The total number of iterations for the inner-most loop is M^c, whereas the total number of iterations for the inner loop (lines 7 to 16) is N. Hence, the loop's time complexity is equal to NM^c. The loop has a higher time complexity than the greedy, WSA, WCA, and WCF algorithms. As a result, our proposed algorithm's worst-case run time complexity is $\mathcal{O}(M^{c3}N)$.

4.3.4 Benchmark: Optimization Problem Without Minimum Power Gap Constraint

Section 4.2 discusses the optimization problem $(P1)$ for sum rate minimization in a downlink NOMA network with subchannel user's limit, QoS, power budget, and minimum power gap constraints. In order to understand the effect of the minimum power gap constraint, we have removed the minimum power gap constraint from $(P1)$; thus, this Subsection 4.3.4 presents an optimization problem $(P3)$ without minimum power gap constraint. As a result, Subsection 4.3.4 provides the optimization problem $(P3)$ as a benchmark for the optimization problem $(P1)$. In $(P3)$, we find the PA for sum rate maximization while keeping QoS, subchannel user's limit, and power budget constraints in mind. As a result, the optimization problem $(P3)$ may be

formulated as follows:

$$(\text{P3}): \max_{\alpha} \sum_{m=1}^{M^c} \sum_{n=1}^{N} s_{m,n} R_{m,n}, \tag{4.17a}$$

$$\textbf{s.t.}\ (6b), (6d), (6e) \text{ and } (6f).$$

We solve the optimization problem $(P3)$ using the same steps and method as in Section 4.3; as a result, all of the steps and explanations are overlooked due to the similarity in solving the optimization problem.

4.4 Simulation Results

This section presents and discusses computer simulation results for our proposed optimization problem $(P1)$. The simulation results of the benchmark method $(P3)$ are discussed in this section. In all the plots, markers denote computer simulation points. In addition, we present and compare simulation results of the greedy, WSA, WCA, and WCF algorithms in order to demonstrate their performance for our proposed and benchmark methods. Furthermore, our simulation results for the proposed method $(P1)$ give the most desirable power gap value for a successful SIC process for constraint (4.8c) and the most appropriate minimum rate requirement for constraint (4.8b). In the simulations, we consider one BS and nine users $(N = 9)$ who are uniformly distributed in the cell range with a radius of 1 kilometer (km) [128]. Three users $(M^c = 3)$ are allowed to use one subchannel at most. The BS uses the same transmit power of 1 W on each subchannel [128]. The performance parameters for all users are obtained in the simulation across 10^5 channel gain realizations of Rayleigh fading [36]. Then, we take the average of channel gain realizations of these performance parameters as shown in algorithm 7. We assume the minimum required power gap is 0.5 W [36]. Further, we assume that the path loss exponent is 3 and the minimum data rate for QoS is 1 bps/Hz [64]. Table 4.2 presents the simulation parameters used to generate the simulation results unless otherwise stated. Table 4.3 summarizes our proposed method's system parameters obtained in simulations for each subchannel for greedy, WSA, WCA, and WCF algorithms. As depicted in the Table 4.3, we present each user's PA coefficients and achievable rates in each subchannel employing greedy, WSA, WCA, and WCF algorithms. Additionally, the sum rate of each subchannel is shown. The sum of the PA coefficients and individual rates

TABLE 4.2: Required system parameters for the simulation.

System Parameter	**Values**
Channel realization $(\mathscr{R})$	10^5
Total number of users (T^c)	9
Number of subchannels (N)	3
Maximum number of users in each subchannel (M^c)	3
Transmit power from BS to each subchannel (P^c)	1 W
Noise power (σ^2)	10 mW
Minimum required power gap (P_g)	0.5 W
Minimum data rate for QoS (R_{min})	1 bps/Hz
Path loss exponent (pl)	3

TABLE 4.3: Simulation results obtained for the proposed method using greedy, WSA, WCA, and WCF algorithm in subchannels 1, 2, and 3.

System Parameter	**Greedy**			**WSA**			**WCA**			**WCF**		
	N1	N2	N3	N1	N2	N3	N1	N2	N3	N1	N2	N3
α^* of user 1	0.16	0.17	0.16	0.16	0.17	0.17	0.17	0.16	0.16	0.16	0.16	0.17
α^* of user 2	0.24	0.25	0.27	0.21	0.25	0.24	0.24	0.24	0.24	0.22	0.25	0.24
α^* of user 3	0.55	0.53	0.56	0.61	0.52	0.55	0.55	0.56	0.56	0.59	0.53	0.55
Rate of user 1	8.15	7.87	6.29	8.14	8.69	7.82	8.16	7.27	8.10	8.15	8.67	8.11
Rate of user 2	1.27	1.33	1.43	1.17	1.32	1.29	1.28	1.30	1.27	1.20	1.32	1.28
Rate of user 3	1.24	1.17	1.10	1.36	1.16	1.22	1.26	1.22	1.25	1.34	1.17	1.23
Sum rate	10.66	10.37	8.83	10.67	11.17	10.33	10.69	9.80	10.62	10.69	11.15	10.62
Network's totat rate	**29.86**			**32.16**			**31.11**			**32.47**		

in each subchannel, as indicated in Table 4.3, guarantees that constraints (4.8b), (4.8c), and (4.8d) are fulfilled. The JFI is a well-known quantitative measure of how well a given level of fairness is guaranteed among multiple users [93]. We use JFI to measure user fairness. The JFI of the proposed method with the greedy algorithm for subchannel $(N1)$, subchannel $(N2)$, and subchannel $(N3)$ are 0.55, 0.55, and 0.61, respectively. For the WCA algorithm, JFI for $N1$, $N2$, and $N3$ are 0.55, 0.57, and 0.55, respectively. Similarly, for the WSA and WCF algorithms, JFI for $N1$, $N2$, and $N3$ are 0.55, 0.53, and 0.55, respectively.

As depicted in Figures 4.3, 4.4, and 4.5 for subchannels 1, 2, and 3, respectively, the variation of sum rates with transmit power are demonstrated for various algorithms in the proposed method $(P1)$ and the benchmark method $(P3)$. Figures 4.3, 4.4, and 4.5 illustrates that when the transmit power of subchannels 1, 2, and 3 increases, the sum rate increases for all algorithms of proposed and benchmark methods. Since we have removed the minimum power gap constraint in the benchmark method $(P3)$, the sum rate of the benchmark method must be higher than the sum rate of the proposed method $(P1)$, as shown in Figures 4.3, 4.4, and 4.5. Note that as transmit

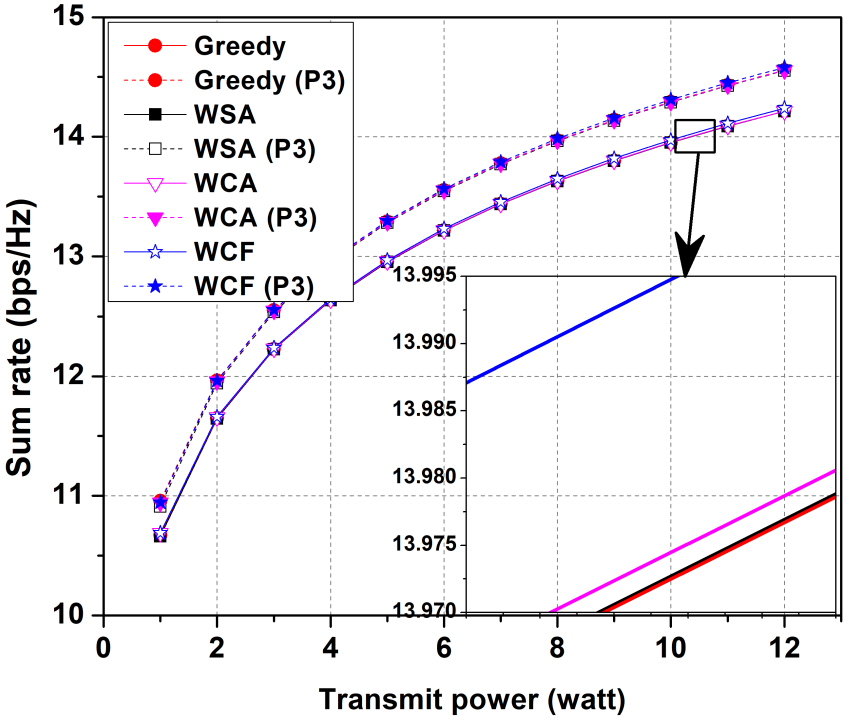

FIGURE 4.3: Sum rate against transmit power in subchannel 1 for proposed and benchmark methods in a downlink transmission NOMA network employing various algorithms.

power increases, the sum rate performance of all algorithms varies more. Hence, at 1 W transmit power ($P^c = 1W$), the subchannels have fewer variations in the sum rate. The WCF algorithm improves the greedy, WSA, and WCA algorithms, it outperforms them in subchannels 1, 2, and 3 for the proposed and benchmark methods, as shown in Figures 4.3, 4.4, and 4.5. Compared to the greedy algorithm, the WSA algorithm can prevent users from being assigned subchannels with the worst subchannel qualities. Thus, the WSA algorithm outperforms the greedy algorithm in all subchannels, as shown in Figures 4.3, 4.4, and 4.5. Compared to the WCA algorithm, the WCF algorithm has only differences in reordered users based on the channel quality of available subcarriers. Since users are selected from available subchannels, sometimes WCF has less circumstance of picking different users in available subchannels. Hence, WCA and WCF algorithms perform almost identically in subchannel 3 for the proposed method. However, the WCF algorithm outperforms the WCA algorithm in subchannels 1 and 2 for the proposed method. In the WCA algorithm, users are ordered based on their subcarrier's poorest channel quality, and then, WCA applies the greedy algorithm to assign subcarriers to users. Since subchannels are not ordered in WCA, subchannel 1 of the greedy and WCA algorithms has a larger chance of

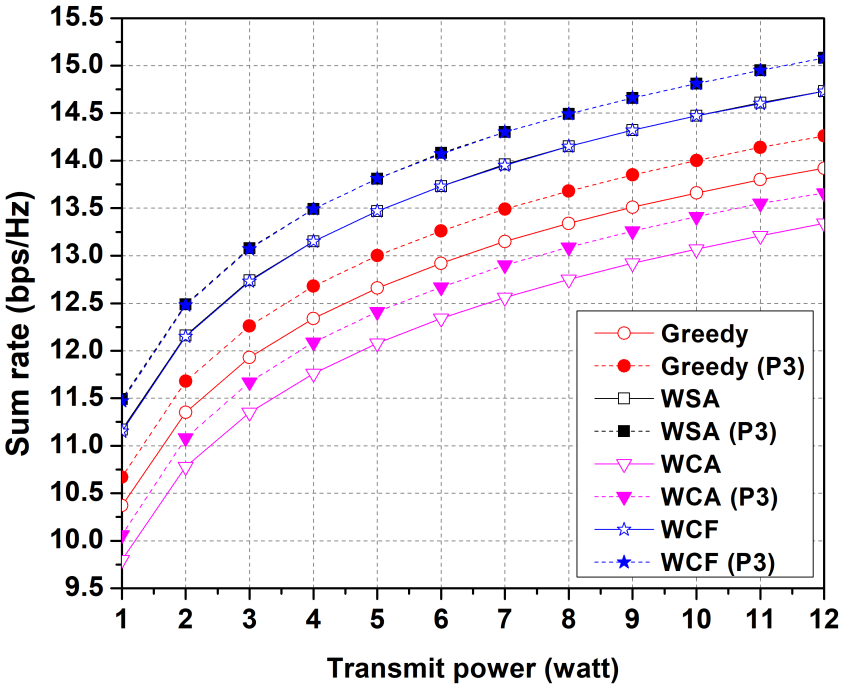

FIGURE 4.4: Sum rate versus transmit power in subchannel 2 for proposed and benchmark methods in a downlink transmission NOMA network employing various algorithms.

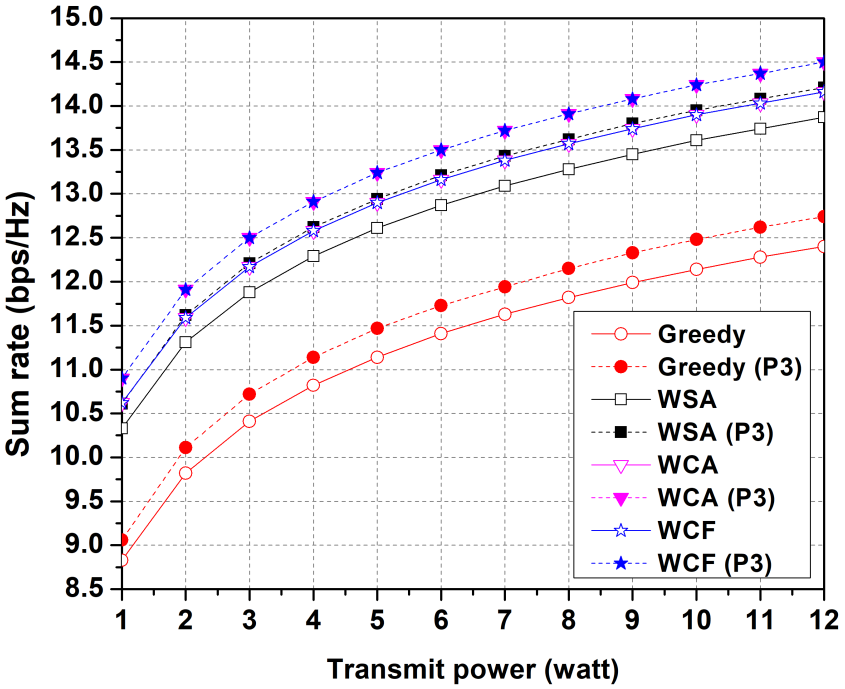

FIGURE 4.5: Sum rate versus transmit power in subchannel 3 for proposed and benchmark methods in a downlink transmission NOMA network employing various algorithms.

selecting the same users. As shown in Figure 4.3, WCA and greedy algorithms have a very small difference in sum rate. In subchannel 2, the WSA and WCF algorithms have identical results, and the WSA and WCF algorithms outperform the greedy and WCA algorithms (see Figure 4.4). The greedy and WSA algorithms are outperformed by the WCA and WCF algorithms in subchannel 3.

Figure 4.6 shows the sum rate comparison for each algorithm for subchannels 1, 2, and 3 for the proposed and benchmark methods. We compare how the algorithms perform in each subchannel

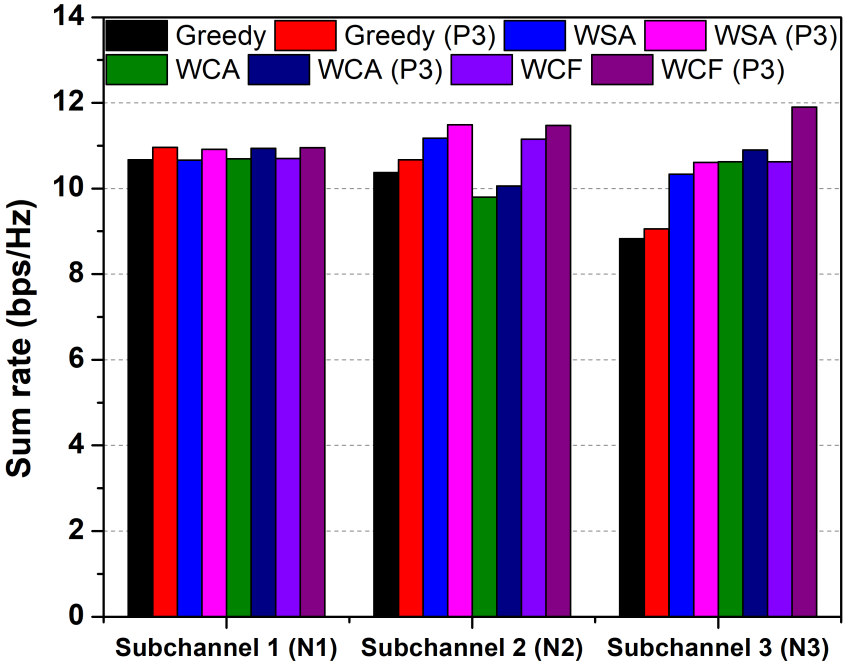

FIGURE 4.6: Sum rate comparison for each algorithm for subchannels 1, 2, and 3 for the proposed and the benchmark methods in the downlink NOMA network.

with respect to the sum rate achieved. Since the WCF algorithm is an improvement of the greedy, WSA, and WCA algorithms, it has a higher sum rate than the greedy, WSA, and WCA algorithms in subchannels 1, 2, and 3 for the proposed and benchmark methods, as shown in Figure 4.6.

Figure 4.7 depicts the sum rate as a function of power gap (P_g) for subchannels 1, 2, and 3 when the WCF algorithm is applied to the proposed method (P1). Figure 4.8 shows how the sum rate changes as a function of the minimum rate requirement (R_{min}) for subchannels 1, 2, and 3 when the WCF algorithm is used with the proposed method $(P1)$. According to Equations

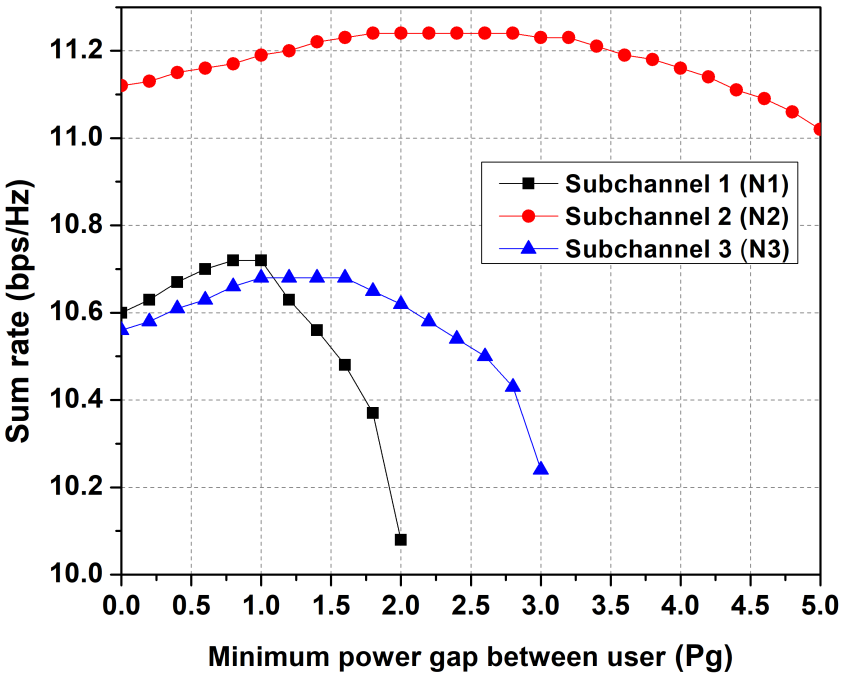

FIGURE 4.7: The sum rate as a function of power gap (P_g) for subchannels 1, 2, and 3 when the WCF algorithm is employed in the proposed method.

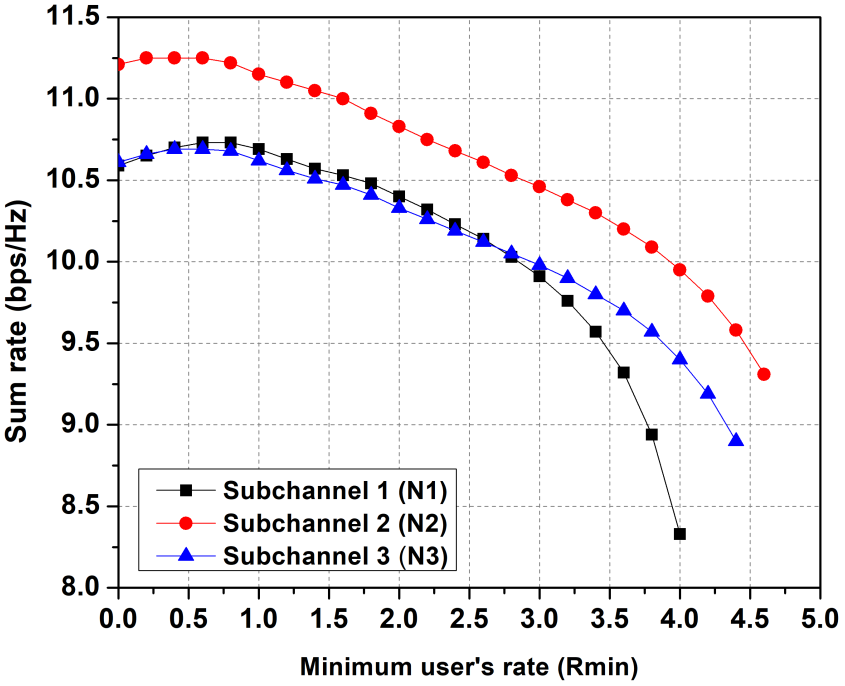

FIGURE 4.8: The sum rate as a function of minimum rate requirement (R_{min}) for subchannels 1, 2, and 3 when the WCF algorithm is employed in the proposed method.

(4.10) and (4.14), we have limitations on P_g and R_{min} for each subchannel. Hence as can be seen in Figures 4.7 and 4.8, we have different P_g and R_{min} limits on the horizontal axis for various subchannels. As indicated in Figures 4.7 and 4.8, the simulations are carried out in accordance with the valid range. PA coefficients can comfortably choose higher values until a specific value of P_g is reached. However, for higher P_g values, Eqn. (4.14) restricts the PA coefficients of users 1 to $m-1$ for user m. Hence, as seen in Figure 4.7, the sum rate for subchannels 1, 2, and 3 rises as P_g rises, then begins to fall as P_g increases more. Therefore, the NOMA system of the proposed method should have P_g set to $1W, 1.75W$ to $2.75W$, and $1W$ to $1.5W$ for subchannels 1, 2, and 3, respectively, in order for it to work nicely. Similarly, PA coefficients can choose higher values comfortably until a specific value of R_{min} is reached. However, Eqn. (4.10) restricts PA coefficients for higher R_{min} values. Hence, as illustrated in Figure 4.8, the sum rate for subchannels 1, 2, and 3 increases as R_{min} increases, then starts to drop as R_{min} increases further. For the proposed method to perform efficiently, the NOMA system should have R_{min} equal to 0.75 W, 0.55 W, and 0.75 W for subchannels 1, 2, and 3, respectively. With the discussion of figures 4.7 and 4.8, we have provided an appropriate power gap value for the minimum power gap constraint as well as the most suitable minimum user's data rate for the QoS constraint in each subchannel for the proposed method $(P1)$ in a downlink NOMA network.

In Figure 4.9, we plot the sum rate of all algorithms in subchannel 3 as a function of transmit power for two different residual components (using the imperfect SINR Eqn. (4.6)). As ε increases, residual interference increases for all users in the NOMA network (except the weakest user). Thus, the sum rate for the proposed method decreases. Therefore, as can be seen from the figure, $\varepsilon = 0.01$ has a higher sum rate than $\varepsilon = 0.05$. In subchannel 3, WCA and WCF have a very small variation in the sum rate for $\varepsilon = 0.05$, and WSA and WCA have a small variation in the sum rate for $\varepsilon = 0.01$ The sum rate for WCA and WCF algorithms in subchannel 3 is 10.62 for $\varepsilon = 0$ at $P^c = 1W$. WCA sum rate is 6.8423 for $\varepsilon = 0.01$, and 4.7436 for $\varepsilon = 0.05$ at $P^c = 1W$. The WCF sum rate is 6.8423 for $\varepsilon = 0.01$, and 4.7475 for $\varepsilon = 0.05$ at $P^c = 1W$. WCA and WCF sum rate decreases by 35.57% with a 1% increase in residual interference. WCA sum rate decreases by 55.33% with a 5% increase in residual interference, and the WCF sum rate decreases by 55.29% with a 5% increase in residual interference. 1% increase in residual interference results in 26.08% decrease, while 5% increase results in 47.88% decrease for the greedy algorithm. Likewise, from Figure 4.9, the WSA algorithm rate decreases significantly

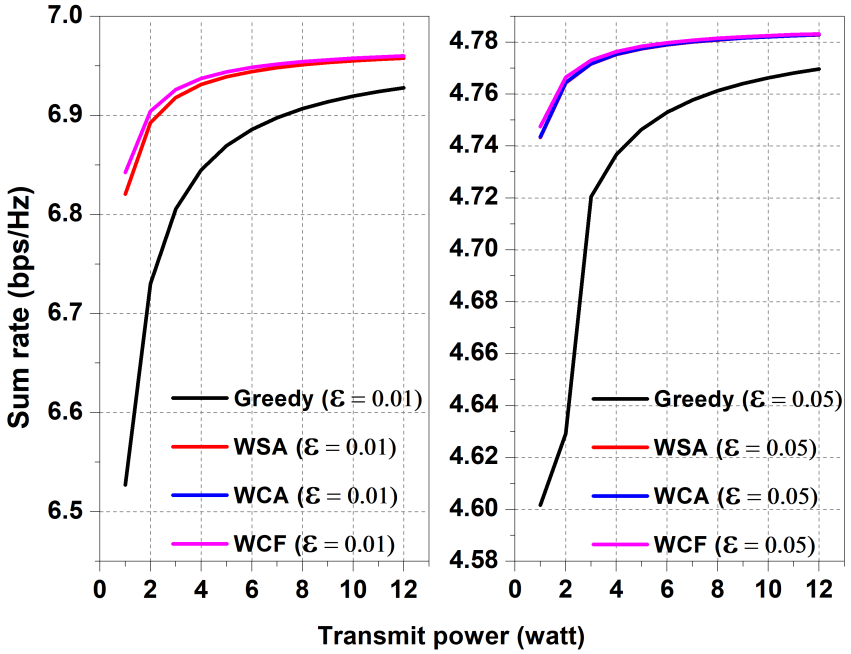

FIGURE 4.9: Sum rate vs. transmit power for two different residual components employing greedy, WSA, WCA, and WCF algorithms in subchannel 3 downlink NOMA network.

by imperfect SIC. Thus, SIC has a significant impact on the proposed method. As a result, considering the minimum power gap for the successful execution of SIC is crucial for the proposed algorithm.

Figure 4.10 shows the WCF algorithm's sum rate versus cell radius in km in subchannels 1, 2, and 3. We consider Rayleigh fading channel denoted by $h_{m,n} = z_{m,n} d_{m,n}^{-pl}$, where $d_{m,n}$ is the distance between BS and user m and $z_{m,n} \sim \mathscr{CN}(0, 1)$. As distance varies, the channel coefficient changes. Hence, the NOMA network's sum rate changes. The distance varies from 0.3 km to 1.2 km, and the sum rate for the WCF algorithm is plotted. The results demonstrate that, as expected, the sum rate decreases with an increase in distance. The subchannel $N2$ sum rate is always higher than the subchannels 1 and 3, regardless of distance.

Figure 4.11 depicts the sum rate versus the number of subchannels (N) employing the WCF algorithm for the proposed method with nine users $(T^c = 9)$. As the number of subchannels increases, users can recommend themselves to subchannels with better sets of preferences in order to obtain a higher rate. Hence, the sum rates increase as the number of subchannels increases in Figure 4.11.

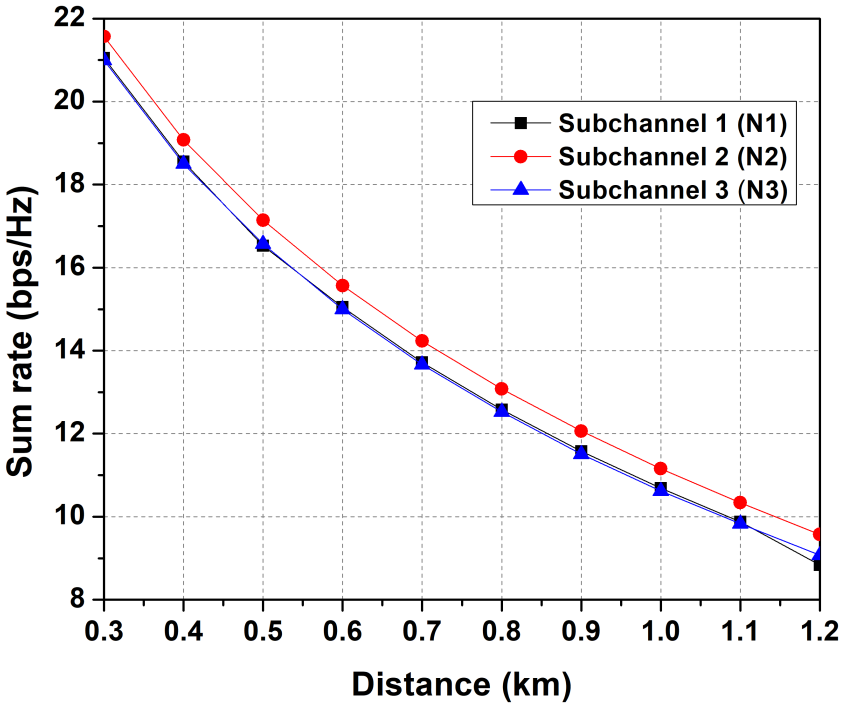

FIGURE 4.10: Sum rate vs. cell radius in subchannels 1, 2, and 3 for WCF algorithm.

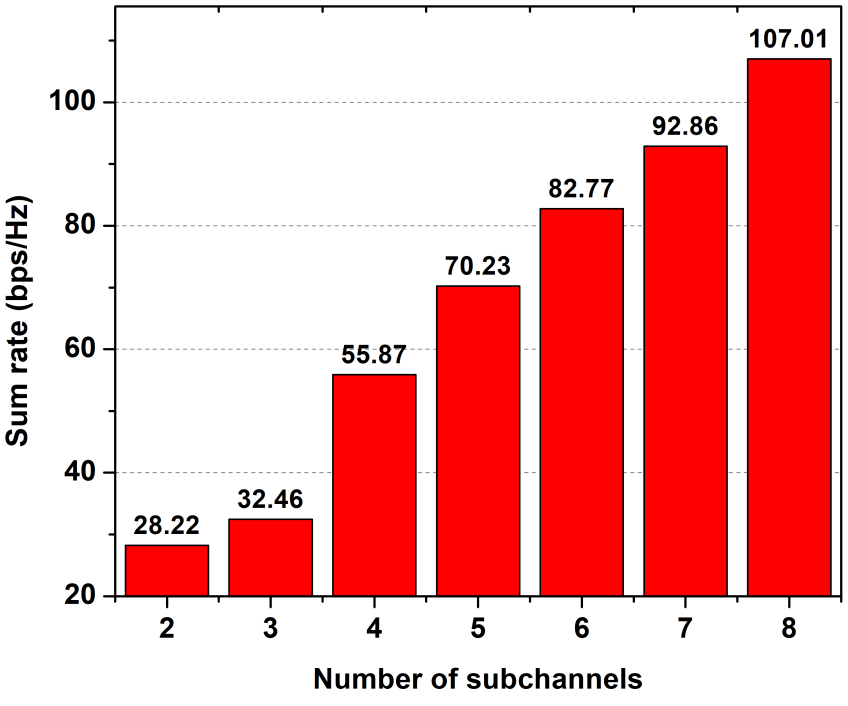

FIGURE 4.11: Sum rate versus the number of subchannels (N) employing the WCF algorithm for the proposed method

4.5 Summary

We formulated and analyzed an optimization problem to maximize the sum rate supporting the transmit power budget, QoS, minimum power gap, and maximum users per subchannel

constraints while optimizing the SA and the PA for the downlink multicarrier NOMA network. We framed the SA and PA as two-stage problems to ensure that the proposed method can be solved in polynomial time. To obtain the SA, we investigated various algorithms. After obtaining SA, the upper bounds for QoS and minimum power gap constraints for each subchannel are computed separately. Then, the common region between these two upper limits is used to determine the PAs. We proved that our solution is unique. Finally, a fast and low-complexity algorithm is proposed to solve the optimization method. We presented simulation results for the proposed method and analyzed the results of the proposed scheme with the results of the benchmark scheme. We also compared the performance of several SA algorithms for the proposed method. In the future, we aspire to improve the energy efficiency of our proposed method for the study of NOMA-based downlink transmission.

Conventional wireless communication technologies cannot meet the essential requirements of 5G wireless networks; therefore, developing new technologies for 5G networks is necessary [23]. In recent years, NOMA and HetNet have been recognized as emerging technologies for developing critical requirements. Chapters 2, 3, and 4 focus on the NOMA technique that enhances essential parameters of the wireless network, like sum rate and user fairness. Chapter 5 focuses on HetNet, the potential technique employed to increase the coverage probability parameter of the wireless network.

Chapter 5

Power Control Algorithm to Improve Coverage Probability in Heterogeneous Networks

One of the main components of 5G technology is the deployment of small cells in the cellular network, called a HetNet [129]. The objective of deploying such small cells is to improve essential features like indoor coverage, user performance at cell-edge, spectrum efficiency using spatial reuse, energy consumption, and capacity. In HetNet, low-power small cells (Microcell, Picocell, and Femtocell) are overlaid with a large-power macrocell. Due to network densification, intense proliferation, and the same frequency used in all cells, interference in the HetNet increases [44, 130]. Consequently, the coverage performance of the cellular network decreases. Hence, interference is one of the leading performance controlling factors in the network [131]. In this work, we mitigate this problem.

5.1 Related Work

In [132], the authors derive the coverage probability of the network by considering blockage, the directionality of the antenna, different fading distributions, and various tiers. In [133], the coverage probability of the wireless network by considering the association of MIMO antennas

with heterogeneous networks is obtained. Paper [133] provided opportunities for researchers to collaborate MIMO with heterogeneous networks to work on coverage probability. The distribution of BSs modeled as PPP or a Matérn hard-core point process (MHCPP) is matching with today's real-life BS distribution scenarios. Compared with the PPP model, where base stations are randomly distributed without restriction, the MHCPP model constructed from a PPP imposes a minimum distance between two BSs so that they are not too close. The BS distribution using PPP is one of the most attractive models for obtaining coverage probability. Hence, active work has been carried out for computation of coverage probability considering BS deployment as PPP [42, 134]. In [42], the authors derived and analyzed coverage probability for K-tier heterogeneous networks with the PPP distribution of BSs. This paper investigated both open and closed access conditions of the network. However, in paper [135], the authors modeled and analyzed coverage probability in HetNet with PPP applied for macrocell BS distribution and the Poisson-point cluster process (PPCP) used for small cell BS distribution. In the article [136], the authors obtained coverage and interference in D2D networks with the PPCP BS deployment. In the paper [137], the coverage probability is increased for nonuniform deployment compared to the uniform deployment of small cells. In [137], the small cell BSs are only located in the uncovered region (outer region) of the macrocell BS, and they are not located in the covered area (inner region) of the macrocell BS. Moreover, there are several methods to reduce interference and improve the performance of coverage in the network. Inter-cell interference coordination (ICIC) and intra-cell diversity (ICD) improve coverage of the cellular network [138]. In the paper [139], the power control algorithm is used to reduce interference and improve the coverage probability of HetNet.

The transmission power level of macrocell and small cells plays a vital role in interference and coverage performance in HetNet. Over the past several years, transmission power has been the most crucial aspect in the management of interference in both the uplink and downlink of cellular networks. The higher transmission power of smaller cells may contribute to better QoS but, at the same time, may cause sufficient interference to other neighboring users of adjacent cells in the network and may lead to degradation in coverage performance. However, a precise selection of transmit power in the small cells can help in the management of interference in the network [139–141]. In [140], the authors use game theory to reduce the power consumption of femtocell BS and hence improve SINR and outage probability performance for femtocell

users of HetNets. In this work [140], the authors repeated the steps of the decision in an almost predictable way to reach a final decision. In the article [139], authors designed a power control algorithm to update the transmission power and improve the coverage probability of interference-limited networks (ignored noise) of [42]. Taking inspiration from their work, we have proposed a power control algorithm for K-tier heterogeneous networks to update the transmit power to increase the coverage probability of interference-limited networks of [42]. In the algorithm, we renew the transmit power of small cells in such a way that it minimizes the interference of another user served by the network. Our proposed algorithm for power control improves the coverage probability more than [139]. Moreover, the convergence rate of our proposed algorithm is higher than the convergence rate of paper [139].

The rest of this Chapter is structured as follows. The system model for the HetNet is described in Section 5.2. In Section 5.3, we introduce the proposed power control algorithm. In Section 5.4, we present simulation results for the validation of theoretical analysis.

5.2 System Model

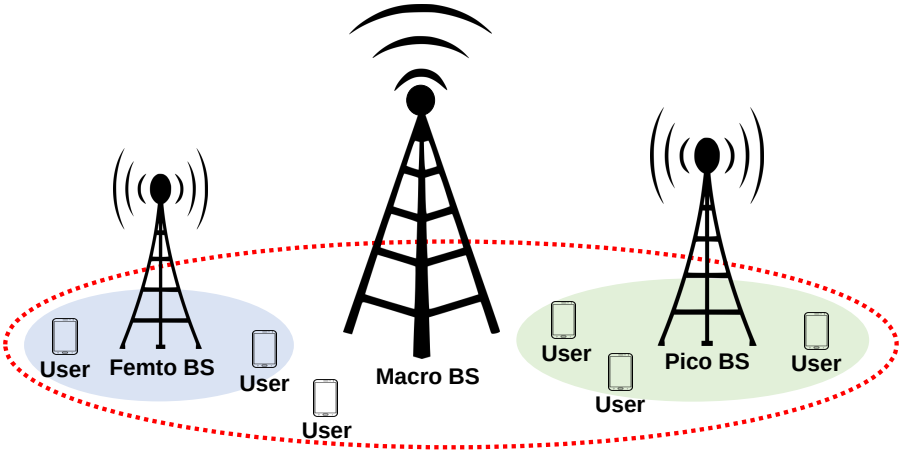

FIGURE 5.1: Representation of a three-tier HetNet consisting of a composite of macro, pico, and femto BSs. Only a single macrocell is shown in the Figure.

Figure 5.1 illustrates the three-tier HetNet. Here, we investigate three types of cells: macrocell, picocell, and femtocell. Each tier BS differs in terms of the transmit power, target SINR, and

density of the BS in the HetNet [42]. Microcells have the highest and femtocells have the lowest coverage areas, and picocells have a coverage area in their midst [43]. The transmission power of each cell depends on the coverage area provided by the particular cell. Large-power macrocell BS provides a larger coverage area (a few km), hence requiring high transmit power (40 W to 100 W) at the BS. Low-power femtocell BS provides a smaller coverage area (less than 100 m) and hence requires low transmit power (less than 200 mW) at the BS. Picocell BS provides 100 m to 200 m coverage area, hence requiring 250 mW to 1 W transmit power [44, 45]. The coverage area of small cells increases when they are away from the macrocell BS. Therefore, whenever macro cell coverage is insufficient, small cells play an essential role in improving coverage [42].

We use stochastic geometry to model the system, BSs in the i^{th} tier are spatial distributed in $\mathbb{R}^2$ as a PPP Φ_i of density λ_i, transmit power P_i^{sc}, and target SINR T_i [42]. In Figure 5.2, we provide

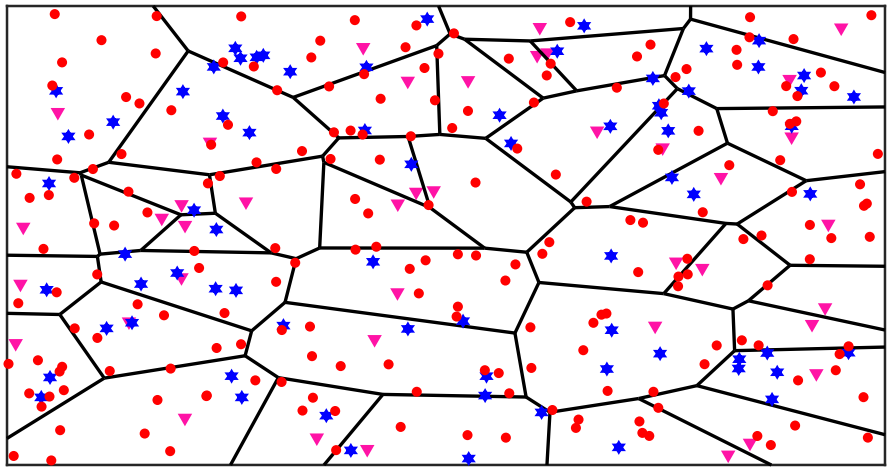

FIGURE 5.2: The system model shows coverage regions for the Three-Tier Heterogeneous Network. Macrocells are indicated by triangles (Pink), Picocells are indicated by stars (Blue), and Femtocells are indicated by circles (Red).

transmitting power to microcells, picocells, and femtocells. Standard values are 50 W, 2 W, and 0.2 W for microcell, picocell, and femtocell, respectively. In system model, BSs of Macrocell, Picocell, and Femtocell are distributed with densities of $\lambda_1, \lambda_2, \lambda_3$, where $\lambda_2 = 2\lambda_1, \lambda_3 = 5\lambda_1$. In our two-dimensional (2D) system model, the BSs are distributed according to the PPP, and Voronoi tessellation is applied to obtain the coverage area of the BS. Voronoi tessellation is the most useful method to obtain a random coverage area of cells in a system model of plane

$\mathbb{R}^2$ [142]. In our model, $i \in \{1,2,3\}$, where i = 1 indicates macrocell. In 2-tier networks, i = 2 indicates femtocells, and in 3-tier networks, i = 2 and 3 indicate picocells and femtocells, respectively. Hence, each tier can uniquely characterized by the tuple $\{P_i^{sc}, T_i, \lambda_i\}$. We organize a conventional mobile user to reside at the origin. The fading coefficient between the user and BS is denoted by h_x and $h_x \sim exp(1)$ is Rayleigh fading with mean 1, and assumed as independent and identical distribution (IID). $\|x_i\|^{-pl}$ is the standard path loss function, pl indicates the path loss exponent, and typically it is greater than 2. We use the same path loss exponent for all K-tier HetNet. From the previous assumptions, the received power by a user located at the origin, from the BS at location $x_i \in \Phi_i$ in the i^{th} tier is represented by [42]:

$$P_r = P_i^{sc} h_i \|x_i\|^{-pl} \tag{5.1}$$

Considering that the user connected to BS of location x_i, then resulting received SINR can then expressed as [42]:

$$\text{SINR}(x_i) = \frac{P_i^{sc} h_i \|x_i\|^{-pl}}{\sum_{j=1}^{K} \sum_{x \in \Phi_j \setminus x_i} P_j^{sc} h_j \left\|x_j\right\|^{-pl} + \sigma^2} \tag{5.2}$$

The first term $\sum_{j=1}^{K} \sum_{x \in \Phi_j \setminus x_i} P_j^{sc} h_j \left\|x_j\right\|^{-pl}$ in the denominator denotes the aggregate interference from all other BSs, excluding the marked BS which is located at x_i, while the second term σ^2 represents the noise power. The coverage probability in a K-tier HetNet can be modeled as [42]:

$$P_c(\{P_i^{sc}\}, \{T_i\}, \{\lambda_i\}) = \mathbb{P}\left(\bigcup_{i \in \kappa, x_i \in \Phi_i} \text{SINR}(x_i) > T_i \right) \tag{5.3}$$

In the article [42], the authors obtained derivation of coverage probability for open access for the randomly located user, and the obtained result indicated as follows:

$$P_c(\{P_i^{sc}\}, \{T_i\}, \{\lambda_i\}) = \sum_{i=1}^{K} \lambda_i \int_{\mathbb{R}^2} e^m e^{\left(-\frac{\sigma^2 T_i}{P_i^{sc}} \|x_i\|^{pl}\right)} dx_i \tag{5.4}$$

where,

$$m = -c(pl) \left(\frac{T_i}{P_i^{sc}}\right)^{\frac{2}{pl}} \left\|x_i^2\right\| \sum_{n=1}^{K} \lambda_n P_n^{sc \frac{2}{pl}},$$

$$c(pl) = \frac{2\Pi^2}{pl} \csc\left(\frac{2\Pi}{pl}\right).$$

The coverage probability for the interference-limited network (no noise) at randomly resided user simplified to the following [42]:

$$P_c(\{P_i^{sc}\},\{T_i\},\{\lambda_i\}) = \frac{\Pi}{c(pl)} \frac{\sum_{i=1}^{K} \lambda_i {P_i^{sc}}^{\frac{2}{pl}} {T_i}^{-\frac{2}{pl}}}{\sum_{i=1}^{K} \lambda_i {P_i^{sc}}^{\frac{2}{pl}}} \tag{5.5}$$

5.3 Algorithm

Coverage probability (equation (5.4) and equation (5.5)) of HetNet is a concave up and monotonically decreasing function. The concave up and monotonically decreasing function must satisfy condition $T_2 \geq T_1$ [139]. Therefore, in the overall discussion, we pay special attention to the condition $T_2 \geq T_1$. In our proposed power control algorithm, we use different target Signal-to-Interference ratio (SIR) T_i for different tiers to make condition $T_2 \geq T_1$ realistic.

In paper [42] shows, each mobile user connects to its most strong BS instantaneously, i.e., to the BS that gives the largest received SINR. Mathematically, the typical user is in the coverage if the following condition is satisfied:

$$\max_{x \in \Phi_i} \text{SINR}(x) > T_i, i \in \{1,2,3\} \tag{5.6}$$

From equation (5.6), In a 2-tier network, the typical user has the selection choice to connect either femto BS or micro BS. Usually, a user connecting to the femto BS provides high throughput coverage in the indoor environment (where this is most required) and hence experiences better QoS compared to the micro BS [143]. To fulfill these, the SIR target of femto BS should be greater than or equal to the SIR target of micro BS, i.e., $T_2 \geq T_1$ [139]. Generally, the SIR provided by femto BS should be higher to maintain the above situation. Therefore, we need to increase the transmit power of the femtocell. However, increased femtocell transmit power can act as additional interference if the user has already connected to another cell (microcell), consequently causing a decrease in the coverage probability of the HetNet. In another case, decreasing the small BSs' transmit power mitigates network interference. As a result, other BSs provide improved SIR value to the user. Accordingly, the maximum SIR in equation (5.6) increases, and there is an improvement in the coverage probability of the network. Therefore, the

power control algorithm aims to decrease the transmission power of small BSs and ensure the SIR is still high but the energy consumption is low. In other circumstances, increasing the transmit power of macrocells improves the coverage probability of HetNet, and decreasing the transmit power of macrocells reduces the coverage probability of HetNet. However, there is very less impact on the coverage probability of the HetNet mentioned in equation (5.5). Hence, updating the transmit power of microcells in the HetNet is futile. The proposed power control system is shown in the Figure 5.3. In an iterative process of the power control algorithm, each time, the

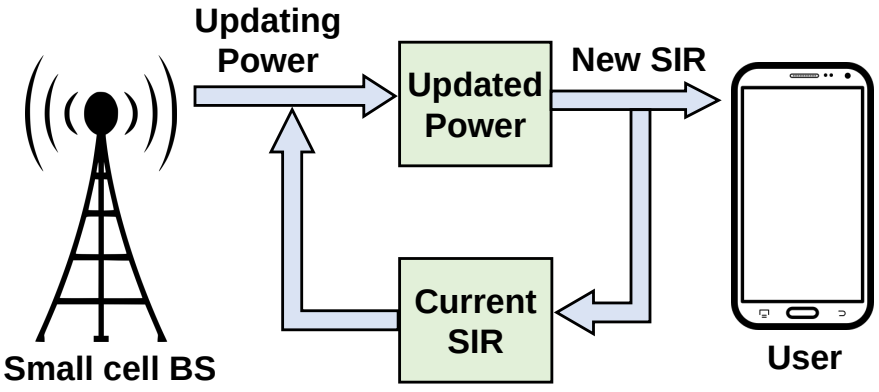

FIGURE 5.3: Power control system.

mobile user measures SIRs arriving from all small cell BSs of K-tier HetNet. After analyzing the current conditions of the network, the mobile user sends back these SIRs information to an appropriate BS for modification of existing power. Based on the current information from the mobile user, BSs update their transmit power, and again, mobile users get new SIRs from the BSs. Once again, the mobile user measures SIRs and sends back this information to BSs. This process continues until it starts converging to the SIRs. The convergence of SIR values in the iterations indicates that we have reached feasible SIRs where the network consists of the lowest interference in the network. In this manner, we approach optimal values of the transmit power of BSs where interference provided by each BS to other BSs is lowest. In the process, all these SIRs are satisfied at the same time.

The proposed power control algorithm for K-tier heterogeneous networks has been provided in this Chapter. Initially, we initialized the system parameters required in the network. In steps 7 to 17 of an algorithm, we updated the transmission power of all small cells present in the network,

Algorithm 8 Proposed power control algorithm in a K-tier heterogeneous network

Requires: $\{\lambda_1, \lambda_2, \cdots, \lambda_K\}$, $\{T_1, T_2, \cdots, T_K\}$;
Requires: $\{P_1^{sc}, P_2^{sc}, \cdots, P_K^{sc}\}$;
Requires: pl, t;
Evaluate small cells SIRs and initial P_c at t;
for (until SIRs start repeating for SCs) **do**
    Calculate SIRs for small cells at $t+1$;
    if $\mathrm{SIR}_2(t+1) > 1$ **then**
        $P_2^{sc}(t+1) = \frac{T_2 \times P_2^{sc}(t)}{\mathrm{SIR}_2(t+1)}$
    else
        $P_2^{sc}(t+1) = T_2 \times P_2^{sc}(t) \times \mathrm{SIR}_2(t+1)$
    end if
    if $\mathrm{SIR}_3(t+1) > 1$ **then**
        $P_3^{sc}(t+1) = \frac{T_3 \times P_3^{sc}(t)}{\mathrm{SIR}_3(t+1)}$
    else
        $P_3^{sc}(t+1) = T_3 \times P_3^{sc}(t) \times \mathrm{SIR}_3(t+1)$
    end if
    proceed if-else for K-tier cells;
    Update $P_c(t+1)$ using equation (5.5) for updated P_i^{sc};
end for
Declare updated P_i^{sc} of small cells as a optimal powers;
Declare updated P_c as a optimal value;

then replaced the updated power in equation (5.5) to find the updated coverage probability. We repeat this process as long as SIRs of small cells start converging. We have proposed an algorithm to implement the idea, as mentioned above. We incorporate the power budget of each tier in the network. The typical small cell transmission power range is specified in Section 5.2. Here, we ensure the power of each tier is within their power constraint. Initially, we assume the transmit powers of all the BSs are fixed.

5.4 Simulation Results

In this Section, we analyzed the coverage probability performance of the proposed power control model. Also, we compared our proposed power control method performance with the existing power control method [139]. To present a quantitative comparison with an existing power control method, we fixed the same system parameter values used in the article [139]. As per the discussion in Section 5.3, we can observe that all the results (Figure 5.5, Figure 5.6, and

Figure 5.4) obtained for an existing power control method as well as for the proposed power control method successfully increases the coverage probability of [42] if the necessary condition $T_2 \geq T_1$ is satisfied. For a more precise explanation, we changed T_2 from 1 decibel (dB) to -1 dB, and the result in Figure 5.4 shows that coverage probability successfully increases for the condition $T_2 \geq T_1$. This condition satisfies the existing power control method as well as the

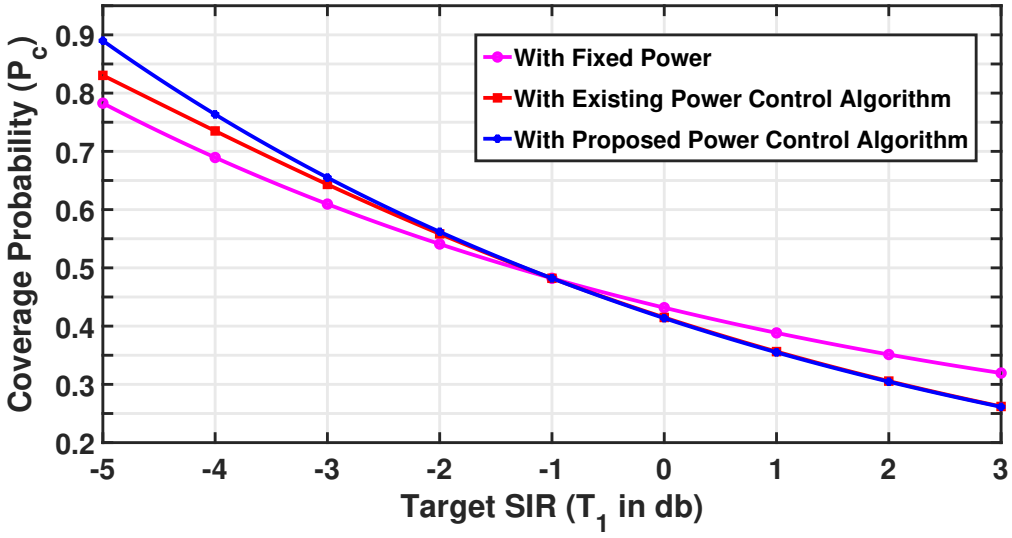

FIGURE 5.4: Coverage Probability of three-tier heterogeneous network with three cases: with fixed power, with existing power control method, and with the proposed power control method (for T_2 = -1 dB)

proposed power control method for general K-tier HetNet. For result in Figure 5.4 we used $K = 3, P_1^{sc} = 25 \times P_2^{sc} = 250 \times P_3^{sc}, pl = 3, \lambda_3 = 5 \times \lambda_1, \lambda_2 = 2 \times \lambda_1$.

In two-tier HetNet, Figure 5.5 shows that the proposed power control method improves the coverage probability compared to the existing power control method and fixed power [42]. For result in Figure 5.5 we used $K = 2, P_1^{sc} = 25 \times P_2^{sc}, pl = 3, \lambda_2 = 2 \times \lambda 1$. When T_1 = -5 dB, then the coverage probability for fixed power is 0.80, 0.84 for the existing power control method, and 0.89 for the proposed power control method. At T_1 = -5 dB, the existing power control method increases coverage probability by 5.0 percent compared to fixed power, and the proposed power control method increases coverage probability by 11.25 percent compared to fixed power. The proposed power control method increases coverage probability by 5.95 percent compared to the existing power control method.

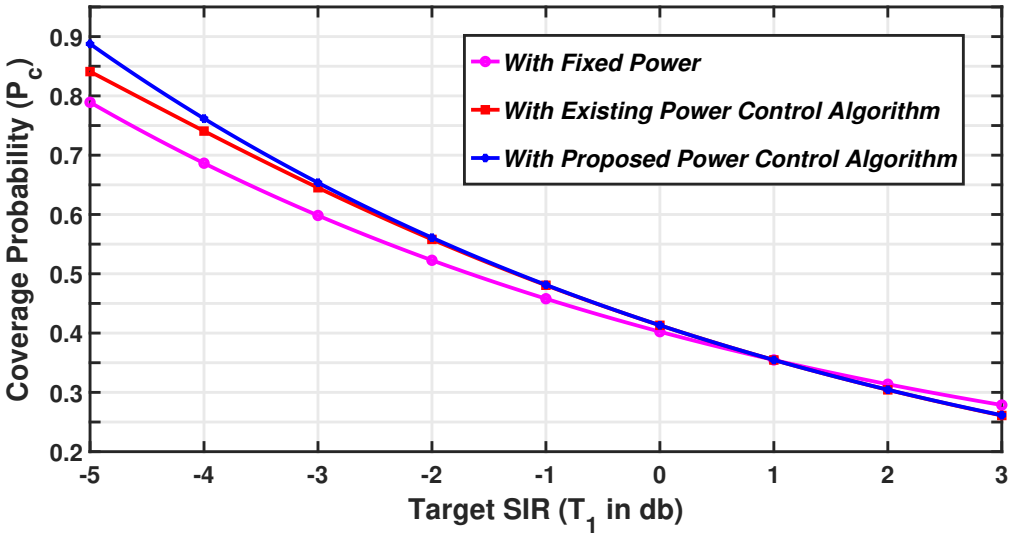

FIGURE 5.5: Coverage Probability of two-tier heterogeneous network with three cases: with fixed power, with existing power control method, and with the proposed power control method (for $T_2 = 1$ dB).

In three-tier HetNet, Figure 5.6 shows that the proposed power control method improves the coverage probability compared to the existing and fixed power control methods. For result

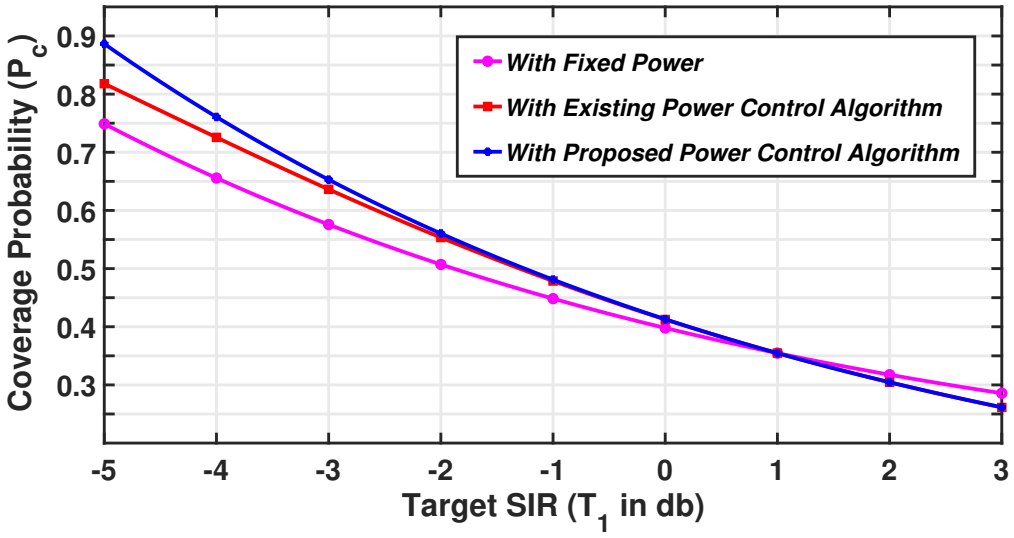

FIGURE 5.6: Coverage Probability of three-tier heterogeneous network with three cases: with fixed power, with existing power control method, and with the proposed power control method (for $T_2 = 1$ dB)

in Figure 5.6 we used $K = 3, P_1^{sc} = 25 \times P_2^{sc} = 250 \times P_3^{sc}, pl = 3, \lambda_3 = 5 \times \lambda_1, \lambda_2 = 2 \times \lambda 1$. When T_1 = -5 dB, then the coverage probability for fixed power is 0.75, 0.82 for the existing

power control method, and 0.89 for the proposed power control method. At T_1 = -5 dB, the existing power control method increases coverage probability by 9.33 percent compared to fixed power, and the proposed power control method increases coverage probability by 18.67 percent compared to fixed power. Compared to the existing power control method, the proposed power control method increases coverage probability by 8.54 percent. Therefore, by comparing numerical results from Figure 5.5 and Figure 5.6, the three-tier HetNet performance is better than the two-tier HetNet for the proposed power control method.

5.4.1 Comparison with an Existing Power Control Method.

The proposed power control method increases not only the coverage probability compared to the existing power control method but also the convergence rate, which is faster than the existing power control method. Figure 5.7 shows the iterations comparison for the proposed and existing

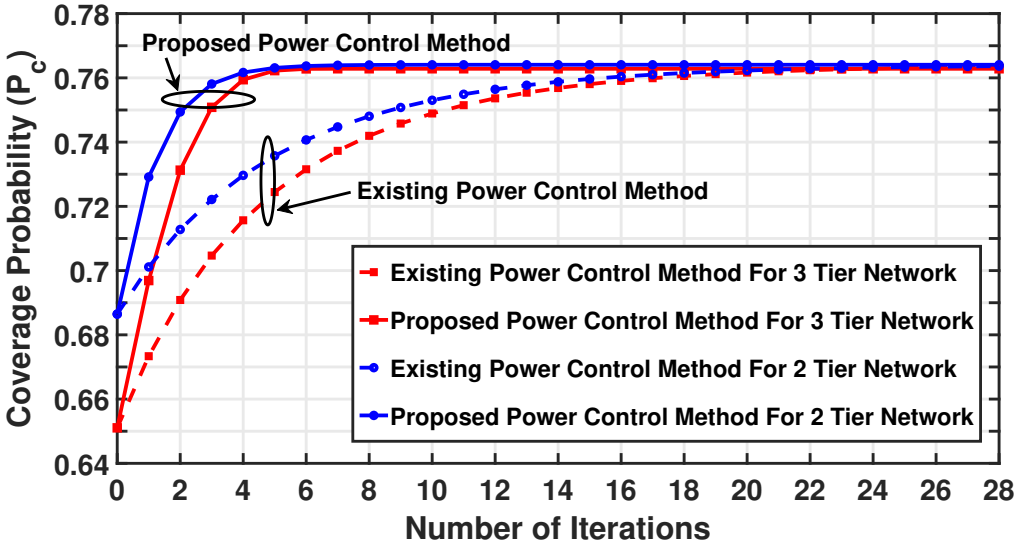

FIGURE 5.7: Iterationwise comparison of convergence of coverage probability with two cases: with existing power control method and with the proposed power control method

power control methods for both two-tier HetNet and three-tier HetNet. In both two-tier HetNet and three-tier HetNet, the existing power control method required approximately 20 iterations to converge, whereas the proposed power control method required just eight iterations to converge. Hence, convergence performance is also better for the proposed power control method than the existing power control method. Additionally, Table 5.1 presents the number of iterations

TABLE 5.1: Number of iterations with two cases: the existing and proposed power control methods.

	Two-tier HetNet		Three-tier HetNet	
	Existing power control method	Proposed power control method	Existing power control method	Proposed power control method
Number of iterations	20	8	20	8

with two cases, the existing power control method and the proposed power control method for downlink heterogeneous networks.

As discussed in Section 5.3, during successive iterations, if SIRs of small cells repeat with some accuracy, then the coverage probability of the network converges. In Figure 5.8, the SIR of picocell and SIR of femtocell converged on the eighth iteration. Therefore, the result in Figure

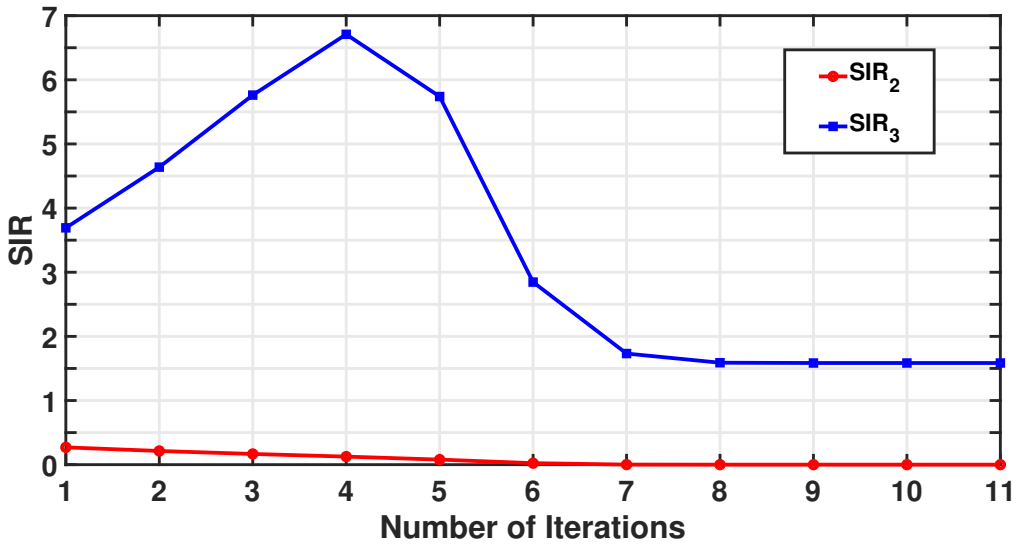

FIGURE 5.8: Iterationwise comparison of convergence of SIR_2 and SIR_3 of three-tier heterogeneous network for the proposed power control method

5.8 is a validation of our proposed theory. Moreover, the result from Figure 5.8 is the justification of the conclusion obtained in Figure 5.7, which has shown that the three-tier heterogeneous network converges to approximately eighth iteration for the proposed power control method.

5.5 Summary

In this work, we proposed the power control algorithm to improve coverage probability in the downlink communication of K-tier heterogeneous networks. In our system model, we used the PPP for the distribution of BSs of three-tier heterogeneous networks. The proposed power control algorithm increases results for necessary condition $T_2 \geq T_1$. Our algorithm updates the transmission power of the BS of all low-power small cells of the heterogeneous network to minimize interference present in the network. It consequently increases coverage probability in the heterogeneous network. The numerical result shows that the proposed method increases coverage probability more than the existing power control method. We also demonstrate that the convergence rate of the proposed power control algorithm is faster than the convergence rate of the existing power control algorithm. Furthermore, it is observed that the proposed power control algorithm converges if the SIRs of the small cell repeat for successive iterations. In the proposed power control algorithm, power control is distributed to all users and, therefore, does not require any centralized controller. Thus, the computational complexity in the network is reduced.

Hybrid systems can improve the system parameters of wireless networks, particularly when NOMA is combined with other techniques. This motivates us to use NOMA in HetNets to enhance system parameters. Chapters 2, 3, and 4 solely deal with the NOMA system, and Chapter 5 deal only with the HetNet system. However, the next Chapter 6 employs hybrid systems combining NOMA with HetNet to enhance the sum rate and outage probability further.

Chapter 6

Optimal Power Allocation for Downlink NOMA HetNets to Improve Sum Rate and Outage Probability

HetNets are composed of low-power small cells (Microcell, Picocell, and Femtocell) superimposed over a high-power macrocell [144]. It is anticipated that the deployment of these small cells over macrocell can enhance essential parameters such as outage probability, user performance at the cell edge, spectrum efficiency, energy consumption, and sum rate [145]. However, interference in HetNets rises as a result of network densification, intensive growth, and the usage of the same frequency by all cells [40, 41]. As a result, the cellular network's outage and data rate performance degrades. Hence, interference is a significant performance constraint in the network [39]. Using NOMA in HetNets helps reduce cross-tier interference and improve system sum rate and outage probability, which we do in this Chapter.

The frequency band in typical OFDMA HetNets may be split into many sub-frequency bands, and users in the macrocell and small cells are allocated to various sub-frequency bands to minimize cross-tier interference [146]. However, in NOMA HetNets, SIC is used at the receivers to enable numerous users to be multiplexed on the same sub-frequency band, resulting in a higher sum rate than in OMA [147]. Strong users can eliminate interference from weak users multiplexed on the same sub-frequency band in the NOMA SIC process. Because several users

in the NOMA network share the same time/frequency resource, different powers are assigned to users, dependent on channel circumstances. PA coefficients can be used to provide different levels of power to different users. The inappropriate selection of PA can reduce the sum rate and increase the outage probability of the NOMA network. As a result, PA is a vital tool for the NOMA network's sum rate and outage improvement. Hence, this Chapter focuses on the minimization of outage probability and maximization of sum rate for downlink NOMA HetNets obtaining optimal PA.

The rest of the Chapter is organized as follows. In Section 6.1, we will present related works. We present the system model in Section 6.2. In Section 6.3, we derive the optimal PA solution for the proposed optimization problem. Section 6.4 presents simulation results and relevant discussions for the proposed scheme. Finally, Section 6.5 provides concluding remarks.

6.1 Related Work

The downlink NOMA network's outage probability has been addressed in a few studies. the work [148] investigates the optimal outage probability problem in the NOMA network while taking power allocation, decoding order selection, and user grouping into consideration. The outage probability and ergodic sum rate of NOMA for randomly deployed users with optimal PA are investigated in paper [149] under perfect and imperfect CSI. The optimum PA is explored in [150] in terms of data rate and outage probability under CSI to optimize fairness among users of a NOMA downlink network. In work [151], closed-form expressions for outage probability and system capacity in simultaneous wireless information and power transmission to NOMA networks are obtained and investigated. The outage probability and diversity order by the cooperative NOMA method are studied in the article [105]. In paper [152], the authors come up with a simple way to find outage probability in downlink HetNet with flexible cell association. The HetNet is modeled as a multi-tier cellular network in which each tier's BSs are distributed at random locations. In [153], a closed-form equation for secrecy outage probability in HetNets and K-tier HetNets based on stochastic geometry is derived with a BS association constraint.

In addition to improving outage probability, another key objective of this Chapter is to maximize the sum rate. For NOMA based HetNets, an iterative subchannel allocation and PA algorithm

is offered to optimize the sum rate of small cells within a limited number of iterations [154]. The subchannel assignment issue and the PA problem in downlink NOMA based HetNets are investigated in article [155]. In [56], the authors find the best PA technique for NOMA networks to maximize the sum rate. They do this while meeting minimum user rate requirements. The work [51] determines the maximum sum rate of a downlink two-user NOMA network under the assumption of an imperfect SIC and minimal QoS constraint. In [57], the authors look into the best PA for a sub-carrier-based NOMA network to maximize its sum rate under a minimum rate and a total power constraint. Work [58] maximizes the total rate using optimum PA in a MIMO NOMA network with layered transmissions. The authors offer an alternating maximization algorithm for instantaneous CSI and statistical CSI at the BS. [59] investigates the subcarrier and PA for a single-cell multicarrier downlink NOMA network. The Double Iterative Waterfilling Algorithm is presented to maximize the NOMA network's sum rate. Paper [36] proposes a multi-objective optimization framework for effectively allocating PA in a downlink transmission NOMA network, which maximizes the total rate while reducing transmit power and considering the QoS, SIC, and transmit power budget.

6.2 System Model

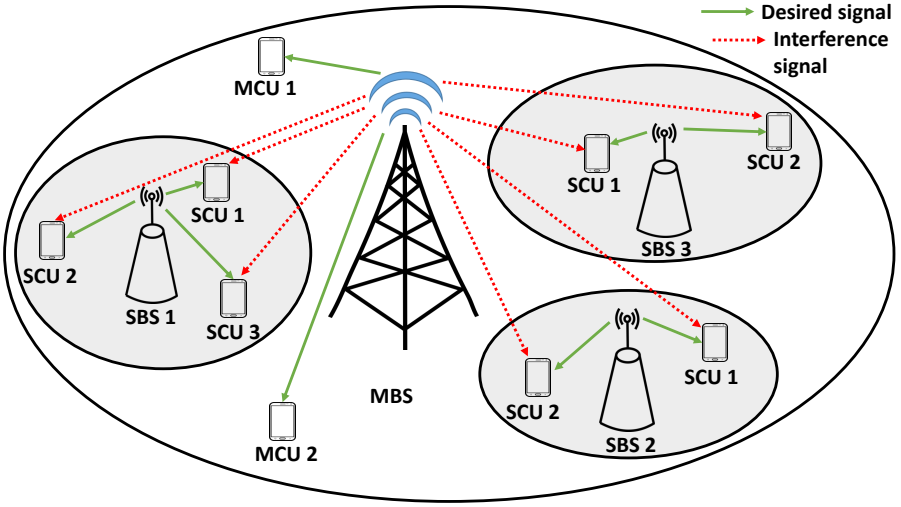

FIGURE 6.1: A downlink NOMA-based Heterogeneous Network

This section introduces the downlink NOMA-based HetNets system model. Let us consider a downlink NOMA-based two-tier heterogeneous wireless network, as shown in Figure 6.1. M^{sc}

small cells are superimposed on a single macrocell in the network. Each small cell has N^{sc} small cell users, while each macrocell has K macrocell users. Let's denote $d^{sc}_{m,n}$ as the user's distance from small cell BS m to small cell user n. Let's denote $h^{sc}_{m,n}$ as Rayleigh fading coefficient from small cell BS m to small cell user n, where $h^{sc}_{m,n} = z^{sc}_{m,n} {d^{sc}_{m,n}}^{-pl}$, $z^{sc}_{m,n}$ is a Rayleigh distribution and pl is the path loss exponent. Let's denote $g_{m,n}$ as a complex Rayleigh fading coefficient from macrocell BS to small cell user n in small cell m, $z_{m,n} = \mathscr{CN}(0,\sigma^2)$ is the Additive AWGN noise. Let's indicate $x_{m,n}$ is data intended for nth user in small cell m. Let's represent $w_{m,n}$ interference plus noise for nth user in small cell m. Without losing generality, we arrange channel coefficients on small cell BS m in descending order as $\left|h^{sc}_{m,1}\right| \geq \left|h^{sc}_{m,2}\right| \geq \cdots \geq \left|h^{sc}_{m,N^{sc}}\right|$.

According to NOMA's principles, the PA coefficients must be sorted as $\alpha^{sc}_{m,1} \leq \alpha^{sc}_{m,2} \leq \alpha^{sc}_{m,3} \cdots \leq \alpha^{sc}_{m,N^{sc}}$, where $\alpha^{sc}_{m,n}$ PA coefficient from small cell BS m to small cell users n. Due to low power and intense penetration loss in small cell, we can ignore interference between different small cell users [146, 156]. The SINR of NOMA network received at the nth small cell user of small cell m can be written as [36],

$$SINR^{sc}_{m,n} = \frac{\alpha^{sc}_{m,n} P^{sc} \left|h^{sc}_{m,n}\right|^2}{\left|h^{sc}_{m,n}\right|^2 P^{sc} \sum_{j=1}^{n-1} \alpha^{sc}_{m,n} + P_k \left|g_{m,n}\right|^2 + \sigma^2} \tag{6.1}$$

where P^{sc} is transmit power from small BS. According to Shannon's capacity formula, the data rate of small cell user n in small cell m is written as [36],

$$R^{sc}_{m,n} = B^{sc} \log(1 + SINR^{sc}_{m,n}) \tag{6.2}$$

where, B^{sc} is bandwidth of small cell. For simplicity, we use $B^{sc} = 1$ Hz. If the data rate falls below the user's required minimum data rate at any point, the user can experience an outage. As a result, the outage probability of small cell user n in small cell m is expressed as,

$$\text{Outage Probability} = \mathbb{P}(R^{sc}_{m,n} < R^{sc*}_{m,n}) \tag{6.3}$$

where, $R^{sc*}_{m,n}$ is target rate of small cell user n of small cell BS m.

6.3 Proposed Method

This section determines the best PA solution that maximizes the sum rate and minimizes the outage probability in NOMA-based HetNets. To achieve optimal PA coefficient while ensuring QoS for user n in small cell m, we choose $\alpha_{m,n}^{sc}$ such that, $R_{m,n}^{sc} \geq R_{m,n}^{sc*}$. To determine the PA coefficient for user 1 (nearest user) in small cell m, we can describe the achievable rate of user 1 as,

$$R_{m,1}^{sc} = \log\left(1 + \frac{\alpha_{m,1}^{sc} P^{sc} \left|h_{m,1}^{sc}\right|^2}{P_k \left|g_{m,1}\right|^2 + \sigma^2}\right) \tag{6.4}$$

To obtain PA coefficient $\alpha_{m,1}^{sc}$, we use $R_{m,1}^{sc} \geq R_{m,1}^{sc*}$, solving, we get,

$$\frac{\alpha_{m,1}^{sc} P^{sc} \left|h_{m,1}^{sc}\right|^2}{P_k \left|g_{m,1}\right|^2 + \sigma^2} \geq 2^{R_{m,1}^{sc*}} - 1$$

Let's denote the target SINR for user n on small cell m as, $\xi_n = 2^{R_{m,n}^{sc*}} - 1$, solving, equation of $\alpha_{m,1}^{sc}$ can be written as,

$$\alpha_{m,1}^{sc} \geq \frac{\xi_1 (P_k \left|g_{m,1}\right|^2 + \sigma^2)}{P^{sc} \left|h_{m,1}^{sc}\right|^2} \tag{6.5}$$

To obtain PA coefficient $\alpha_{m,2}^{sc}$, we can use $R_{m,2}^{sc} \geq R_{m,2}^{sc*}$, solving, we get,

$$\frac{\alpha_{m,2}^{sc} P^{sc} \left|h_{m,2}^{sc}\right|^2}{\alpha_{m,1}^{sc} P^{sc} \left|h_{m,2}^{sc}\right|^2 + P_k \left|g_{m,1}\right|^2 + \sigma^2} \geq 2^{R_{m,2}^{sc*}} - 1$$

solving, $\alpha_{m,2}^{sc}$ equation can be written as,

$$\alpha_{m,2}^{sc} \geq \frac{\xi_1 \xi_2 (P_k \left|g_{m,1}\right|^2 + \sigma^2)}{P^{sc} \left|h_{m,1}^{sc}\right|^2} + \frac{\xi_2 (P_k \left|g_{m,2}\right|^2 + \sigma^2)}{P^{sc} \left|h_{m,2}^{sc}\right|^2}$$

Therefore, using the deduction method and taking the lower limit of $\alpha_{m,n}^{sc}$, the PA coefficient for user n in small cell m can be written as shown in equation (6.6). This equation can be expressed in terms of previously determined PA coefficients, which are as shown in equation (6.7). Thus, we achieve the optimal $\alpha_{m,n}^{sc}$ in the NOMA-based HetNets while adhering to the

$$\alpha_{m,n}^{sc} = \sum_{i=1}^{n} \left(\xi_i \left(1 + \underbrace{\sum_{j=i+1}^{n-1} \xi_j}_{\text{ST}} + \text{Sum of all possible two product terms of ST} + \right. \right. \\ \left. \left. \text{Sum of all possible three product terms of ST} + \cdots \right) \left(\frac{\xi_n (P_k |g_{m,i}|^2 + \sigma^2)}{P^{sc} \left| h_{m,i}^{sc} \right|^2} \right) \right) \tag{6.6}$$

$$\alpha_{m,n}^{sc} = \sum_{i=1}^{n-1} \left(\alpha_{m,i}^{sc} \left(1 + \underbrace{\sum_{j=i+1}^{n-1} \xi_j}_{\text{ST}} + \text{Sum of all possible two product terms of ST} \right. \right. \\ \left. \left. + \text{Sum of all possible three product terms of ST} + \cdots \right) \right) + \frac{\xi_n (P_k |g_{m,n}|^2 + \sigma^2)}{P^{sc} \left| h_{m,n}^{sc} \right|^2} \tag{6.7}$$

QoS constraint. In the context of the preceding description, we now propose algorithm 9 for acquiring the optimum sum rate and outage probability with PA in a downlink NOMA-based HetNets while sticking to the QoS constraint. We assume that all users' target rates $R_{m,n}^{sc*}$ are the

Algorithm 9 Outage probability and sum rate in small cell of NOMA based HetNets

1: **Requires:** S,P_k,P^{sc},pl,M^{sc},N^{sc}, σ^2.
2: $x = \text{zeros}(1, S)$;
3: Obtain $h_{m,n}^{sc}$ and $g_{m,n}$;
4: Generate equally spaced $\mathbf{R^{sc*}}$ vector.
5: **for** $i = 1$ to length($\mathbf{R^{sc*}}$) **do**
6: Compute $\alpha_{m,n}^{sc}$ from eqn. (6.7);
7: Find data rates for each user in small cells;
8: **for** $u = 1$ to S **do**
9: **if** $R_{m,n}^{sc}(u) \leq R^{sc*}(i)$ **then**
10: $x(u) = x(u) + 1$ for each users
11: **end if**
12: **end for**
13: OP = x/S for each user;
14: Calculate Sum rate in each small cell;
15: **end for**

same in the algorithm. Lines 13 and 14 provide the outage probability and sum rate, respectively.

We can now examine the time complexity of our proposed algorithm. The algorithm's *if* statement does not affect the time complexity. The time complexity of the $\alpha_{m,n}^{sc}$ equation is

N^{sc}. Since the inner loop (lines 5 to 12) repeats S times, the worst-case time complexity of the inner loop is S, provided S is greater than N^{sc}. Let us suppose R has a length of L. The outer loop repeats L times, giving a worst-case time complexity of LS. Consequently, the worst-case run time complexity of our proposed algorithm is $\mathcal{O}(LS)$. Thus, we have developed a simple algorithm that has a low time complexity and can be used with real-world wireless communication networks.

6.4 Simulation Results

This section presents and discusses the simulation results for our proposed problem. Furthermore, we compare the simulation results of the proposed method with OMA to demonstrate comparable performance. Unless otherwise specified, Table 6.1 contains the simulation parameters used to obtain all the simulation results. In the simulation, we obtain the performance parameters for all users across 10^5 Rayleigh fading channel gain realizations ($\mathscr{R}$), and then we take the average of these performance parameters. The system parameters obtained in simulations for our proposed

TABLE 6.1: System parameters required for simulation.

System Parameters	**Values**
Channel realization ($\mathscr{R}$)	10^5
Number of small cells (M^{sc})	1
Number of users in small cell (N^{sc})	2 and 3
Total transmit power from macrocell BS (P_k)	1 Watt
Total transmit power from small cell BS (P^{sc})	0.1 Watt
Variance of AWGN noise (σ^2)	10^{-4}
The minimum required rate for QoS (R^{sc*}_{min})	1 bps/Hz
Path loss exponent (pl)	3

method are summarised in Table 6.2. We provide the PA coefficients and the achievable rates for each user in a small cell for two and three user cases for the proposed method in Table 6.2. Additionally, the sum rate for two and three users in small cell is shown. The PA coefficients are between 0 and 1, and their sum equal to 1 indicates that users take power in such a way that their total power equals P^{sc}, as seen in Table 6.2. Individual rates in Table 6.2 ensure that each user's minimum rate constraint is fulfilled.

TABLE 6.2: Simulation results obtained for the proposed method.

System Parameters	Obtained values	
	2 Users	3 Users
α_1^{sc}	0.1845	0.1924
α_2^{sc}	0.8155	0.2420
α_3^{sc}	-	0.5656
R_1^{sc}	1.0000 bps/Hz	1.0000 bps/Hz
R_2^{sc}	4.1729 bps/Hz	1.0000 bps/Hz
R_3^{sc}	-	2.9909 bps/Hz
Sum rate	5.1729 bps/Hz	4.9909 bps/Hz

Figures (6.2) and (6.3) depict the fluctuation of outage probability with target rate for the proposed NOMA method and OMA method for two and three users in a small cell of NOMA-based HetNets. The outage probability of NOMA-based HetNets outperforms the OMA method

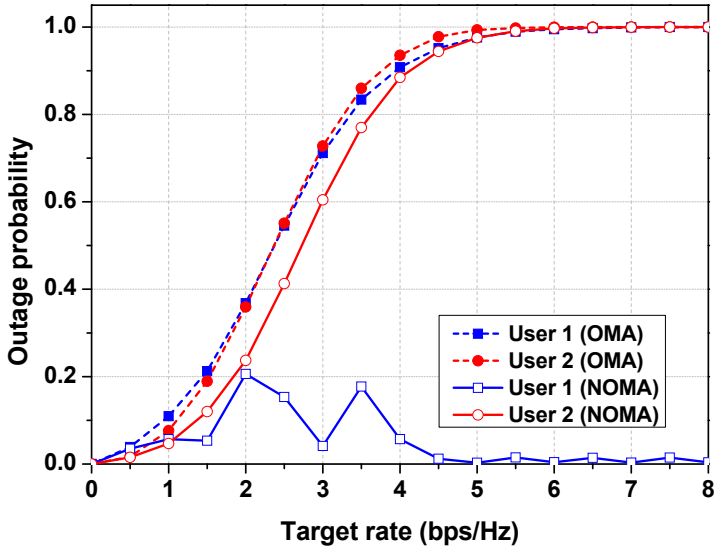

FIGURE 6.2: Outage probability Vs. target Rate for the proposed NOMA method and OMA method for two users case in a small cell of NOMA-based HetNets.

irrespective of target rates, as seen in Figures (6.2) and (6.3). This is obvious because PA coefficients are dynamically modified whenever the channels and the target rates change. It's straightforward to notice in Figures (6.2) and (6.3) that the small cell user's performance worsens as the target rate rises. This should happen because the small cell user's chances of meeting the

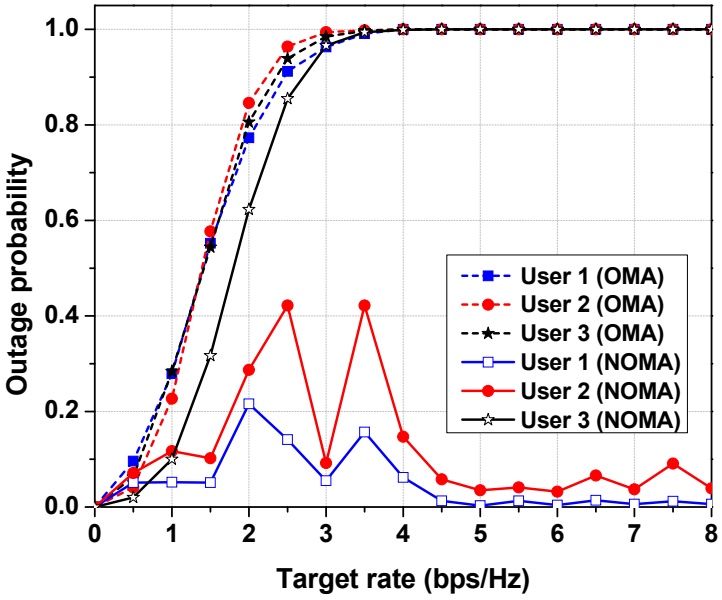

FIGURE 6.3: Outage probability Vs. target Rate for the proposed NOMA method and OMA method for three users case in a small cell of NOMA-based HetNets.

target rate reduces as the target rate rises. Hence, R_{min}^{sc*} must be smaller in order for the proposed and OMA methods to perform better for two and three users, as seen in Figures (6.2) and (6.3).

In Figure (6.2), we can observe that the strong user performs well for the proposed method, but the weak user reaches an outage. In the proposed method, the far user's outage increases rapidly for the initial R_{min}^{sc*}, and beyond 5 bps/Hz, the far user is continuously in an outage. The strong and weak user outage performance is almost the same for the OMA method. The OMA method shows a transition around values of 1 to 5 bps/Hz for both users and beyond that, users are always in an outage. Thus, for two users in small cell, NOMA-based HetNets outperform the OMA method. In Figure (6.3), we can observe that users 1 and 2 outage performance is satisfactory for all R_{min}^{sc*} in the proposed method, but the weakest user is quickly approaching outage. The outage performance of user 3 has quite a sharp transition around 0.5 to 3.5 bps/Hz, and exceeding that, user 3 is always in an outage. The outage of all users is almost the same for the OMA method. Initially, users show transition around values 0 to 3 bps/Hz; after that, they are always in an outage. Thus, NOMA-based HetNets outperforms the OMA method for three users in small cell.

The change of sum rate with transmit power is shown in Figures (6.4) and (6.5) for the proposed NOMA and OMA methods for two and three users in a small cell of NOMA-based HetNets.

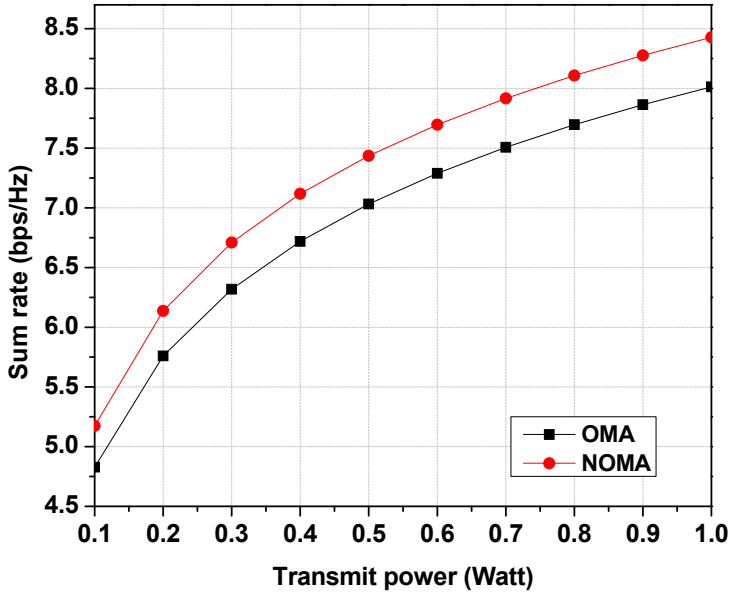

FIGURE 6.4: Sum rate versus transmit power for proposed NOMA method and OMA method for two users case in a small cell of NOMA-based HetNets.

Figures (6.4) and (6.5) show that when transmit power increases, the sum rate of NOMA-based HetNets and OMA methods for two and three users increases as well. Given that we use the QoS constraint to obtain the optimum PA in the proposed method, the proposed method's sum rate may be higher than the OMA method, as shown in Figures (6.4) and (6.5). The NOMA sum rate outperforms the OMA sum rate because each user in OMA must share bandwidth with all other users compared to NOMA, where each user shares the entire bandwidth. Additionally, in Figures (6.4) and (6.5), the separation between NOMA and OMA sum rates increases as transmit power increases. This happens because PA is inextricably linked to the SIC process. The user with the small PA is greatly affected by noise when the BS's transmit power is low, resulting in a sum rate degradation of NOMA compared to OMA. For low transmit power, this is exactly what we see in Figures (6.4) and (6.5). The receiver can detect the signal more accurately, and SIC can be carried out more efficiently if the transmit power is sufficiently high, resulting in a

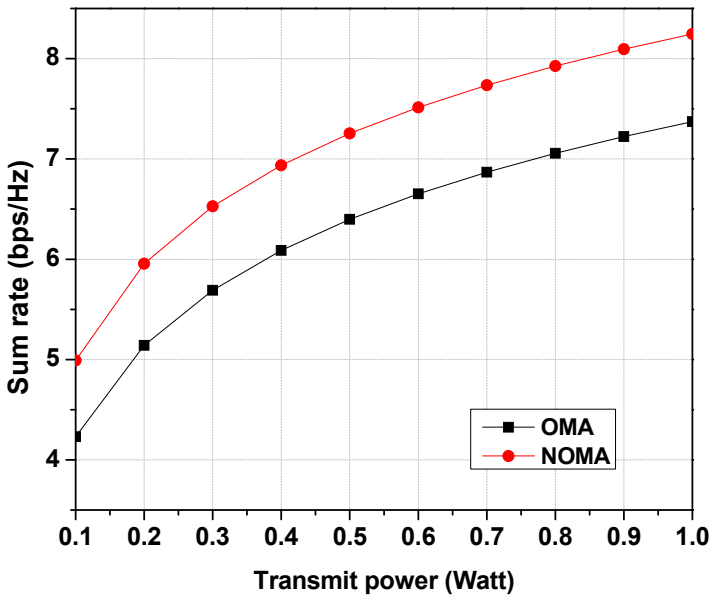

FIGURE 6.5: Sum rate versus transmit power for proposed NOMA method and OMA method for three users case in a small cell of NOMA-based HetNets.

significant rate increase. As a result, at higher transmit power, the NOMA sum rate increases more than the OMA sum rate, as illustrated in Figures (6.4) and (6.5).

6.5 Summary

This Chapter aims to find the optimal PA problem for downlink transmission NOMA-based HetNets to optimize the sum rate and outage. We devised a problem to maximize the sum rate and minimize the outage probability while adhering to the minimum data rate requirement with optimal PA coefficients. A novel technique is investigated to get the solution of the proposed method in a NOMA-based HetNets for downlink transmission. In the small cell of NOMA-based HetNets, we derived a generalized optimal PA coefficient equation. We then offered a low-complexity, fast algorithm for our proposed method to maximize the sum rate and minimize outage probability. It is demonstrated that the proposed method functions efficiently in a NOMA network for downlink communication. In this Chapter, we presented simulation results for the proposed method and compared them to results from the OMA scheme.

Chapter 7

Conclusions

Chapter 2 introduced a MOO scheme to investigate the trade-off between sum rate and user fairness for downlink transmission NOMA networks. The study examined a novel approach and demonstrated that the proposed technique works well for the NOMA network. We formulated an original MOO problem for joint maximization of sum rate and user fairness to optimize PA incorporating transmit power and QoS requirement constraints. Using the weighted sum method, we converted a MOO problem into a single-objective optimization problem. To solve the optimization problem, we employed the Lagrange dual decomposition method and KKT conditions. Finally, simulation results demonstrated joint maximization of sum rate and user fairness with optimal PA for downlink NOMA networks.

Chapter 3 presented a MOO method for investigating the trade-off between sum rate and user fairness in downlink communication NOMA networks, including the minimum power gap for successful SIC constraint. The chapter examines a novel method and shows that the proposed method works effectively in downlink NOMA networks. First, we formulated the MOO problem for jointly maximizing sum rate and user fairness while optimizing PA under a minimum power gap among users, transmit power, and QoS requirement constraints. Then, we transformed a MOO problem into a single-objective optimization problem using the weighted sum method. To solve the optimization problem, we employ the Lagrange dual decomposition method and the KKT conditions. Finally, simulation results show how downlink NOMA networks can obtain optimal PA to maximize the sum rate and be fair to all users while maintaining a quick

convergence rate for the proposed method. We also examined how well our method performed compared to benchmark methods.

The sum rate maximization problem is formulated and analyzed in Chapter 4 to optimize SA and the PA, incorporating the transmit power budget, QoS, minimum power gap, and maximum users per subchannel constraints for the downlink multicarrier NOMA network. We set up the SA and PA as two-stage problems in order to ensure that the proposed method can be solved in polynomial time. We investigated various algorithms to obtain the SA. After obtaining SA, the upper bounds for QoS and minimum power gap constraints for each subchannel are computed separately. Then, the PAs are calculated using the common region between these two upper bounds. We have shown that our solution is unique. A fast and low-complexity algorithm is proposed to solve the optimization method. Finally, we presented simulation results for the proposed method and analyzed the results of the proposed method with the results of the benchmark method. For the proposed method, we also compared the performance of several SA algorithms.

To improve the coverage probability in the downlink transmission of K-tier heterogeneous networks, we proposed the power control algorithm in Chapter 5. We used the PPP in our system model to distribute BSs of three-tier heterogeneous networks. The proposed power control algorithm increases results for necessary condition $T_2 \geq T_1$. Our method changes the transmission power of the BS of all low-power small cells in a heterogeneous network to keep interference to a minimum. As a result, the coverage probability in the heterogeneous network increases. It has been seen that the proposed power control method converges if the SIRs of the small cell repeat for successive iterations. The result shows that the proposed method increases coverage probability more than the existing power control method. We also show that the proposed power control algorithm's convergence rate is faster than the existing power control algorithm's convergence rate. In the proposed power control algorithm, power control is distributed to all users, eliminating the need for a centralized controller. Thus the computational complexity in the network is reduced.

Chapter 6 formulated and analyzed the optimization problem to find the optimal PA to optimize the sum rate and outage for downlink communication NOMA-based HetNets. We came up with a problem to maximize the sum rate and minimize the probability of an outage while

fulfilling the minimum data rate requirement with optimal PA coefficients. A novel method is investigated to get the solution of the proposed method in a NOMA-based HetNets.We proposed a generalized optimal PA coefficient equation in the small cell of NOMA-based HetNets. Then, we presented a low-complexity, fast algorithm for our proposed method to maximize the sum rate and minimize outage probability. It has been shown that the proposed method works well for downlink transmission in a NOMA network. Finally, we present simulation results for the proposed method and compare them to results from the OMA scheme.

7.1 Future Scope

1. It is obvious that hybrid systems can improve the system parameters of 5G networks, especially those that integrate NOMA and HetNet techniques. The MOO problem in downlink transmission NOMA networks is formulated and investigated in Chapters 2 and 3 to achieve optimal PA for joint optimization of sum rate and user fairness. We intend to further study the performance of our proposed method for combining NOMA and heterogeneous networks for downlink transmission.

2. In Chapter 4, the subchannel and power allocation are obtained to maximize the sum rate objective while adhering to the minimum power gap constraint for downlink transmission NOMA-based 5G networks. We intend to study on how well our proposed method works for integrating NOMA and heterogeneous networks for downlink multicarrier systems.

3. Massive MIMO has been identified as the key technology for the 5G network to boost the sum rate over the current network. Chapters 2, 3, 4, and 6 maximize the sum rate for the SISO system, which the BS transmits, and the users receive using a single antenna. We intend to investigate the MIMO system's performance for downlink transmission for a combination of NOMA and heterogeneous-based 5G networks.

Appendix A

Concavity Proof of $g_1(t_m)$

In this appendix, we prove the concavity of $g_1(t_m)$. We do this by showing that the Hessian matrix is negative definite. Let Δ_i represent the determinant of the leading principal sub-matrix of first i rows and i columns of the Hessian matrix $\mathbf{A}$. If $\Delta_i < 0$, for odd $i \in \{1,2,\cdots,M\}$ and $\Delta_i > 0$, for even $i \in \{1,2,\cdots,M\}$, then we say $\mathbf{A}$ is negative definite. First term in Eqn. (2.13) can be written as,

$$U_{sum} = \sum_{m=1}^{M} \frac{t_m^{1-l}}{1-l},\ l \geq 0.$$

The Hessian matrix for U_{sum} can then be calculated as follows:

$$\mathbf{A_{M\times M}} = \left[a_{ij}\right],\ \text{where, } a_{ij} = \frac{\partial}{\partial t_i}\left(\frac{\partial U_{sum}}{\partial t_j}\right).$$

After solving, we get,

$$\mathbf{A_{M\times M}} = \left(-\frac{l}{t_i^{(1+l)}}\right) \times \mathbf{I_{M\times M}},\ \text{where, } \mathbf{I} \text{ is Identity matrix.}$$

The determinant of a diagonal matrix is the product of its diagonal elements, Hence, we get, $\Delta_i < 0$, for odd $i \in \{1,2,\cdots,M\}$ and $\Delta_i > 0$, for even $i \in \{1,2,\cdots,M\}$. Hence, Hessian matrix $\mathbf{A}$ is negative definite. Hence, U_{sum} is concave. It can be noted that the second term $\sum_{m=1}^{M} \mu_m t_m$ in Eqn. (2.13) is a linear function of t_m. Therefore it is strictly concave-convex. Thus, $g_1(t_m)$ is concave function.

Appendix B

Concavity Proof of $g_2(P_m)$

The concavity proof of $g_2(P_m)$ is shown here. Since the channels are ordered $|h_1| \leq |h_2| \leq \cdots \leq |h_M|$, then we can write the sum rate as,

$$R_{sum} = \sum_{m=1}^{M} \log_2 \left(1 + \frac{P_m |h_m|^2}{\sum_{n=m+1}^{M} P_n |h_m|^2 + \sigma^2} \right).$$

Denoting Hessian matrix for R_{sum} as:

$$\mathbf{B_{M \times M}} = \left[b_{ij} \right].$$

After solving, we obtain the coefficients of the Hessian matrix **B** as:

$$b_{ij} = b_{ji}, \quad \text{for } j \geq i, \text{ constant } i.$$

where, matrix elements b_{ij} for user m is given by,

$$b_{mm} = \sum_{i=1}^{m} \left[-T_{ii} + T_{i(i+1)} \right], \text{ excluding } T_{m(m+1)},$$

where, T_{ij} is given as,

$$T_{ij} = \left(\frac{|h_i|^2}{\left(\sum_{n=j}^{M} P_n \right) |h_i|^2 + \sigma^2} \right)^2,$$

Here, the determinant of the leading principal sub-matrix Δ_m for user m can be written as,

$$\Delta_m = \begin{bmatrix} -T_{11} & -T_{11} & -T_{11} & \cdots & -T_{11} \\ 0 & T_{12}-T_{22} & T_{12}-T_{22} & \cdots & T_{12}-T_{22} \\ 0 & 0 & T_{23}-T_{33} & \cdots & T_{23}-T_{33} \\ \vdots & \vdots & \vdots & \ddots & \vdots \\ 0 & 0 & 0 & \cdots & T_{(m-1)m}-T_{mm} \end{bmatrix}$$

Since $|h_1| \leq |h_2| \leq \cdots \leq |h_M|$, therefore $T_{12} < T_{22}, T_{23} < T_{33}, \cdots, T_{(M-1)M} < T_{MM}$ and hence $\Delta_M > 0$ if M is even else $\Delta_M < 0$ if M is odd. Therefore, $\Delta_i < 0$ for odd $i \in \{1,2,\cdots,M\}$ and $\Delta_i > 0$ for even $i \in \{1,2,\cdots,M\}$. Consequently, Hessian matrix $\mathbf{B}$ is negative definite. Hence, R_{sum} is concave function. As, R_{sum} is concave function, therefore first term $\omega \sum_{m=1}^{M} R_m$, second term $\sum_{m=1}^{M} \chi_m (R_m - R_{min})$, and fourth term $\sum_{m=1}^{M} \mu_m R_m$ are concave function. Also, it is important to note that in Eqn. (2.15), the third term $\beta_m (P_{BS} - \sum_{m=1}^{M} P_m)$ is a linear function of P. Hence the third term in Eqn. (2.15) is concave-convex. Therefore, $g_2(P_m)$ is concave function.

Appendix C

Derivation of a Closed-form Expression t_m

The equation for $g_1(t_m)$ is,

$$g_1(t_m) = (1-\omega)\sum_{m=1}^{M} U(t_m) - \sum_{m=1}^{M} \mu_m t_m.$$

The first partial derivative of $g_1(t_m)$ with respect to t_m is,

$$\frac{\partial g_1(t_m)}{\partial t_m} = (1-\omega)\sum_{m=1}^{M} \frac{t_m^{(1-l)}}{1-l} - \sum_{m=1}^{M} (\mu_m t_m),$$

We can determine the optimal value of t_m in Eqn. (2.17) by solving the partial derivative equated to zero.

Appendix D

Derivation of a Closed-form Expression P_m

The equation for $g_2(P_m)$ is given as,

$$g_2(P_m) = \omega \sum_{m=1}^{M} R_m + \sum_{m=1}^{M} \chi_m (R_m - R_{min}) + \beta_m (P_{BS} - \sum_{m=1}^{M} P_m) + \sum_{m=1}^{M} \mu_m R_m.$$

Now, we can derive a closed-form expression of P_m for u_m, as shown here. The first partial derivative of $g_2(P_m)$ with respect to P_m can be written as,

$$\frac{\partial g_2(P_m)}{\partial P_m} = \sum_{i=1}^{m-1} \left(\left(\frac{-(\omega + \chi_i + \mu_i)}{\log 2} \right) \times \left(\frac{P_i^2 \left(|h_i|^2 \right)^2}{\left(\sum_{n=i}^{M} P_n |h_i|^2 + \sigma^2 \right) \left(\sum_{n=i+1}^{M} P_n |h_i|^2 + \sigma^2 \right)} \right) \right) + \frac{(\omega + \chi_m + \mu_m)}{\log 2} \frac{|h_m|^2}{\sum_{n=m}^{M} P_n |h_m|^2 + \sigma^2} - \beta_m,$$

We can now solve the partial derivation equal to zero to get the optimal solution of P_m^* for user m as seen in Eqn. (2.18).

Appendix E

Proof of $g_3(t_m)$ is Concave Function

We prove the concavity of $g_3(t_m)$ in this appendix. This is accomplished by demonstrating that the Hessian matrix is negative definite. Let Δ_i represent the determinant of the leading principal sub-matrix of the first i rows and i columns of the Hessian matrix $\mathbf{C}$. If $\Delta_i > 0$, for even $i \in \{1,2,\cdots,M\}$ and $\Delta_i < 0$, for odd $i \in \{1,2,\cdots,M\}$, then we say $\mathbf{C}$ is negative definite. The first term in Eqn. (3.7) can be written as,

$$U_{sum} = (1-\omega)\sum_{m=1}^{M} \frac{t_m^{1-l}}{1-l},\ l \geq 0.$$

The Hessian matrix for U_{sum} can then be calculated as follows:

$$\mathbf{C} = \begin{bmatrix} \frac{\partial}{\partial t_1}\left(\frac{\partial U_{sum}}{\partial t_1}\right) & \frac{\partial}{\partial t_1}\left(\frac{\partial U_{sum}}{\partial t_2}\right) & \cdots & \frac{\partial}{\partial t_1}\left(\frac{\partial U_{sum}}{\partial t_3}\right) \\ \frac{\partial}{\partial t_2}\left(\frac{\partial U_{sum}}{\partial t_1}\right) & \frac{\partial}{\partial t_2}\left(\frac{\partial U_{sum}}{\partial t_2}\right) & \cdots & \frac{\partial}{\partial t_2}\left(\frac{\partial U_{sum}}{\partial t_3}\right) \\ \vdots & \vdots & \ddots & \vdots \\ \frac{\partial}{\partial t_M}\left(\frac{\partial U_{sum}}{\partial t_1}\right) & \frac{\partial}{\partial t_M}\left(\frac{\partial U_{sum}}{\partial t_2}\right) & \cdots & \frac{\partial}{\partial t_M}\left(\frac{\partial U_{sum}}{\partial t_M}\right) \end{bmatrix}$$

After solving, we get,

$$\mathbf{C} = \begin{bmatrix} -\frac{(1-\omega)x}{t_1^{(1+x)}} & 0 & \cdots & 0 \\ 0 & -\frac{(1-\omega)x}{t_2^{(1+x)}} & \cdots & 0 \\ \vdots & \vdots & \ddots & \vdots \\ 0 & 0 & \cdots & -\frac{(1-\omega)x}{t_M^{(1+x)}} \end{bmatrix}$$

The determinant of a diagonal matrix is the product of its diagonal elements, Hence, we get, $\Delta_i > 0$, for even $i \in \{1,2,\cdots,M\}$. and $\Delta_i < 0$, for odd $i \in \{1,2,\cdots,M\}$. Hence, Hessian matrix $\mathbf{C}$ is negative definite. Hence, U_{sum} function is concave. It is worth noting that in Eqn. (3.7), the second term $\sum_{m=1}^{M} \mu_m t_m$ is a linear function of t_m. As a result, it is strictly concave-convex. Hence, $g_3(t_m)$ is a concave function.

Appendix F

Proof of $g_4(\alpha_m)$ is Concave Function

In this appendix, we prove the concavity of the $g_4(\alpha_m)$ function. Since the channels are sorted as $|h_1| \leq |h_2| \leq \cdots \leq |h_M|$, then we can express the sum rate as,

$$R_{sum} = \sum_{m=1}^{M} \log_2 \left(1 + \frac{\alpha_m P |h_m|^2}{\sum_{n=m+1}^{M} \alpha_n P |h_m|^2 + \sigma^2} \right).$$

Denoting Hessian matrix for R_{sum} as, $\mathbf{D_{M \times M}} = \left[d_{ij} \right]$. After solving, we get the coefficients of the Hessian matrix $\mathbf{D}$ as shown below,

$d_{11} = d_{12} = d_{13} = \cdots = d_{1M} = -C_{11}$,

$d_{21} = d_{31} = d_{41} = \cdots = d_{M1} = -C_{11}$,

$d_{22} = d_{23} = d_{24} = \cdots = d_{2M} = -C_{11} + C_{12} - C_{22}$,

$d_{32} = d_{42} = d_{52} = \cdots = d_{M2} = -C_{11} + C_{12} - C_{22}$,

$d_{33} = d_{34} = d_{35} = \cdots = d_{3M} = -C_{11} + C_{12} - C_{22} + C_{23} - C_{33}$,

$d_{43} = d_{53} = d_{63} = \cdots = d_{M3} = -C_{11} + C_{12} - C_{22} + C_{23} - C_{33}$,

$\vdots$

$d_{MM} = -C_{11} + C_{12} - C_{22} + C_{23} - C_{23} + \cdots + C_{(M-1)(M-1)} - C_{(M-1)M} + C_{MM}$. By performing

elementary matrix operations to reduce the matrix to upper triangular form, we get,

$$\mathbf{D} = \begin{bmatrix} -C_{11} & -C_{11} & -C_{11} & \cdots & -C_{11} \\ 0 & C_{12}-C_{22} & C_{12}-C_{22} & \cdots & C_{12}-C_{22} \\ 0 & 0 & C_{23}-C_{33} & \cdots & C_{23}-C_{33} \\ \vdots & \vdots & \vdots & \ddots & \vdots \\ 0 & 0 & 0 & \cdots & C_{(M-1)M}-C_{MM} \end{bmatrix}$$

Since $|h_1| \leq |h_2| \leq \cdots \leq |h_M|$, therefore $C_{12} < C_{22}, C_{23} < C_{23}, \cdots, C_{(M-1)M} < C_{MM}$. Therefore, $\Delta_i > 0$ for even $i \in \{1,2,\cdots,M\}$ and $\Delta_i < 0$ for odd $i \in \{1,2,\cdots,M\}$. As a result, Hessian matrix $\mathbf{D}$ is negative definite. Hence, R_{sum} is concave function. As, R_{sum} is concave function, therefore first term $\omega \sum_{m=1}^{M} R_m$, second term $\sum_{m=1}^{M} \chi_m (R_m - R_{min})$, and fourth term $\sum_{m=1}^{M} \mu_m R_m$ are concave function. Also, it is important to note that in Eqn. (3.9), the third term $\sum_{m=1}^{M-1} \psi_m \left(\alpha_m P |h_{m+1}|^2 - \sum_{i=m+1}^{M} \alpha_i P |h_{m+1}|^2 - P_g \right)$ and the fourth term $\beta_m (P_{BS} - \sum_{m=1}^{M} \alpha_m P)$ are linear function of α. Hence, the third and fourth terms in Eqn. (3.9) are concave-convex. Therefore, $g_4(\alpha_m)$ is concave function.

Appendix G

Derivation of a Closed-form Expression v_m

The equation for $g_3(v_m)$ is,

$$g_3(v_m) = (1-\omega)\sum_{m=1}^{M} U(v_m) - \sum_{m=1}^{M} \xi_m v_m.$$

The first partial derivative of $g_3(v_m)$ with regards to v_m is given as,

$$\frac{\partial g_3(v_m)}{\partial v_m} = (1-\omega)\sum_{m=1}^{M} \frac{v_m^{(1-l)}(1-l)}{1-l} - \sum_{m=1}^{M} (\xi_m v_m),$$

By solving the partial derivative and equal to zero, we may get the optimal value of v_m in equation (3.11).

Appendix H

Derivation of a Closed-form Expression α_m

The equation for $g_4(\alpha_m)$ is given as,

$$g_4(\alpha_m) = \omega \sum_{m=1}^{M} R_m + \sum_{m=1}^{M} \chi_m (R_m - R_{min}) + \beta_m (P_{BS} - \sum_{m=1}^{M} \alpha_m P) + \sum_{m=1}^{M-1} \psi_m \left(\alpha_m P |h_{m+1}|^2 - \sum_{i=m+1}^{M} \alpha_i P |h_{m+1}|^2 - P_g \right) + \sum_{m=1}^{M} \mu_m R_m$$

To get a closed-form expression for α_m, compute the first partial derivative of $g_4(\alpha_m)$ concerning α_m, as shown below,

$$\frac{\partial g_4(\alpha_m)}{\partial \alpha_m} = \frac{(\omega + \chi_m + \mu_m)}{\log 2} \frac{P|h_m|^2}{\sum_{n=m}^{M} \alpha_n P |h_m|^2 + \sigma^2} - \beta_m P - \psi_m P |h_{m+1}|^2 + \sum_{i=1}^{m-1} \left(\left(\frac{-(\omega + \chi_i + \mu_i)}{\log 2} \right) \times \left(\frac{\alpha_i P^2 \left(|h_i|^2 \right)^2}{\left(\sum_{n=i}^{M} \alpha_n P |h_i|^2 + \sigma^2 \right) \left(\sum_{n=i+1}^{M} \alpha_n P |h_i|^2 + \sigma^2 \right)} \right) + \psi_i P |h_{i+1}|^2 \right) \tag{H.1}$$

We may now solve the partial derivation and equal it to zero to get the optimal solution α_m^* for user m, as shown in Eqn. (3.12).

Appendix I

Proof of Matrix E is a Non-singular Matrix.

We present in this appendix that matrix **E** is a non-singular matrix. The determinant of matrix **E** can be written as,

$$\Delta_E = (1+\xi)\cdot \begin{vmatrix} 0 & 1 & 1 & \cdots & 1 \\ 1 & 0 & 1+\xi & \cdots & 1+\xi \\ 1 & 1 & 0 & \ddots & 1+\xi \\ \vdots & \ddots & \ddots & \ddots & \vdots \\ 1 & 1 & 1 & \cdots & 0 \end{vmatrix}$$

By performing matrix row operations, we can reduce matrix Δ_A to its upper triangular form as,

$$\Delta_E = (1+\xi)\cdot \begin{vmatrix} 1 & 1 & 1 & 1 & \cdots & 0 \\ 0 & -1 & 1+\xi & 0 & \cdots & 0 \\ 0 & 0 & -1 & 1+\xi & \cdots & 0 \\ \vdots & \ddots & \ddots & \ddots & \ddots & \vdots \\ 0 & 0 & 0 & 0 & \cdots & 1+\xi \\ 0 & 0 & 0 & 0 & \cdots & v \end{vmatrix}$$

Where, $v = \xi^{(M^c-2)} + (M^c-1)\sum_{p=3}^{M^c} \xi^{(M^c-p)}$. Matrix **E** has the rank of M^c, as can be seen. As a result, matrix **E** is a non-singular matrix.

Appendix J

Proof of matrix G is a Non-singular Matrix.

In this appendix, we show that matrix **G** is a non-singular matrix. We can write determinant of matrix **G** as,

$$\Delta_G = \prod_{i=1}^{M^c-1} P|h_{i,n}|^2 \cdot \begin{vmatrix} 1 & 1 & 1 & \cdots & 1 \\ 2 & 0 & 1 & \cdots & 1 \\ 2 & 2 & 0 & \ddots & 1 \\ \vdots & \ddots & \ddots & \ddots & \vdots \\ 2 & 2 & 2 & \cdots & 0 \end{vmatrix}$$

By performing elementary matrix operations to reduce matrix Δ_G to upper triangular form, we get,

$$\Delta_G = \prod_{i=1}^{M^c-1} P|h_{i,n}|^2 \cdot \begin{vmatrix} 1 & 1 & 1 & \cdots & 1 \\ 0 & -2 & -1 & \cdots & -1 \\ 0 & 0 & -2 & \ddots & -1 \\ \vdots & \ddots & \ddots & \ddots & \vdots \\ 0 & 0 & 0 & \cdots & -2 \end{vmatrix}$$

We can see that the rank of matrix **G** is M^c. Therefore, matrix **G** is a non-singular matrix.

Appendix K

Proof for Sum Rate is Concave Down Function to $\alpha_{m,n}$

Here we prove that the sum rate to $\alpha_{m,n}$ is a concave down function. Since the channels are ordered on subchannel n as, $\left|h_{1,n}\right| \geq \left|h_{2,n}\right| \geq \cdots \geq |h_{M^c,n}|$, then we can write the sum rate on subchannel n as,

$$R_{sum} = \sum_{m=1}^{M^c} \log_2 \left(1 + \frac{\alpha_{m,n} P^c \cdot |h_{m,n}|^2}{|h_{m,n}|^2 \cdot \sum_{i=1}^{m-1} \alpha_{i,n} P^c + \sigma^2} \right),$$

The first partial derivative of R_{sum} with respect to $\alpha_{1,n}$ can be written as,

$$\frac{\partial R_{sum}}{\partial \alpha_{1,n}} = \frac{P^c \left|h_{1,n}\right|^2}{\alpha_{1,n} P^c \left|h_{1,n}\right|^2 + \sigma^2} - \frac{P^c \left|h_{2,n}\right|^2}{\alpha_{1,n} P^c \left|h_{2,n}\right|^2 + \sigma^2} + \frac{P^c \left|h_{2,n}\right|^2}{(\sum_{i=1}^{2} \alpha_{i,n}) P^c \left|h_{2,n}\right|^2 + \sigma^2} - \frac{P^c \left|h_{3,n}\right|^2}{(\sum_{i=1}^{2} \alpha_{i,n}) P^c \left|h_{3,n}\right|^2 + \sigma^2} + \cdots + \frac{P^c |h_{M^c,n}|^2}{\sum_{i=1}^{M} \alpha_{i,n} P^c |h_{M^c,n}|^2 + \sigma^2},$$

The first partial derivative of R_{sum} with respect to $\alpha_{2,n}$ is,

$$\frac{\partial R_{sum}}{\partial \alpha_{2,n}} = \frac{P^c \left|h_{2,n}\right|^2}{(\sum_{i=1}^{2} \alpha_{i,n}) P^c \left|h_{2,n}\right|^2 + \sigma^2} - \frac{P^c \left|h_{3,n}\right|^2}{(\sum_{i=1}^{2} \alpha_{i,n}) P^c \left|h_{3,n}\right|^2 + \sigma^2} + \frac{P^c \left|h_{3,n}\right|^2}{(\sum_{i=1}^{3} \alpha_{i,n}) P^c \left|h_{3,n}\right|^2 + \sigma^2} - \frac{P^c \left|h_{4,n}\right|^2}{(\sum_{i=1}^{3} \alpha_{i,n}) P^c \left|h_{4,n}\right|^2 + \sigma^2} + \cdots + \frac{P^c |h_{M^c,n}|^2}{\sum_{i=1}^{M^c} \alpha_i P^c |h_{M^c,n}|^2 + \sigma^2},$$

Therefore, by deduction method, the first partial derivative of R_{sum} concerning $\alpha_{m,n}$ can be written as,

$$\frac{\partial R_{sum}}{\partial \alpha_{m,n}} = \sum_{i=m}^{M^c} \left[\frac{P^c \left|h_{i,n}\right|^2}{\sum_{j=1}^{i} \alpha_{j,n} P^c \left|h_{i,n}\right|^2 + \sigma^2} - \frac{P^c \left|h_{i+1,n}\right|^2}{\sum_{j=1}^{i} \alpha_{j,n} P^c \left|h_{i+1,n}\right|^2 + \sigma^2} \right], \tag{K.1}$$

Since, $\left|h_{1,n}\right| \geq \left|h_{2,n}\right| \geq \cdots \geq \left|h_{M^c,n}\right|$, Therefore, Eqn. (K.1) is positive. Hence, The sum rate is increasing function as an increasing $\alpha_{m,n}$ value. By doing a similar procedure, we get the second derivative of R_{sum} with respect to $\alpha_{m,n}$,

$$\frac{\partial^2 R_{sum}}{\partial \alpha_{m,n}^2} = \sum_{i=m}^{M^c} \left(\left(\frac{P^c \left|h_{i+1,n}\right|^2}{(\sum_{j=1}^{i} \alpha_{j,n} P^c \left|h_{i+1,n}\right|^2 + \sigma^2} \right)^2 - \left(\frac{P^c \left|h_{i,n}\right|^2}{\sum_{j=1}^{i} \alpha_{j,n} P^c \left|h_{i,n}\right|^2 + \sigma^2} \right)^2 \right). \tag{K.2}$$

Since, $\left|h_{1,n}\right| \geq \left|h_{2,n}\right| \geq \cdots \geq \left|h_{M^c,n}\right|$, Therefore, the second derivative of the sum rate of $\alpha_{m,n}$ is negative. Thus, the first derivative is positive, while the second derivative is negative of R_{sum}; hence, it is important to note that R_{sum} function is a concave down and strictly increasing function for $\alpha_{m,n}$.

Bibliography

[1] F. A. Tobagi, "Modeling and performance analysis of multihop packet radio networks," *Proceedings of the IEEE*, vol. 75, no. 1, pp. 135–155, 1987.

[2] J. G. Andrews, S. Buzzi, W. Choi, S. V. Hanly, A. Lozano, A. C. Soong, and J. C. Zhang, "What will 5G be?" *IEEE Journal on selected areas in communications*, vol. 32, no. 6, pp. 1065–1082, 2014.

[3] V. W. Wong, R. Schober, D. W. K. Ng, and L.-C. Wang, *Key technologies for 5G wireless systems*. Cambridge university press, 2017.

[4] A. Goldsmith, *Wireless communications*. Cambridge university press, 2005.

[5] S. S. Hussain, S. M. Yaseen, and K. Barman, "An overview of massive MIMO system in 5G," *IJCTA*, vol. 9, no. 11, 2016.

[6] I. Parvez, A. Rahmati, I. Guvenc, A. I. Sarwat, and H. Dai, "A survey on low latency towards 5G: RAN, core network and caching solutions," *IEEE Communications Surveys & Tutorials*, vol. 20, no. 4, pp. 3098–3130, 2018.

[7] S. Kano, "Technical innovations, standardization and regional comparison—a case study in mobile communications," *Telecommunications Policy*, vol. 24, no. 4, pp. 305–321, 2000.

[8] M. Alnaas, E. Laias, S. Alghol, and H. Akeel, "An overview of the development of mobile wireless communication technologies," *American Journal of Computer Science and Engineering (AMCSE)*, vol. 5, no. 2, pp. 22–29, 2018.

[9] A. Agarwal and K. Agarwal, "Implementation and performance evaluation of OFDM system in diverse transmission channel using simulink," *American Journal of Electrical and Electronic Engineering*, vol. 3, no. 5, pp. 117–123, 2015.

[10] A. Ahad, M. Tahir, and K.-L. A. Yau, "5G-based smart healthcare network: architecture, taxonomy, challenges and future research directions," *IEEE access*, vol. 7, pp. 100 747–100 762, 2019.

[11] A. A. Labade, G. V. Lohar, P. R. Dike, and N. N. Pachpor, "Spectral efficiency enhancement through wavelet transform (wt) for 5g," in *2014 IEEE Global Conference on Wireless Computing & Networking (GCWCN)*. IEEE, 2014, pp. 268–272.

[12] S. Mumtaz, J. M. Jornet, J. Aulin, W. H. Gerstacker, X. Dong, and B. Ai, "Terahertz communication for vehicular networks," *IEEE Transactions on Vehicular Technology*, vol. 66, no. 7, 2017.

[13] I. Union, "Imt traffic estimates for the years 2020 to 2030," *Report ITU*, vol. 2370, 2015.

[14] G. Fettweis and S. Alamouti, "5G: Personal mobile internet beyond what cellular did to telephony," *IEEE Communications Magazine*, vol. 52, no. 2, pp. 140–145, 2014.

[15] F. Tariq, M. R. Khandaker, K.-K. Wong, M. A. Imran, M. Bennis, and M. Debbah, "A speculative study on 6G," *IEEE Wireless Communications*, vol. 27, no. 4, pp. 118–125, 2020.

[16] D. Center, "Samsung 5G vision white paper," 2015.

[17] M. Z. Chowdhury, M. Shahjalal, S. Ahmed, and Y. M. Jang, "6G wireless communication systems: Applications, requirements, technologies, challenges, and research directions," *IEEE Open Journal of the Communications Society*, vol. 1, pp. 957–975, 2020.

[18] S. Huaizhou, R. V. Prasad, E. Onur, and I. Niemegeers, "Fairness in wireless networks: Issues, measures and challenges," *IEEE Communications Surveys & Tutorials*, vol. 16, no. 1, pp. 5–24, 2013.

[19] Q. Wu, G. Y. Li, W. Chen, D. W. K. Ng, and R. Schober, "An overview of sustainable green 5G networks," *IEEE wireless communications*, vol. 24, no. 4, pp. 72–80, 2017.

[20] C. H. News, "Tsunami of data could consume one-fifth of global electricity by 2025," *Online:https://www.climatechangenews.com*.

[21] A. Al-Dulaimi, X. Wang, and I. Chih-Lin, *5G Networks: fundamental requirements, enabling technologies, and operations management*. John Wiley & Sons, 2018.

[22] N. Radio, "User equipment (UE.) radio transmission and reception part 1: Range 1 standalone (release 16), 3gpp ts 38101-1-g30, technical specification. 2020."

[23] A. Osseiran, F. Boccardi, V. Braun, K. Kusume, P. Marsch, M. Maternia, O. Queseth, M. Schellmann, H. Schotten, H. Taoka *et al.*, "Scenarios for 5G mobile and wireless communications: the vision of the METIS project," *IEEE communications magazine*, vol. 52, no. 5, pp. 26–35, 2014.

[24] Y. Xu, G. Gui, H. Gacanin, and F. Adachi, "A survey on resource allocation for 5G heterogeneous networks: Current research, future trends and challenges," *IEEE Communications Surveys & Tutorials*, 2021.

[25] X. Wang, L. Kong, F. Kong, F. Qiu, M. Xia, S. Arnon, and G. Chen, "Millimeter wave communication: A comprehensive survey," *IEEE Communications Surveys & Tutorials*, vol. 20, no. 3, pp. 1616–1653, 2018.

[26] L. Dai, B. Wang, Y. Yuan, S. Han, I. Chih-Lin, and Z. Wang, "Non-orthogonal multiple access for 5G: solutions, challenges, opportunities, and future research trends," *IEEE Communications Magazine*, vol. 53, no. 9, pp. 74–81, 2015.

[27] L. Lu, G. Y. Li, A. L. Swindlehurst, A. Ashikhmin, and R. Zhang, "An overview of massive MIMO: Benefits and challenges," *IEEE journal of selected topics in signal processing*, vol. 8, no. 5, pp. 742–758, 2014.

[28] F. Jameel, Z. Hamid, F. Jabeen, S. Zeadally, and M. A. Javed, "A survey of device-to-device communications: Research issues and challenges," *IEEE Communications Surveys & Tutorials*, vol. 20, no. 3, pp. 2133–2168, 2018.

[29] L. Dai, B. Wang, Z. Ding, Z. Wang, S. Chen, and L. Hanzo, "A survey of non-orthogonal multiple access for 5G," *IEEE communications surveys & tutorials*, vol. 20, no. 3, pp. 2294–2323, 2018.

[30] M. Aldababsa, M. Toka, S. Gökçeli, G. K. Kurt, and O. Kucur, "A tutorial on nonorthogonal multiple access for 5G and beyond," *wireless communications and mobile computing*, vol. 2018, 2018.

[31] M. Rumney *et al.*, *LTE and the evolution to 4G wireless: Design and measurement challenges*. John Wiley & Sons, 2013.

[32] N. M. Balasubramanya, A. Gupta, and M. Sellathurai, "Combining code-domain and power-domain NOMA for supporting higher number of users," in *2018 IEEE global communications conference (GLOBECOM)*. IEEE, 2018, pp. 1–6.

[33] Z.-g. Ding, M. Xu, Y. Chen, M.-g. Peng, and H. V. Poor, "Embracing non-orthogonalmultiple access in future wireless networks," *Frontiers of Information Technology & Electronic Engineering*, vol. 19, no. 3, pp. 322–339, 2018.

[34] Z. Ding, X. Lei, G. K. Karagiannidis, R. Schober, J. Yuan, and V. K. Bhargava, "A survey on non-orthogonal multiple access for 5G networks: Research challenges and future trends," *IEEE Journal on Selected Areas in Communications*, vol. 35, no. 10, pp. 2181–2195, 2017.

[35] M. S. Ali, H. Tabassum, and E. Hossain, "Dynamic user clustering and power allocation for uplink and downlink non-orthogonal multiple access (NOMA) systems," *IEEE access*, vol. 4, pp. 6325–6343, 2016.

[36] W. U. Khan, F. Jameel, T. Ristaniemi, S. Khan, G. A. S. Sidhu, and J. Liu, "Joint spectral and energy efficiency optimization for downlink noma networks," *IEEE Transactions on Cognitive Communications and Networking*, vol. 6, no. 2, pp. 645–656, 2019.

[37] A. J. Muhammed, Z. Ma, P. D. Diamantoulakis, L. Li, and G. K. Karagiannidis, "Energy-efficient resource allocation in multicarrier NOMA systems with fairness," *IEEE Transactions on Communications*, vol. 67, no. 12, pp. 8639–8654, 2019.

[38] W. Saetan and S. Thipchaksurat, "Power allocation for sum rate maximization in 5G NOMA system with imperfect SIC: A deep learning approach," in *2019 4th International Conference on Information Technology (InCIT)*. IEEE, 2019, pp. 195–198.

[39] M. Wildemeersch, T. Q. S. Quek, M. Kountouris, A. Rabbachin, and C. H. Slump, "Successive interference cancellation in heterogeneous networks," *IEEE Transactions on Communications*, vol. 62, no. 12, pp. 4440–4453, 2014.

[40] D. Lopez-Perez, I. Guvenc, G. de la Roche, M. Kountouris, T. Q. Quek, and J. Zhang, "Enhanced intercell interference coordination challenges in heterogeneous networks," *IEEE Wireless Communications*, vol. 18, no. 3, pp. 22–30, 2011.

[41] Y.-S. Liang, W.-H. Chung, G.-K. Ni, I.-Y. Chen, H. Zhang, and S.-Y. Kuo, "Resource allocation with interference avoidance in OFDMA femtocell networks," *IEEE Transactions on Vehicular Technology*, vol. 61, no. 5, pp. 2243–2255, 2012.

[42] H. S. Dhillon, R. K. Ganti, F. Baccelli, and J. G. Andrews, "Modeling and analysis of k-tier downlink heterogeneous cellular networks," *IEEE Journal on Selected Areas in Communications*, vol. 30, no. 3, pp. 550–560, 2012.

[43] A. Ghosh, N. Mangalvedhe, R. Ratasuk, B. Mondal, M. Cudak, E. Visotsky, T. A. Thomas, J. G. Andrews, P. Xia, H. S. Jo *et al.*, "Heterogeneous cellular networks: From theory to practice," *IEEE communications magazine*, vol. 50, no. 6, pp. 54–64, 2012.

[44] D. Lopez-Perez, I. Guvenc, G. De la Roche, M. Kountouris, T. Q. Quek, and J. Zhang, "Enhanced intercell interference coordination challenges in heterogeneous networks," *IEEE Wireless communications*, vol. 18, no. 3, pp. 22–30, 2011.

[45] A. Tikhomirov, E. Omelyanchuk, and A. Semenova, "Recommended 5G frequency bands evaluation," in *2018 Systems of Signals Generating and Processing in the Field of on Board Communications*. IEEE, 2018, pp. 1–5.

[46] Y. Kim and J. Kim, "A 2-D subcarrier allocation scheme for capacity enhancement in a clustered OFDM system," *IEICE Trans. Commun.*, vol. 90-B, pp. 1880–1883, 2007.

[47] T. Liu, C. Yang, and L.-L. Yang, "A low-complexity subcarrier-power allocation scheme for frequency-division multiple-access systems," *IEEE Transactions on Wireless Communications*, vol. 9, no. 5, pp. 1564–1570, 2010.

[48] J. Shi and L.-L. Yang, "Novel subcarrier-allocation schemes for downlink MC DS-CDMA systems," *IEEE Transactions on Wireless Communications*, vol. 13, no. 10, pp. 5716–5728, 2014.

[49] R. Vannithamby and S. Talwar, *Towards 5G: Applications, requirements and candidate technologies*. John Wiley & Sons, 2017.

[50] S. R. Islam, N. Avazov, O. A. Dobre, and K.-S. Kwak, "Power-domain non-orthogonal multiple access (NOMA) in 5G systems: Potentials and challenges," *IEEE Communications Surveys & Tutorials*, vol. 19, no. 2, pp. 721–742, 2016.

[51] I. A. Mahady, E. Bedeer, S. Ikki, and H. Yanikomeroglu, "Sum-rate maximization of NOMA systems under imperfect successive interference cancellation," *IEEE Communications Letters*, vol. 23, no. 3, pp. 474–477, 2019.

[52] C.-H. Wang, J.-Y. Lin, and J.-M. Wu, "Resource allocation and user grouping for sum rate and fairness optimization in NOMA and IoT," in *2018 IEEE Conference on Standards for Communications and Networking (CSCN)*. IEEE, 2018, pp. 1–6.

[53] K. S. Ali, H. ElSawy, A. Chaaban, M. Haenggi, and M.-S. Alouini, "Analyzing non-orthogonal multiple access (NOMA) in downlink poisson cellular networks," in *2018 IEEE International Conference on Communications (ICC)*. IEEE, 2018, pp. 1–6.

[54] Z. Ding, P. Fan, and H. V. Poor, "Impact of user pairing on 5G nonorthogonal multiple-access downlink transmissions," *IEEE Transactions on Vehicular Technology*, vol. 65, no. 8, pp. 6010–6023, 2015.

[55] P. Swami, M. K. Mishra, V. Bhatia, and T. Ratnarajah, "Performance analysis of noma enabled hybrid network with limited feedback," *IEEE Transactions on Vehicular Technology*, vol. 69, no. 4, pp. 4516–4521, 2020.

[56] Z. Yang, W. Xu, C. Pan, Y. Pan, and M. Chen, "On the optimality of power allocation for NOMA downlinks with individual qos constraints," *IEEE Communications Letters*, vol. 21, no. 7, pp. 1649–1652, 2017.

[57] Z. Q. Al-Abbasi and D. K. So, "Power allocation for sum rate maximization in non-orthogonal multiple access system," in *2015 IEEE 26th Annual International Symposium*

on Personal, Indoor, and Mobile Radio Communications (PIMRC). IEEE, 2015, pp. 1649–1653.

[58] J. Choi, "On the power allocation for MIMO-NOMA systems with layered transmissions," *IEEE Transactions on Wireless Communications*, vol. 15, no. 5, pp. 3226–3237, 2016.

[59] Y. Fu, L. Salaün, C. W. Sung, C. S. Chen, and M. Coupechoux, "Double iterative waterfilling for sum rate maximization in multicarrier NOMA systems," in *2017 IEEE International Conference on Communications (ICC)*. IEEE, 2017, pp. 1–6.

[60] Z. Li, S. Wang, P. Mu, and Y.-C. Wu, "Sum rate maximization of secure noma transmission with imperfect CSI," in *ICC 2020-2020 IEEE International Conference on Communications (ICC)*. IEEE, 2020, pp. 1–6.

[61] M. F. Hanif, Z. Ding, T. Ratnarajah, and G. K. Karagiannidis, "A minorization-maximization method for optimizing sum rate in the downlink of non-orthogonal multiple access systems," *IEEE Transactions on Signal Processing*, vol. 64, no. 1, pp. 76–88, 2015.

[62] M. Zeng, A. Yadav, O. A. Dobre, G. I. Tsiropoulos, and H. V. Poor, "On the sum rate of MIMO-NOMA and MIMO-OMA systems," *IEEE Wireless communications letters*, vol. 6, no. 4, pp. 534–537, 2017.

[63] A. Ali, A. Baig, G. M. Awan, W. U. Khan, Z. Ali, and G. A. S. Sidhu, "Efficient resource management for sum capacity maximization in 5G NOMA systems," *Applied System Innovation*, vol. 2, no. 3, p. 27, 2019.

[64] S. Trankatwar and P. Wali, "Optimal power allocation for downlink NOMA heterogeneous networks to improve sum rate and outage probability," in *2022 IEEE India Council International Subsections Conference (INDISCON)*. IEEE, 2022, pp. 1–6.

[65] X. Wang, R. Chen, Y. Xu, and Q. Meng, "Low-complexity power allocation in NOMA systems with imperfect SIC for maximizing weighted sum-rate," *IEEE Access*, vol. 7, pp. 94 238–94 253, 2019.

[66] S. Trankatwar and P. Wali, "Subchannel and power optimization for sum rate maximization in downlink multicarrier NOMA networks," *Physical Communication*, p. 102050, 2023.

[67] S. Timotheou and I. Krikidis, "Fairness for non-orthogonal multiple access in 5G systems," *IEEE Signal Processing Letters*, vol. 22, no. 10, pp. 1647–1651, 2015.

[68] Y. Lin, Z. Yang, and H. Guo, "Proportional fairness-based energy-efficient power allocation in downlink MIMO-NOMA systems with statistical CSI," *China Communications*, vol. 16, no. 12, pp. 47–55, 2019.

[69] M.-R. Hojeij, C. A. Nour, J. Farah, and C. Douillard, "Waterfilling-based proportional fairness scheduler for downlink non-orthogonal multiple access," *IEEE wireless communications letters*, vol. 6, no. 2, pp. 230–233, 2017.

[70] H. Xing, Y. Liu, A. Nallanathan, and Z. Ding, "Sum-rate maximization guaranteeing user fairness for NOMA in fading channels," in *2018 IEEE Wireless Communications and Networking Conference (WCNC)*. IEEE, 2018, pp. 1–6.

[71] P. Xu, K. Cumanan, and Z. Yang, "Optimal power allocation scheme for NOMA with adaptive rates and alpha-fairness," in *GLOBECOM 2017-2017 IEEE Global Communications Conference*. IEEE, 2017, pp. 1–6.

[72] Y. Sun, Y. Guo, S. Li, D. Wu, and B. Wang, "Optimal resource allocation for NOMA-TDMA scheme with α-fairness in industrial internet of things," *Sensors*, vol. 18, no. 5, p. 1572, 2018.

[73] A. S. de Sena, F. R. M. Lima, D. B. da Costa, Z. Ding, P. H. Nardelli, U. S. Dias, and C. B. Papadias, "Massive MIMO-NOMA networks with imperfect SIC: Design and fairness enhancement," *IEEE Transactions on Wireless Communications*, vol. 19, no. 9, pp. 6100–6115, 2020.

[74] F. Liu, P. Mähönen, and M. Petrova, "Proportional fairness-based power allocation and user set selection for downlink noma systems," in *2016 IEEE International Conference on Communications (ICC)*. IEEE, 2016, pp. 1–6.

[75] Y. Liu, X. Chen, L. X. Cai, Q. Chen, R. Gong, and D. Tang, "On the fairness performance of NOMA-based wireless powered communication networks," in *ICC 2019-2019 IEEE International Conference on Communications (ICC)*. IEEE, 2019, pp. 1–6.

[76] J. Choi, "Power allocation for max-sum rate and max-min rate proportional fairness in NOMA," *IEEE Communications Letters*, vol. 20, no. 10, pp. 2055–2058, 2016.

[77] H. Al-Obiedollah, K. Cumanan, J. Thiyagalingam, A. G. Burr, Z. Ding, and O. A. Dobre, "Sum rate fairness trade-off-based resource allocation technique for MISO NOMA systems," in *2019 IEEE Wireless Communications and Networking Conference (WCNC)*. IEEE, 2019, pp. 1–6.

[78] K. Higuchi and A. Benjebbour, "Non-orthogonal multiple access (NOMA) with successive interference cancellation for future radio access," *IEICE Transactions on Communications*, vol. 98, no. 3, pp. 403–414, 2015.

[79] Y. Sawaragi, H. NAKAYAMA, and T. TANINO, *Theory of multiobjective optimization*. Elsevier, 1985.

[80] K. Miettinen, *Nonlinear multiobjective optimization*. Springer Science & Business Media, 2012, vol. 12.

[81] R. T. Marler and J. S. Arora, "The weighted sum method for multi-objective optimization: new insights," *Structural and multidisciplinary optimization*, vol. 41, no. 6, pp. 853–862, 2010.

[82] S. Boyd, S. P. Boyd, and L. Vandenberghe, *Convex optimization*. Cambridge university press, 2004.

[83] J. Chen, L. Yang, and M.-S. Alouini, "Physical layer security for cooperative NOMA systems," *IEEE Transactions on Vehicular Technology*, vol. 67, no. 5, pp. 4645–4649, 2018.

[84] A. Jee, K. Janghel, and S. Prakriya, "Performance of adaptive multi-user underlay NOMA transmission with simple user selection," *IEEE Transactions on Cognitive Communications and Networking*, vol. 8, no. 2, pp. 871–887, 2022.

[85] Y. Cheng, X. You, P. Fu, and Z. Wang, "An energy efficient algorithm based on clustering formulation and scheduling for proportional fairness in wireless sensor networks," *KSII Transactions on Internet and Information Systems (TIIS)*, vol. 10, no. 2, pp. 559–573, 2016.

[86] H. Shi, R. V. Prasad, E. Onur, and I. Niemegeers, "Fairness in wireless networks: Issues, measures and challenges," 2014.

[87] H. Felfel, O. Ayadi, and F. Masmoudi, "A decision-making approach for a multi-objective multisite supply network planning problem," *International Journal of Computer Integrated Manufacturing*, vol. 29, no. 7, pp. 754–767, 2016.

[88] Z. Tahira, H. M. Asif, A. A. Khan, S. Baig, S. Mumtaz, and S. Al-Rubaye, "Optimization of non-orthogonal multiple access based visible light communication systems," *IEEE Communications Letters*, vol. 23, no. 8, pp. 1365–1368, 2019.

[89] T. C.-Y. Ng and W. Yu, "Joint optimization of relay strategies and resource allocations in cooperative cellular networks," *IEEE Journal on Selected areas in Communications*, vol. 25, no. 2, pp. 328–339, 2007.

[90] S. Boyd, L. Xiao, and A. Mutapcic, "Subgradient methods," *lecture notes of EE392o, Stanford University, Autumn Quarter*, vol. 2004, pp. 2004–2005, 2003.

[91] A. Benjebbour, Y. Saito, Y. Kishiyama, A. Li, A. Harada, and T. Nakamura, "Concept and practical considerations of non-orthogonal multiple access (NOMA) for future radio access," in *2013 International Symposium on Intelligent Signal Processing and Communication Systems*. IEEE, 2013, pp. 770–774.

[92] Y. Saito, A. Benjebbour, Y. Kishiyama, and T. Nakamura, "System-level performance evaluation of downlink non-orthogonal multiple access (NOMA)," in *2013 IEEE 24th Annual International Symposium on Personal, Indoor, and Mobile Radio Communications (PIMRC)*. IEEE, 2013, pp. 611–615.

[93] R. K. Jain, D.-M. W. Chiu, W. R. Hawe *et al.*, "A quantitative measure of fairness and discrimination," *Eastern Research Laboratory, Digital Equipment Corporation, Hudson, MA*, 1984.

[94] J. Zhao, Y. Liu, K. K. Chai, A. Nallanathan, Y. Chen, and Z. Han, "Spectrum allocation and power control for non-orthogonal multiple access in hetnets," *IEEE Transactions on Wireless Communications*, vol. 16, no. 9, pp. 5825–5837, 2017.

[95] P. Xu and K. Cumanan, "Optimal power allocation scheme for non-orthogonal multiple access with α-fairness," *IEEE Journal on Selected Areas in Communications*, vol. 35, no. 10, pp. 2357–2369, 2017.

[96] Z. Yang, W. Xu, Y. Pan, C. Pan, and M. Chen, "Optimal fairness-aware time and power allocation in wireless powered communication networks," *IEEE Transactions on Communications*, vol. 66, no. 7, pp. 3122–3135, 2018.

[97] H. Sun, B. Xie, R. Q. Hu, and G. Wu, "Non-orthogonal multiple access with sic error propagation in downlink wireless MIMO networks," in *2016 IEEE 84th Vehicular Technology Conference (VTC-Fall)*. IEEE, 2016, pp. 1–5.

[98] Z. Ali, G. A. S. Sidhu, M. Waqas, and F. Gao, "On fair power optimization in nonorthogonal multiple access multiuser networks," *Transactions on Emerging Telecommunications Technologies*, vol. 29, no. 12, p. e3540, 2018.

[99] J. Zhao, X. Yue, S. Kang, and W. Tang, "Joint effects of imperfect CSI and SIC on NOMA based satellite-terrestrial systems," *IEEE Access*, vol. 9, pp. 12 545–12 554, 2021.

[100] C.-H. Wang, J.-Y. Lin, and J.-M. Wu, "Joint fairness and sum rate resource allocation for NOMA communications," in *2017 IEEE Conference on Standards for Communications and Networking (CSCN)*. IEEE, 2017, pp. 269–274.

[101] D. W. K. Ng, E. S. Lo, and R. Schober, "Energy-efficient resource allocation in multicell OFDMA systems with limited backhaul capacity," *IEEE Transactions on Wireless Communications*, vol. 11, no. 10, pp. 3618–3631, 2012.

[102] D. Yuan, J. Joung, C. K. Ho, and S. Sun, "On tractability aspects of optimal resource allocation in OFDMA systems," *IEEE transactions on vehicular technology*, vol. 62, no. 2, pp. 863–873, 2012.

[103] Y. Dursun, K. Wang, and Z. Ding, "Secrecy sum rate maximization for a MIMO-NOMA uplink transmission in 6G networks," *Physical Communication*, vol. 53, p. 101675, 2022.

[104] P. Swami, V. Bhatia, S. Vuppala, and T. Ratnarajah, "User fairness in noma-hetnet using optimized power allocation and time slotting," *IEEE Systems Journal*, vol. 15, no. 1, pp. 1005–1014, 2020.

[105] Z. Ding, M. Peng, and H. V. Poor, "Cooperative non-orthogonal multiple access in 5G systems," *IEEE Communications Letters*, vol. 19, no. 8, pp. 1462–1465, 2015.

[106] M. S. Ali, H. Tabassum, and E. Hossain, "Dynamic user clustering and power allocation for uplink and downlink non-orthogonal multiple access (NOMA) systems," *IEEE Access*, vol. 4, pp. 6325–6343, 2016.

[107] W. U. Khan, F. Jameel, M. A. Jamshed, H. Pervaiz, S. Khan, and J. Liu, "Efficient power allocation for NOMA-enabled IoT networks in 6G era," *Physical Communication*, vol. 39, p. 101043, 2020.

[108] J. Zhu, J. Wang, Y. Huang, S. He, X. You, and L. Yang, "On optimal power allocation for downlink non-orthogonal multiple access systems," *IEEE Journal on Selected Areas in Communications*, vol. 35, no. 12, pp. 2744–2757, 2017.

[109] L. Lei, D. Yuan, C. K. Ho, and S. Sun, "Power and channel allocation for non-orthogonal multiple access in 5G systems: Tractability and computation," *IEEE Transactions on Wireless Communications*, vol. 15, no. 12, pp. 8580–8594, 2016.

[110] H. Zhang, F. Fang, J. Cheng, K. Long, W. Wang, and V. C. Leung, "Energy-efficient resource allocation in NOMA heterogeneous networks," *IEEE Wireless Communications*, vol. 25, no. 2, pp. 48–53, 2018.

[111] H. Zhang, M. Feng, K. Long, G. K. Karagiannidis, and V. C. Leung, "Energy-efficient resource allocation in NOMA heterogeneous networks with energy harvesting," in *2018 IEEE Global Communications Conference (GLOBECOM)*. IEEE, 2018, pp. 206–212.

[112] F. Fang, J. Cheng, and Z. Ding, "Joint energy efficient subchannel and power optimization for a downlink NOMA heterogeneous network," *IEEE Transactions on Vehicular Technology*, vol. 68, no. 2, pp. 1351–1364, 2018.

[113] L. Lei, D. Yuan, C. K. Ho, and S. Sun, "Joint optimization of power and channel allocation with non-orthogonal multiple access for 5G cellular systems," in *2015 IEEE Global Communications Conference (GLOBECOM)*. IEEE, 2015, pp. 1–6.

[114] Y. Xu, Y. Yang, G. Li, and Z. Wang, "Joint subchannel and power allocation for cognitive noma systems with imperfect CSI," in *2019 IEEE Global Conference on Signal and Information Processing (GlobalSIP)*. IEEE, 2019, pp. 1–5.

[115] X. Sun, L. Yu, and Y. Yang, "Jointly optimizing user clustering, power management, and wireless channel allocation for NOMA-based internet of things," *Digital Communications and Networks*, vol. 7, no. 1, pp. 29–36, 2021.

[116] M. Abd-Elnaby, G. G. Sedhom, and M. Elwekeil, "Subcarrier-user assignment in downlink NOMA for improving spectral efficiency and fairness," *IEEE Access*, vol. 9, pp. 5273–5284, 2020.

[117] B. Di, L. Song, and Y. Li, "Sub-channel assignment, power allocation, and user scheduling for non-orthogonal multiple access networks," *IEEE Transactions on Wireless Communications*, vol. 15, no. 11, pp. 7686–7698, 2016.

[118] Y. Sun, D. W. K. Ng, Z. Ding, and R. Schober, "Optimal joint power and subcarrier allocation for MC-NOMA systems," in *2016 IEEE Global Communications Conference (GLOBECOM)*, 2016, pp. 1–6.

[119] M. Kim, C.-H. Cho, and B. C. Chung, "Joint power and subchannel allocation regarding energy harvesting in MC-NOMA based wireless networks," *ICT Express*, 2022.

[120] A. B. Adam, X. Wan, and Z. Wang, "User scheduling and power allocation for downlink multi-cell multi-carrier NOMA systems," *Digital Communications and Networks*, 2022.

[121] C. Chaieb, F. Abdelkefi, and W. Ajib, "Deep reinforcement learning for resource allocation in multi-band and hybrid OMA-NOMA wireless networks," *IEEE Transactions on Communications*, 2022.

[122] X. Li, Z. Xie, G. Huang, J. Zhang, M. Zeng, and Z. Chu, "Sum rate maximization for RIS-aided NOMA with direct links," *IEEE Networking Letters*, vol. 4, no. 2, pp. 55–58, 2022.

[123] A. Jee, K. Agrawal, and S. Prakriya, "A coordinated direct AF/DF relay-aided NOMA framework for low outage," *IEEE Transactions on Communications*, vol. 70, no. 3, pp. 1559–1579, 2021.

[124] X. Li, X. Gao, S. A. Shaikh, M. Zeng, G. Huang, N. M. F. Qureshi, and D. Qiao, "NOMA-based cognitive radio network with hybrid FD/HD relay in industry 5.0," *Journal of King Saud University-Computer and Information Sciences*, 2022.

[125] H. Semira, F. Kara, H. Kaya, and H. Yanikomeroglu, "Multi-user joint maximum-likelihood detection in uplink NOMA-IoT networks: Removing the error floor," *IEEE Wireless Communications Letters*, vol. 10, no. 11, pp. 2459–2463, 2021.

[126] M. R. Garey and D. S. Johnson, *Computers and intractability*. freeman San Francisco, 1979, vol. 174.

[127] D. Palomar, J. Cioffi, and M. Lagunas, "Joint tx-rx beamforming design for multicarrier MIMO channels: a unified framework for convex optimization," *IEEE Transactions on Signal Processing*, vol. 51, no. 9, pp. 2381–2401, 2003.

[128] A. Kiani and N. Ansari, "Edge computing aware NOMA for 5G networks," *IEEE Internet of Things Journal*, vol. 5, no. 2, pp. 1299–1306, 2018.

[129] Y. S. Soh, T. Q. Quek, M. Kountouris, and H. Shin, "Energy efficient heterogeneous cellular networks," *IEEE Journal on selected areas in communications*, vol. 31, no. 5, pp. 840–850, 2013.

[130] Y.-S. Liang, W.-H. Chung, G.-K. Ni, Y. Chen, H. Zhang, and S.-Y. Kuo, "Resource allocation with interference avoidance in OFDMA femtocell networks," *IEEE Transactions on Vehicular Technology*, vol. 61, no. 5, pp. 2243–2255, 2012.

[131] M. Wildemeersch, T. Q. Quek, M. Kountouris, A. Rabbachin, and C. H. Slump, "Successive interference cancellation in heterogeneous networks," *IEEE Transactions on Communications*, vol. 62, no. 12, pp. 4440–4453, 2014.

[132] D. Maamari, N. Devroye, and D. Tuninetti, "Coverage in mmwave cellular networks with base station co-operation," *IEEE transactions on Wireless Communications*, vol. 15, no. 4, pp. 2981–2994, 2016.

[133] M. M. Fadoul, "Rate and coverage analysis in multi-tier heterogeneous network using stochastic geometry approach," *Ad Hoc Networks*, vol. 98, p. 102038, 2020.

[134] W. Yi, Y. Liu, and A. Nallanathan, "Modeling and analysis of D2D millimeter-wave networks with poisson cluster processes," *IEEE Transactions on Communications*, vol. 65, no. 12, pp. 5574–5588, 2017.

[135] V. Suryaprakash, J. Møller, and G. Fettweis, "On the modeling and analysis of heterogeneous radio access networks using a poisson cluster process," *IEEE Transactions on Wireless Communications*, vol. 14, no. 2, pp. 1035–1047, 2014.

[136] S. Joshi and R. K. Mallik, "Coverage and interference in D2D networks with poisson cluster process," *IEEE Communications Letters*, vol. 22, no. 5, pp. 1098–1101, 2018.

[137] H. Wang, X. Zhou, and M. C. Reed, "Coverage and throughput analysis with a non-uniform small cell deployment," *IEEE transactions on wireless communications*, vol. 13, no. 4, pp. 2047–2059, 2014.

[138] X. Zhang and M. Haenggi, "Cellular network coverage with inter-cell interference coordination and intra-cell diversity," in *2014 IEEE International Symposium on Information Theory*. IEEE, 2014, pp. 996–1000.

[139] S. Arabameri, M. J. Dehghani, and J. Haghighat, "Improving coverage probability in heterogeneous networks based on poisson point process," *Iranian Journal of Science and Technology, Transactions of Electrical Engineering*, vol. 43, no. 3, pp. 415–425, 2019.

[140] M. Çakir and A. Kalaycioglu, "Power adjustment based interference management in dense heterogeneous femtocell networks," in *2017 2nd International Conference on Computer and Communication Systems (ICCCS)*. IEEE, 2017, pp. 133–137.

[141] M. Chiang, P. Hande, T. Lan, C. W. Tan *et al.*, "Power control in wireless cellular networks," *Foundations and Trends® in Networking*, vol. 2, no. 4, pp. 381–533, 2008.

[142] F. Aurenhammer, "Voronoi diagrams—a survey of a fundamental geometric data structure," *ACM Computing Surveys (CSUR)*, vol. 23, no. 3, pp. 345–405, 1991.

[143] A. Mukherjee, S. Bhattacherjee, S. Pal, and D. De, "Femtocell based green power consumption methods for mobile network," *Computer Networks*, vol. 57, no. 1, pp. 162–178, 2013.

[144] Y. S. Soh, T. Q. S. Quek, M. Kountouris, and H. Shin, "Energy efficient heterogeneous cellular networks," *IEEE Journal on Selected Areas in Communications*, vol. 31, no. 5, pp. 840–850, 2013.

[145] S. Trankatwar and P. Wali, "Power control algorithm to improve coverage probability in heterogeneous networks," *Wireless Personal Communications*, vol. 121, no. 3, pp. 1821–1833, 2021.

[146] H. Zhang, C. Jiang, N. C. Beaulieu, X. Chu, X. Wang, and T. Q. S. Quek, "Resource allocation for cognitive small cell networks: A cooperative bargaining game theoretic approach," *IEEE Transactions on Wireless Communications*, vol. 14, no. 6, pp. 3481–3493, 2015.

[147] H. Zhang, F. Fang, J. Cheng, K. Long, W. Wang, and V. C. M. Leung, "Energy-efficient resource allocation in NOMA heterogeneous networks," *IEEE Wireless Communications*, vol. 25, no. 2, pp. 48–53, 2018.

[148] S. Shi, L. Yang, and H. Zhu, "Outage balancing in downlink nonorthogonal multiple access with statistical channel state information," *IEEE Transactions on Wireless Communications*, vol. 15, no. 7, pp. 4718–4731, 2016.

[149] Z. Ding, Z. Yang, P. Fan, and H. V. Poor, "On the performance of non-orthogonal multiple access in 5G systems with randomly deployed users," *IEEE Signal Processing Letters*, vol. 21, no. 12, pp. 1501–1505, 2014.

[150] S. Timotheou and I. Krikidis, "Fairness for non-orthogonal multiple access in 5G systems," *IEEE Signal Processing Letters*, vol. 22, no. 10, pp. 1647–1651, 2015.

[151] Y. Liu, Z. Ding, M. Elkashlan, and H. V. Poor, "Cooperative non-orthogonal multiple access with simultaneous wireless information and power transfer," *IEEE Journal on Selected Areas in Communications*, vol. 34, no. 4, pp. 938–953, 2016.

[152] H.-S. Jo, Y. J. Sang, P. Xia, and J. G. Andrews, "Outage probability for heterogeneous cellular networks with biased cell association," in *2011 IEEE Global Telecommunications Conference - GLOBECOM 2011*, 2011, pp. 1–5.

[153] H. Wu, X. Tao, N. Li, and J. Xu, "Secrecy outage probability in multi-rat heterogeneous networks," *IEEE Communications Letters*, vol. 20, no. 1, pp. 53–56, 2016.

[154] J. Zhao, Y. Liu, K. K. Chai, A. Nallanathan, Y. Chen, and Z. Han, "Spectrum allocation and power control for non-orthogonal multiple access in hetnets," *IEEE Transactions on Wireless Communications*, vol. 16, pp. 5825–5837, 2017.

[155] X. Chu, H. Zhang, W. Huangfu, W. Liu, Y. Ren, J. Dong, and K. Long, "Subchannel assignment and power optimization for energy-efficient NOMA heterogeneous network," in *2019 IEEE Global Communications Conference (GLOBECOM)*, 2019, pp. 1–6.

[156] H. Zhang, M. Feng, K. Long, G. K. Karagiannidis, V. C. Leung, and H. V. Poor, "Energy efficient resource management in swipt enabled heterogeneous networks with NOMA," *IEEE Transactions on Wireless Communications*, vol. 19, no. 2, pp. 835–845, 2019.

List of Publications

List of Journals

[1] Sachin Trankatwar and Prashant Wali, "Power allocation scheme for sum rate and fairness trade-off in downlink NOMA networks," Computer Communications, Elseveir, 2024, issn: 0140-3664. doi: https://doi.org/10.1016/j.comcom.2024.04.018.

[2] 3. Sachin Trankatwar and Prashant Wali, "Subchannel and power optimization for sum rate maximization in downlink multicarrier NOMA networks," Physical Communication, Elseveir, vol. 58, p. 102 050, 2023, issn: 1874-4907.
doi: https://doi.org/10.1016/j.phycom.2023.102050.

[3] Sachin Trankatwar and Prashant Wali, "Power control algorithm to improve coverage probability in heterogeneous networks," Wireless Personal Communications, Springer, vol. 121, no. 3, pp. 1821–1833, 2021. doi: https://doi.org/10.1007/s11277-021-08739-y.

List of Conferences

[1] Sachin Trankatwar and Prashant Wali, "Power allocation for sum rate maximization under SIC constraint in NOMA networks," in 2024 16th IEEE International Conference on COMmunication Systems NETworkS (COMSNETS), 2024, pp. 646–650.
doi: 10.1109/COMSNETS59351.2024.10427001.

[2] Sachin Trankatwar and Prashant Wali, "Optimal power allocation for downlink NOMA heterogeneous networks to improve sum rate and outage probability," in 2022 IEEE India

Council International Subsections Conference (INDISCON), 2022, pp. 1–6.
doi: 10.1109/INDISCON54605.2022.9862842.

List of Papers Communicated

[1] Sachin Trankatwar, and Prashant Wali, “Power Allocation for Joint Sum Rate and Fairness Optimization in Downlink NOMA Networks,” International Journal of Communication Systems, Wiley, 2023 (under review).

Biography

Trankatwar Sachin Ravikant received a B.E. degree in Electronics and Telecommunications Engineering from IETE, New Delhi, in 2010 and a Master's degree in Electronics and Telecommunications Engineering from DBATU, Lonere, Raigad, India, in 2013. He is currently pursuing a Ph.D. degree from BITS Pilani, Hyderabad Campus, Hyderabad, India. His current research interest includes Efficient techniques for 5G cellular networks. He qualified GATE examination six times. He has over six years of teaching experience at an undergraduate level.

Prashant K. Wali received his Masters degree from the Dept. of Electrical Communication Engineering, Indian Institute of Science, Bangalore, India in 2008 and his Ph.D. from the International Institute of Information Technology-Bangalore in 2017. Currently, he is working as an Assistant Professor in the Department of Electrical and Electronics Engineering at BITS-Pilani, Hyderabad Campus, India. His research interests include the design and analysis of energy-efficient algorithms for broadband wireless cellular systems and estimation techniques for event-based networked control systems.